69-8021

DEEHR, Charles Sterling, 1936-
THE TWILIGHT ENHANCEMENT OF THE AURORAL AND NEBULAR LINES OF NEUTRAL ATOMIC OXYGEN.

University of Alaska, Ph.D., 1968
Physics, general

University Microfilms, Inc., Ann Arbor, Michigan

THE TWILIGHT ENHANCEMENT OF THE AURORAL AND NEBULAR LINES OF NEUTRAL ATOMIC OXYGEN

A

DISSERTATION

Presented to the Faculty of the
University of Alaska in Partial Fulfillment
of the Requirements
for the Degree of
DOCTOR OF PHILOSOPHY

by

Charles Sterling Deehr, B.A., M.S.

College, Alaska
May, 1968

THE TWILIGHT ENHANCEMENT OF THE AURORAL

AND NEBULAR LINES OF NEUTRAL ATOMIC OXYGEN

APPROVED:

Gerald J. Romick

Tunis Wentink Jr.

T. Neil Davis
Chairman

Roger Sheridan
Department Head

APPROVED: _____ DATE: 5/13/68
Dean of the College of Mathematics,
Physical Sciences, and Engineering

_____
Vice President for Research and
Advanced Study

I am very often convinced
that the angle of man
is necessarily inconducive
to higher thoughts.
Walking, as we do,
at right angles to the earth,
we are prevented from looking,
as much as we should
at the legendary sky above us...
Probably this was the divine plan, anyway,
but I certainly intend
to spend more time
lying on my back...

---Dylan Thomas
Resolutions for 1934

THE TWILIGHT ENHANCEMENT OF THE AURORAL

AND NEBULAR LINES OF NEUTRAL ATOMIC OXYGEN

(Order No.)

Charles Sterling Deehr, Ph.D.

University of Alaska, 1968

Supervisor_____

ABSTRACT

A study of the auroral (5577 A) and nebular (6300 A) emissions of [OI] in the twilight airglow was carried out at College, Alaska (65°N, 147°W) during the IQSY period (1963-1965). An analysis of morning twilight observations, taken with a birefringent filter photometer, showed the twilight enhancement of both emissions to be due to photodissociation of O_2. Analytical expressions were developed which described the intensities to be expected from this mechanism in the twilight, and then the physical parameters used in these expressions were varied to match the intensities observed under changing atmospheric conditions. Because only one production mechanism was important, it was possible to draw conclusions about the physical processes involved and about the state of the atmosphere at the time of the observation.

Observations during undisturbed, magnetically quiet winter twilights indicated an atmosphere which is best described by the 1965 COSPAR Reference Atmosphere with an exospheric temperature of approximately 750°K. Under these conditions, the production efficiency for the 5577 A emission was approximately 1/200 of that for the 6300 A line, which was taken as 4.4×10^{-6} photons sec^{-1} $molecule^{-1}$.

The altitude of the main emitting region was found to vary from 250 km to 150 km during the course of the morning twilight observations. This variation accounts for the difficulty which has resulted from previous attempts to measure the scale height of the emitting species without allowing for the altitude change.

As magnetic activity increased, the enhancement increased and the altitude of the emitting region was lowered; the data indicated that an increase of O_2 near the 200 km level was more important than the expected increase in exospheric temperature with magnetic activity. The 5577 A enhancement increased far more than that of the 6300 A line under these conditions, probably because of selective quenching of the latter emission at lower altitudes. The quenching of the 6300 A $O(^1D)$ emission was probably by N_2 with a rate of 10^{-11} cm^3 sec^{-1}.

In order to show that photodissociation was the dominant process in these observations, an analysis was made of the possible contribution to the 6300 A emission by the precipitation into the atmosphere of photoelectrons (5 to 50 ev) traveling along magnetic lines of force from the conjugate hemisphere. This re-evaluation of previous work leads to a new description of both the world-wide occurrence and the local characteristics of this phenomenon.

1) The altitude and intensity of the 6300 A emission associated with conjugate photoelectrons is proportional to the solar cycle variation in atmospheric density above 300 km.

2) The approach and departure of the emitting region with conjugate sunrise and sunset over any single station changes as much as 90° in azimith with the yearly change in solar declination.

3) The displacement of the geomagnetic pole from the geographic pole results in the existence of a region of continuous precipitation of photoelectrons in certain areas of the earth.

4) The extent and occurrence of the photoelectron precipitation are predictably dependent on the solar activity.

Comparison of maps prepared to show the world-wide distribution of conjugate photoelectron precipitation with airglow data indicates that the 6300 A emission due to conjugate photoelectron precipitation must have been less than 5 Rayleighs at College. It is concluded that precipitation poleward of L=5 during a magnetically quiet period is probably negligible.

ACKNOWLEDGEMENTS

I am indebted to T. N. Davis, G. J. Romick and T. Wentink for advice and critical reading of the manuscript, and to A. E. Belon, S.-I.Akasofu, W. B. Murcray and C. T. Elvey for helpful discussion of the material. A large amount of computer time was donated to the effort of calculating the photoelectron precipitation patterns by Major E. W. Pittenger and Dr. G. Gassman of Air Force Cambridge Research Laboratories and Dr. N. Glass and Dr. L. Miller of Los Alamos Research Laboratories. The maps, on which the computer results were plotted, were provided by J. K. Hargreaves of ITS-ESSA, Boulder.

The research was supported by National Science Foundation grants GA-468 and GA-1008 and by the Advanced Research Projects Agency with technical direction by Air Force Technical Applications Center, Contract No. AF33(657)-13703, as part of Project VELA.

TABLE OF CONTENTS

LIST OF ILLUSTRATIONS

LIST OF TABLES

CHAPTER I

INTRODUCTION

High latitudes are well known for long winter nights and eternal summer days. The light that we recall, however, is the long, slow twilight. Because the rising and the setting of the sun is a matter of such concern near the poles, it is always heartening to know in midst of winter that the sun is shining on the earth itself just a few degrees away beyond the pole. The solar rays then never truly leave the atmosphere above, and this sunlight line is always closer to the earth in the "infinite polar night" than during any night at lower latitudes. This geometric situation results in atmospheric phenomena which differ markedly from those at lower latitudes. The number of twilights per year decreases as we move toward the pole but the higher latitude observatory is then allowed the longer single observation of the twilit sky.

Because the history of twilight observations has been written in the middle latitudes, it was assumed that the different viewpoint given by observations made at higher latitudes would enable one to solve some of the problems which have been raised. An observing program utilizing a birefringent filter photometer was begun at College, Alaska (64° 52.8'N, 148° 03.4'W) in the spring of 1963 and continued until the spring of 1965. The birefringent filter photometer and the observing program were almost identical to those employed by Megill (1960). The rejection of the scattered solar continuum by this photometer allows almucantar (constant altitude, changing azimuth) scans to be made until the height of the intersection of the instrumental field of view toward the sun with the earth's geometric shadow

is approximately 40 km. The ground based observation of the twilight airglow is not unlike a photometric rocket flight: it documents the effect of the change of solar flux with altitude during dusk and dawn. Additional information on the change of layers with time is available to an observer using azimuth scans, because a number of effective shadow heights are seen in any single scan. Inhomogeneities in geographical distribution become evident in this program, again improving the ability to separate the phenomena.

Theoretically, the different processes for the production of atmospheric emissions should manifest themselves in a characteristic pattern across the sky. If a seasonal or diurnal variation happens to separate the patterns and the observational data have sufficient resolution in time and space, then the processes should be easily deduced. The procedure can ultimately be reversed and the observational data can then be interpreted to monitor the "meteorology" of the upper atmosphere. The attainment of this goal has been a slow process. When fortunate circumstances allowed observations with sufficient resolution in time and space, new phenomena were found instead of old questions resolved.

In a most complete review of spectroscopic studies of the twilight airglow, Hunten (1967) divides the twilight phenomena into three classes, roughly according to height. First in order are the bands O_2 and perhaps OH, probably emitted below an altitude of 80 km. Secondly are listed the metallic emissions, most of which are resonantly scattered between 80 km and the F region. The third class includes the F region (150 km) and above.

Because the birefringent filter is not designed to measure band emissions, the first named class is not of interest here. In the second category, two metallic emissions were included in the observing program. Prefilters isolating wavelength regions around 5893A and 6708A were included in order to observe the abundance-height profile of Na and Li , respectively. Because the all-sky observing program did not allow a large enough signal-to-noise ratio for the very low intensities encountered in the Li emission, it was never positively identified during the observations. The Na emission in the twilight has been previously observed at College and briefly discussed by Rees and Deehr (1962). The azimuth scan allows one to detect geographic inhomogenietics and improves the luminosity-height profile for this emission but this matter will not be treated here.

Of the twilight emissions comprising the third named class, including the F region and above, the lines of [NI] 5200A, and [OI] 5577A and 6300A were measured. The first of these emissions was not observed in twilight except in the presence of aurora. The latter two emissions are the forbidden green and red lines of oxygen which are the subject of the work presented here.

The green line is only sporadically enhanced in twilight as first reported by Dufay and Dufay (1948). Other investigators were not able to substantiate the existence of the enhancement until Megill (1960) used a birefringent filter photometer during the IGY in 1957-1958 and documented a seasonal variation of the occurrence at 44°N. The nature of the excitation mechanism was left in doubt.

Early observations of the red line are listed by Chamberlain (1961, p. 384). The observation of this line in twilight is complicated by the number of processes which lead to the transition. Barbier (1960) observed with a time and spatial resolution which was adequate to describe at least the major processes involved in the production of [OI] ^1D in the twilight. Dividing the observations according to morphology, Barbier observed the red line to be present in at least five different forms: the "aurora", the "true twilight enhancement", the "western sheet", the "subpolar sheet" and the "intertropical arcs". He was able to describe the different phenomena in terms of certain excitation processes. There were left, however, a number of questions to be answered before such observations could be used to describe the upper atmosphere. Hunten's summary (1967) of advances since the work of Barbier essentially substantiated Barbier's hypotheses about the types of excitation of the line. Questions related to the altitude and geographic distribution have remained unanswered.

The "western sheet" has been observed to be closely associated with the height and electron density of the F region. It is almost certainly due to dissociative recombination of O_2^+ (Hunten, 1967, p. 557). This phenomenon, predominantly observed in the evening twilight and the airglow until early morning, will not be considered here. The aurora, i.e. luminosity produced by particles from the outer magnetosphere, will not be included either. The intertropical arcs are, of course, not observable from College. The remaining two effects, which have been observed in twilight are: 1) the true twilight effect, i.e. direct enhancement by solar radiation, which has been observed in

morning and evening in both the red and green lines, and 2) the predawn enhancement of 6300A emission, called the subpolar sheet.

It is the purpose of this study to describe these effects and compare previous observations with those made here at College. From the observed morphology, one can infer the mechanisms involved in the production of the observed emissions, predict the occurrence of the emissions at other times and places, and draw some conclusions as to the state of the atmosphere during the observations.

CHAPTER II

INSTRUMENTATION

2.1 The Photometer

Birefringent filter photometers have been used extensively for airglow and aurora observation; instruments similar to the one used here are described by Megill (1960) and Dunn and Manring (1955). The instrument used in this study at College was built at the National Bureau of Standards Laboratory in Boulder, Colorado, by L. R. Megill and F. E. Roach. It was sent to the Geophysical Institute in 1958 as a part of the IGY program and has been used since then for airglow and aurora studies. Improvements made over the years kept pace with the development of improved interference filters and electronic equipment. The following is a brief description of the photometer as it was used for the observations reported here.

The basic photometric system is shown by the block diagram in Figure 2.1. The telescope has a 6" dia. objective, a 2.5" dia. Ross corrector containing the optical interference prefilter, and a field lens in front of the photomultiplier to limit the field of view to 5° at the half-transmission points. The typical prefilter has a nominal peak transmission of 40 percent at the wavelength of interest and transmission of less than 10^{-2} percent at ± 50A from the peak. The prefilters are mounted on a wheel and are changed by a geneva gear system which is activated by engaging a magnetic clutch on the shaft of a continuously running 60 rpm motor. The prefilters used in this

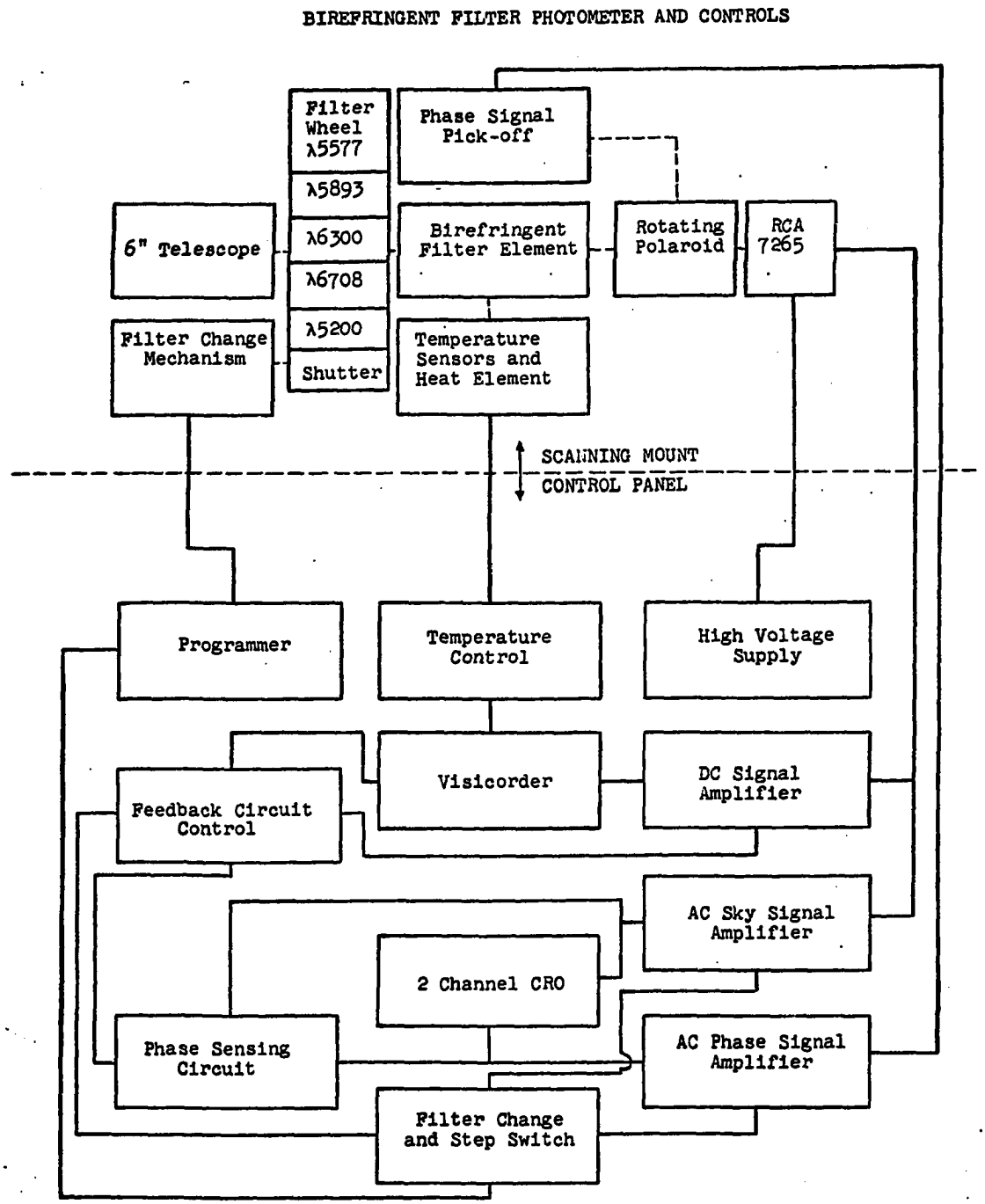

Fig. 2.1 Block diagram of the birefringent quartz filter photometer with phase sensitive electronics and related systems.

study were peaked to include the following wavelengths: 5577 A [OI], 5890 A - 5896 A (NaI), 6300 A [OI], 6708 A (LiI), 5200 A [NI].

Immediately behind the prefilter and the Ross corrector is the birefringent filter. This filter was first developed by Blamont and Kastler (1951) and was later applied to airglow measurements by Koomen et al (1951), Dunn and Manring (1955), and Megill (1960). The design of the filter used here is due to R. B. Dunn. Light entering the filter is elliptically polarized and retarded so that the major axis of polarization which is perpendicular to the optic axis is rotated about the optic axis to an angle of magnitude proportional to the wavelength of the incident light. An analyzer polaroid at the back of the birefringent element then produces a channel spectrum with the wavelength of the transmission peaks dependent on the angular position of the plane of polarization. Rotating this last polaroid effectively moves the channels (in this case 3A wide, 6A apart), within the transmission envelope of the prefilter. Discontinuities in the continuum (e.g. emission lines) which are less than 6A wide are thus modulated in proportion to the angular displacement of the polaroid. A separate electrical measure of this displacement provides a reference voltage with the same frequency of modulation, which is used as a phase comparison signal. The light reaches a RCA 7265 photomultiplier operated at 2500 volts. The total current from this tube is amplified by a Keithley 610 electrometer; the output is then fed to a feedback control and is recorded on a strip chart as a measure of the total light incident on the tube.

Modulation of the emission line intensity described above produces an alternating component of the tube current which is amplified by an ac amplifier with a peak sensitivity at 73 cycles (chopping frequency) and a bandwidth of approximately 12 cycles. The phase reference voltage is shaped and amplified by a "twin T" amplifier and is fed to the phase sensing circuit along with the chopped sky signal. The output from the phase sensing circuit enters the feedback control which adds or subtracts an amount to the signal in proportion to the total current of the photomultiplier. This is to allow for the chopping of the continuum by the birefringent filter and is adjusted for each wavelength region during a time when the brightness of the continuum is far in excess of that of the signal. The final output of the phase sensitive amplifier is recorded in 2 gains on the strip chart and represents the intensity of the emission line.

The photometer was calibrated by comparison with an interference filter photometer, which had been calibrated previously using Strontium-90 activated phosphors manufactured by the U. S. Radium Corporation under the trade name of "Isolite" sources. The two instruments were run simultaneously with 5577 A filters while pointing at an aurora in the zenith. The brightness of the aurora was approximately 4 kR, thereby eliminating the necessity of correcting for the intensity of the background radiation, which probably amounted to approximately 6 Rayleighs/A. The calibration was extended to other wavelengths by means of the known characteristics of the photomultiplier and the filters. Because the temperature of the birefringent element was held to ± 0.1°C, the

calibration of filter, photomultiplier and other temperature sensitive elements remained quite constant.

2.2 The Scanning Mount and Programmer

The telescope and associated equipment, as indicated in Figure 2.1 are mounted in a yoke which is driven in altitude and azimuth according to instructions from an electronic programmer. The programmer, shown in Figure 2.2, commands the scanning mount in 5 programs: 1) vertical circle sweeps, 2) vertical circle survey, 3) manual, 4) almucantar survey, 5) almucantar sweeps. Analog information as to the position of the telescope in azimuth and altitude is brought to the control panel by selsyn motors where it is transferred to digital position and light commands by photoelectric cells looking through slits in the edge of disks attached to the shafts of the receiver selsyns.

Accurate digital information on the position of the telescope (± 0.1 degrees) is obtained by pulses from a photoelectric cell looking through slots in a disk which is geared to rotate 18 times for each revolution of each mount shaft. For ease of scaling the azimuth sweeps every 22 1/2 degrees, small magnets were attached to the rotating platform and a reed switch was mounted on the base. Activation of the reed switch by the magnets provided additional position information which was recorded on the strip chart. Universal Time was transmitted from the College Minitrack Station and recorded in digital form on the strip chart.

The twilight observing program normally consisted of an almucantar survey in each of the six positions of the prefilter and shutter wheel.

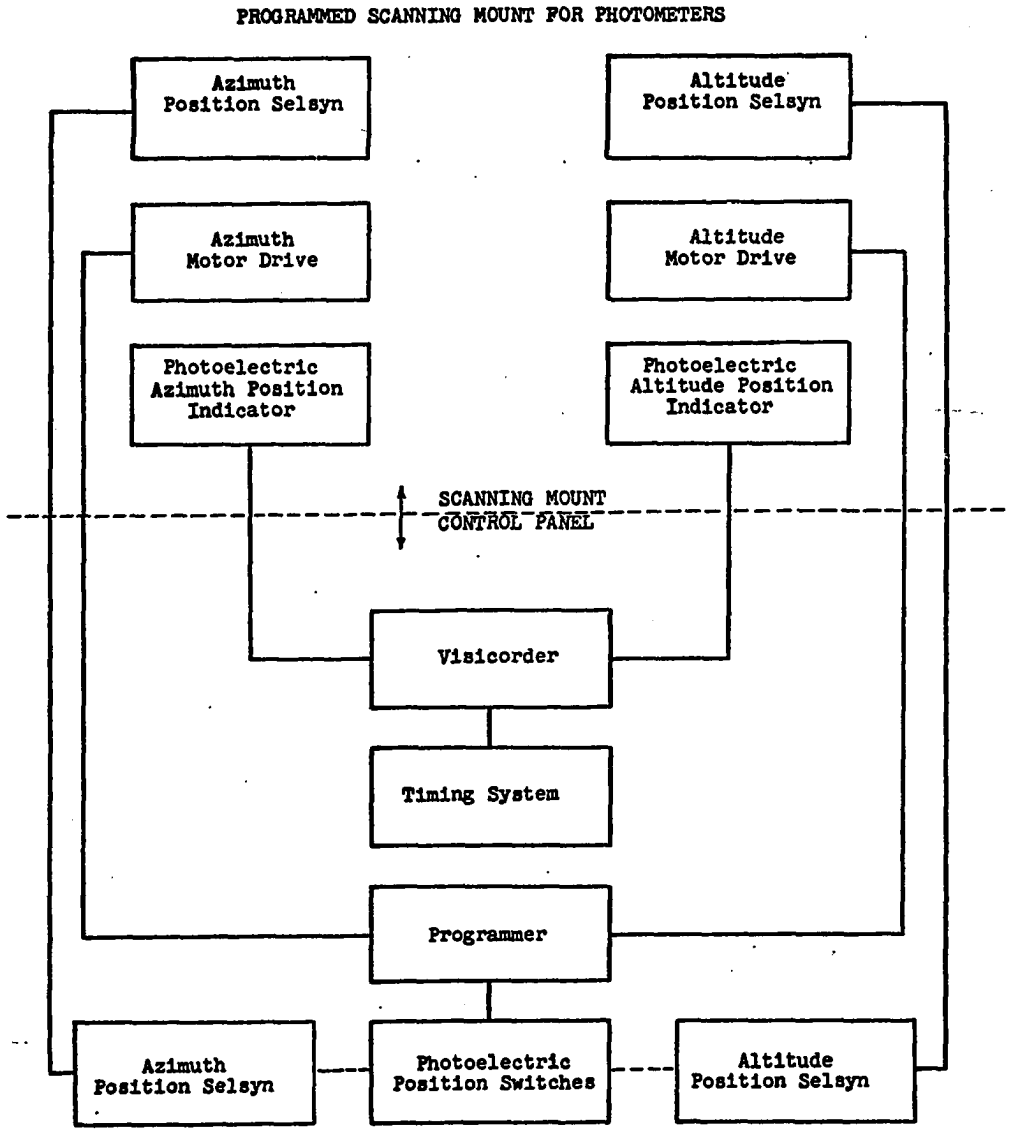

Fig. 2.2 Block diagram of scanning photometer mount and related controls.

Sweeps were made at 0, 45, 65 and 75 degrees zenith angle. The system was programmed to change filters at the completion of each survey. The filter change signal also advanced the signal amplifier load resistance, filter indicator, phase control and feedback control to values set for the corresponding prefilter. The sweeps were begun in the geographic south, covering 360° in azimuth in 20 seconds.

The purpose of the zenith almucantar (as opposed to a motionless zenith reading), is to give an indication of the amount of signal contamination by sunlight. This is accomplished by making use of the stationary polaroid built in to the photometer. As the photometer turns around its optic axis, polarized sky light reaching the photomultiplier is modulated in proportion to the azimuth of the sweep. The total photomultiplier current is recorded directly on the same chart as the alternating component (phase detected signal). The greatest amount of polarization that one can expect, which occur in the case of resonance scattering of Na, is approximately 7 percent. On the other hand, scattered sunlight is polarized to approximately 60 percent in twilight. In the analysis of the records, the phase detected signal is compared with the total photomultiplier current on the record, and is assumed to be contaminated when it begins to follow the polarization curve of the scattered sunlight either positively or negatively.

CHAPTER III

THE OBSERVATIONS AND DATA HANDLING

3.1 Observational Program

The observational program consisted of a series of all-sky almucantar surveys taken between civil and astronomical twilights. A survey consists of almucantar sweeps at each of 3 or 4 zenith angles, typically 0, 45, and 65 degrees. Each survey requires 1 minute for its completion, so the sequence covering the five wavelength regions and the one shutter position is completed in approximately 6 minutes. The data are recorded at a chart speed of 5 inches/minute.

Any one of the almucantar sweeps intercepts the sun's rays in the upper atmosphere in a range of altitudes determined by the solar depression angle and the zenith angle of the photometer. Figure 3.1 shows an example of the range of heights over which the field of view of the photometer intercepts the edge of the earth's shadow as a function of azimuth for a single solar depression angle(see also Fig. 5.1, p.70).

Thus, the family of curves generated by the change in the solar depression angle includes all altitudes of interest over a circle bounded by the largest zenith angle of observation and the lowest altitude of interest. In the case of sodium emission, which originates near 90 km, the intensity in a circle of radius 250 km is monitored by an almucantar survey with sweeps at 0, 45, 65, and 80 degrees zenith angle. If the program were extended to include a sweep nearer the horizon, emission intensities from the 100 km altitude region could be

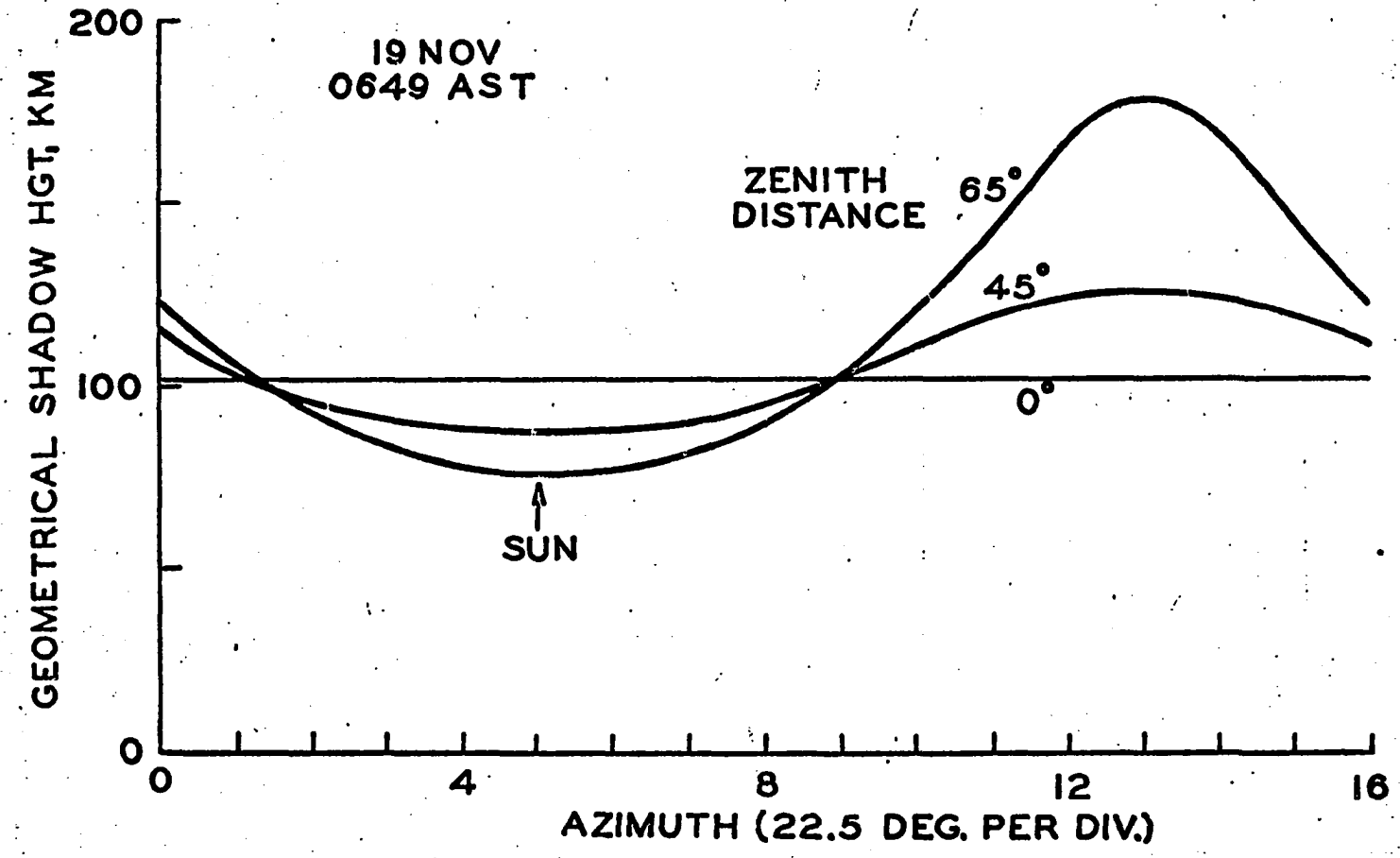

Fig. 3.1 A graph of the altitude of the intersection of the instrumental field of view with the edge of the earth's shadow versus the azimuth of the observation. Three almucantar sweeps are shown, for the observer's solar depression angle of 10 degrees.

monitored over an area of more than 20,000 km^2. If the emitting layer has a uniform geographic distribution, the ordinary twilight observation is greatly extended, because a number of height-luminosity profiles can be made. Again in the case of Na, the zenith measurement program lasts roughly 20 minutes due to the duration of the twilight at the zenith, the survey program enables four or more profiles to be taken over an extended period of up to two hours, in different parts of the sky. Because of the twilight emitting layers show some evidence of non-uniformity, the program suggested here should provide a basis for determining the degree of inhomogeneity. In the case of the red oxygen emission, however, the non-uniformity is not only horizontal in extent, but the emission altitude changes in height, depending upon the variation in solar illumination during the twilight period. Thus, the range of altitudes available in a single sweep allows one to study the changing characteristics of the emitting layer. The all-sky survey program can provide basic information regarding the morphology of the emitting layers during twilight which is not possible to obtain from measurements made in a single direction.

The increase in the amount of information from a single twilight is acquired at the cost of increased complexity in data reduction. In fact, the program is not readily feasible without the use of automatic scaling, computing, and plotting machines. An almucantar twilight program at zenith angles 0, 45, and 65 degrees yields roughly 700 data points for each of five emissions. Extinction and scattering corrections are made for each intensity reading; the result is plotted versus the

computed geometric shadow height at the intersection of the field of view and the shadow for that particular azimuth and zenith angle. Plots of three emission lines in one twilight would ordinarily take approximately two man-months if manual methods were employed. The computer program, as it is set up, completes the same data reduction in approximately three hours of IBM 1620 computer time.

3.2 Conversion of Chart Deflection to Absolute Intensity

The calibration factor (Rayleighs/mm chart deflection, Q(L)) was obtained from an intercalibration with a calibrated interference filter photometer. As stated in section 2.1, the intercalibration was performed during a 4 kilorayleigh aurora in order to overcome any contribution due to background sky emissions in the data from the interference filter photometer. The calibration by this method agreed very well with intercalibrations made with three separate groups of experimenters during the 20 July 1963 solar eclipse (Deehr and Rees, 1964); the installation of the photometer in a B-17 aircraft for the eclipse experiment may have affected the calibration somewhat, however. The intensities observed as a part of the twilight program were all very low and the downward extrapolation from the auroral observation may have resulted in errors as large as a factor of two, even though the instrument response was known to be fairly linear. It is this factor of two which is of concern.

Photometric calibrations over the years normally develop a consistent pattern among the instruments at a single observatory. A comparison of the birefringent filter photometer with the meridian

scanning photometer at a number of intensities showed that at the lower intensities, the latter photometer required an abnormally large correction for background continuum. The birefringent calibration, on the other hand, seemed to be somewhat low when compared with plates from two different spectrographs in operation at the observatory. For instance, the Huet f/0.75 prism spectrograph did not record the 6300A line above the OH background which was just detectable during the night of 21 January 1964. The birefringent photometer measured 5R for the same period. On the night of 19 November 1963, the spectrograph recorded 6300A, but not 6364A. The birefringent value for this time was 10R. Theoretically, the intensity ratio of 6300A to 6364A is 3. The resolution of the spectrograph in the 6300A region is 25A; the background OH emission is about 30R, which is easily recorded. The threshold is thus about 15R for a one-hour exposure time. On 19 November 1963, when 6364A was not observed, it was less than 15R and 6300A must have been about 20R. The birefringent values were doubled therefore, to meet the spectrograph line emission values. After a similar argument, the scanning photometer readings had to be halved in order to compare with the spectrograph background intensities. This procedure resulted in a consistent agreement with the other spectrographs at the observatory. The final corrections then tested favorably in a comparison between the birefringent and the meridian scanning photometer over a large range of intensities concurrently observed on 4/5 January 1965. It is thought that the absolute intensities quoted in this study are accurate to within ± 50%.

The emission intensity data for 18 twilights have been scaled on an 'Oscar' scaling machine and analyzed with the aid of an IBM 1620 computer. Uncorrected intensity data input consists of punched cards from the 'Oscar'. Each card is identified by date, time, and coded wavelength, zenith angle and load resistor. Sixteen data points were scaled from each almucantar, spaced at 22.5°, beginning with the south point on clockwise sweeps and ending with the south point on counter clockwise sweeps. Each card has one data point, so sixteen cards are required for each sweep. For zenith observations, a single data point and a single card is used. Since consecutive sweeps were in opposite directions, an indicator was entered on baseline cards to enable the computer to determine the direction from the wavelength and zenith angle. The computer program accommodates a 3 decade range of instrument gain. The gain is inversely proportional to the load resistor which is recorded with values from 001 to 999. The baseline, obtained from the record with the shutter in position, remains constant for many observations, and is entered on a separate card preceding the data cards to which it applies.

3.3 Corrections for Extinction and Scattering

The uncorrected intensity values read off the strip chart onto the cards were first corrected by subtracting the baseline, applying the calibration factor ($Q(\lambda)$), and the gain of the instrument. Typical deflections were from 1 to 5 cm. The least count of the 'Oscar' is 0.2 mm. The measured intensity, I_{obs} must then be corrected for extinction by absorption and scattering in the lower atmosphere and

for the scattering into the field of view of light from other parts of the same emission layer.

The first correction, that of extinction by the lower atmosphere, is made by multiplying the data by $e^{\tau m}$ where m is the number of air masses traversed and τ is the coefficient of extinction per unit air mass which includes ozone absorption and Rayleigh scattering. τ' is the coefficient of Rayleigh scattering alone. The values for τ and τ' used in this study were taken from Tables 16-15, 16-16C, 16-18 and 16-19 of the Handbook of Geophysics (1960).

The correction for light of the same wavelength scattered into the field from other parts of the emitting layer is not so easily made, but the correction is small and an approximation to it is probably adequate. The problem has been treated for a point source by Chandrasekar (1950) and for a uniform source covering the entire sky (Barbier and Pettit, 1952). Neither of these methods applied in the twilight situation, so an approximation used by Megill (1960) is adapted here. An average of the 16 points of each almucantar sweep is used as representative of the sky intensity contributing to the scattered light component of the observed intensity. The development of the correction for the uncorrected data follows in some detail.

If I_i is the observed slant intensity at a zenith angle and azimuth angle (ζ,ϕ) then

$$I_i \frac{\exp[\tau m(\zeta)]}{V(\zeta)} \qquad (3.1)$$

is the slant intensity at (ζ,ϕ_i) outside the atmosphere, corrected to the zenith using the Van Rhijn function, V.

$$V = [1 - (\frac{R}{R+h})^2 \sin^2 \zeta]^{-1/2} \tag{3.2}$$

where R = radius of the earth, and h is taken as 250 km.

This zenith intensity inside the atmosphere is then

$$I_{ti} = I_i \frac{\exp[\tau m(\zeta)]}{V(\zeta)} \exp[-\tau m(0)]. \tag{3.3}$$

I_{ti} is the source function for the scattering correction. The observed intensity at (ζ,ϕ_i) due to scattering of I_{ti} is given by

$$I_{si} = I_{ti} (1 - \exp [-\tau' m(\zeta)]) = I_{ti} Sc(\zeta) \tag{3.4}$$

where $Sc(\zeta) = (1-\exp[-\tau' m(\zeta)])$ and τ' is the coefficient of Rayleigh scattering alone. When the scattered component is subtracted from I_i, and the result is similarly corrected to outside the atmosphere and referred to the zenith, one obtains the relation:

$$I_{pi} = [I_i - I_{si}] \frac{\exp[\tau\ m(\zeta)]}{V(\zeta)} \tag{3.5}$$

or

$$I_{pi} = I_i \left[1 - \frac{\exp[\tau m(\zeta)]}{V(\zeta)} \exp[-\tau m(0)]\ Sc(\zeta)\right] \frac{\exp[\tau m(\zeta)]}{V(\zeta)} \tag{3.6}$$

as the actual intensity of a thin, uniform layer outside the atmosphere at (ζ,ϕ_i), corrected for extinction and scattering and referred to the zenith. When I_{pi} is brought inside the atmosphere, the correction for

scattering and extinction is given by the factor

$$A = \exp[-\tau m(0)]\ (1 + Sc(0)) \tag{3.7}$$

The average intensity of the sky is then

$$\frac{1}{n} \sum_{i=1}^{n} AI_{pi} = I_{avg.} \tag{3.8}$$

where each value of i corresponds to a reading in azimuth on a single sweep. $I_{avg.}$ is then used to correct the observed reading for scattering from other parts of the sky. The final steps are to correct the slant intensities to outside the atmosphere and to the zenith. Then the corrected intensity I_{ci} is given by

$$I_{ci} = [I_i - Sc(\zeta)\ I_{avg.}] \frac{\exp[\tau m(\zeta)]}{V(\zeta)} \tag{3.9}$$

For computation this equation becomes

$$I_{ci} = C(\lambda,\zeta) \left[I_i - B(\lambda,\zeta) \sum_{i=1}^{16} I_i \right] \tag{3.10}$$

Where

$$C(\lambda,\zeta) = \frac{\exp[\tau(\lambda)\ m\ (\zeta)]}{V(\zeta)} \tag{3.11}$$

and

$$B(\lambda,\zeta) = Sc(\zeta)\ \frac{A}{16} \left[1 - \frac{\exp[\tau(\lambda)m(\zeta)]}{V(\zeta)} \exp[-\tau(\lambda)m(0)]\ Sc(\zeta) \right] \frac{\exp[\tau(\lambda)m(\zeta)]}{V(\zeta)} \tag{3.12}$$

The two coefficients, $B(\lambda,\zeta)$ and $C(\lambda,\zeta)$, are required for these corrections. Table 3.1 lists their values for the five wavelengths (λ) and six zenith angles (ζ) included in the observing program. For use in the data reduction program, $10B(\lambda,\zeta)$ is read into the computer, rather than $B(\lambda,\zeta)$. Note that this is an approximate correction involving assumptions as to the morphology of the emitting layer. In the case of sodium, the intensity is so great in a narrow region near the sun that the scattering correction, formulated from the average intensity, seems to subtract too much from the lower readings over much of the azimuth sweep. The program was changed so as not to include the four points near the sun in the averaging process.

3.4 Shadow Height Program and Data Display

I am indebted to M. H. Rees for providing a computer program which was prepared by L. R. Megill for calculating shadow heights using the iterative method described by Chamberlain (eqs. 10.1, 10.2, 10.3, 10.4, (1961) pp. 395-396). This program was modified and incorporated into the data analysis program, so that a single pass through the computer yielded output cards with corrected intensity and shadow height. A major modification to the above program was made by substituting a closed solution (eqs. 10.5, 10.6, 10.7, Chamberlain, (1961) p. 396) for the iteration. For large zenith angles this reduced the time required for the computer to make the calculation, an important consideration when the rather slow IBM 1620 was used.

The output cards list for each observation the identification from the input card, the original observation corrected for baseline, the

TABLE 3.1

$B(\lambda,\zeta)$ *

	λ	5577 1	5893 2	6300 3	6708 4	5200 5
NZA	ζ					
0°	1	0.005176	0.004175	0.003216	0.002502	0.006738
45°	2	.005372	.004326	.003327	.002571	.006994
65°	3	.005978	.004810	.003655	.002784	.007760
75°	4	.007163	.005759	.004322	.003206	.009251
80°	5	.009002	.007251	.005371	.003893	.011510
50°	6	.005448	.004385	.003362	.002596	.007088

*These values are multiplied by 10 before reading into the computer.

$C(\lambda,\zeta)$

λ	1	2	3	4	5
ζ					
1	1.1211	1.1073	1.0836	1.0553	1.1381
2	0.8434	0.8286	0.8039	0.7746	0.8615
3	0.5908	0.5735	0.5452	0.5125	0.6124
4	0.4767	0.4541	0.4186	0.3792	0.5060
5	0.5489	0.4268	0.3792	0.3291	0.5023
6	0.7839	0.7688	0.7436	0.7138	0.8025

azimuth of the observation and of the sun, the final corrected intensity, and the geometric twilight height in km. The azimuths are measured clockwise from the north (N-E-S-W) in units of 22.5°. The IBM 1620 computer is then programmed to plot data using the IBM 1627 plotter showing 1 or 2 decades of intensity and 400 km of shadow height on a plot 10 inches high and 20 inches long. Figure 3.2 shows tracings of two of these plots, using only one symbol for all points, regardless of direction or time.

While it is of interest to note the general trend of the emission as the earth's shadow moves through the sky, the separation of distinct patterns is necessary in order to determine the excitation process. Therefore, each direction of observation, with respect to the sun, was assigned a certain symbol according to the pattern indicated in Figure 3.1. This procedure established an adequate spatial resolution on the plots. An adequate temporal resolution was achieved by simply leaving the plotter pen on the paper between the symbols of a single scan. Thus, the spatial temporal relationship with the change of solar radiation can establish the change of emission height and position during the twilight period. This relationship can be interpreted directly from the computer plot with some practice and reference to supplementary information, such as spectrograms and the usual geophysical indices. An example of this computer plot is given in Figure 3.3.

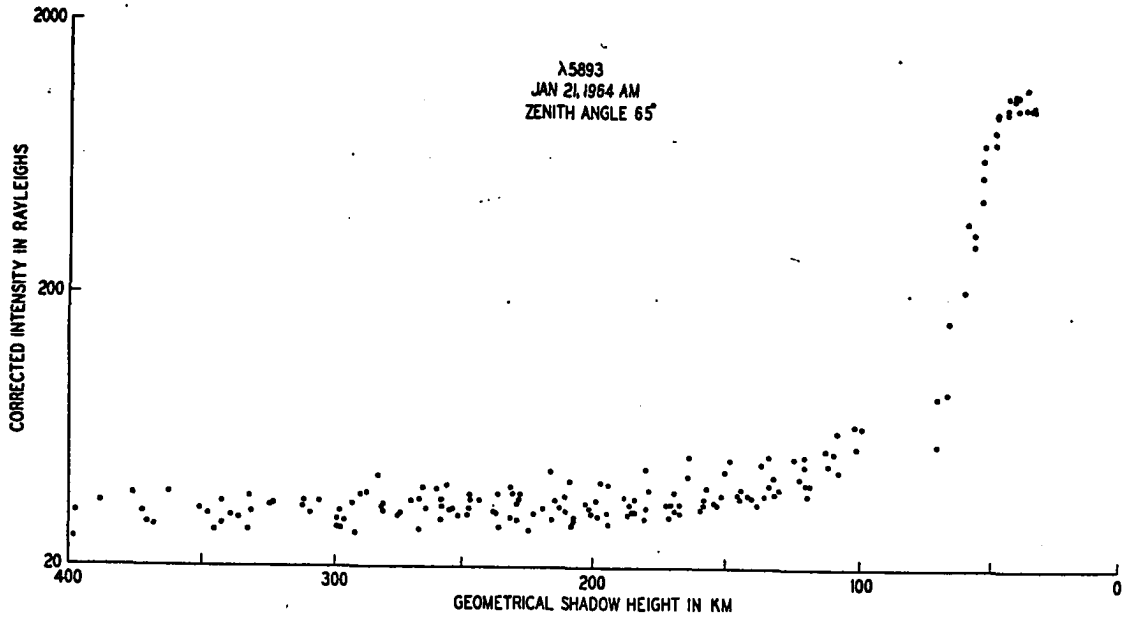

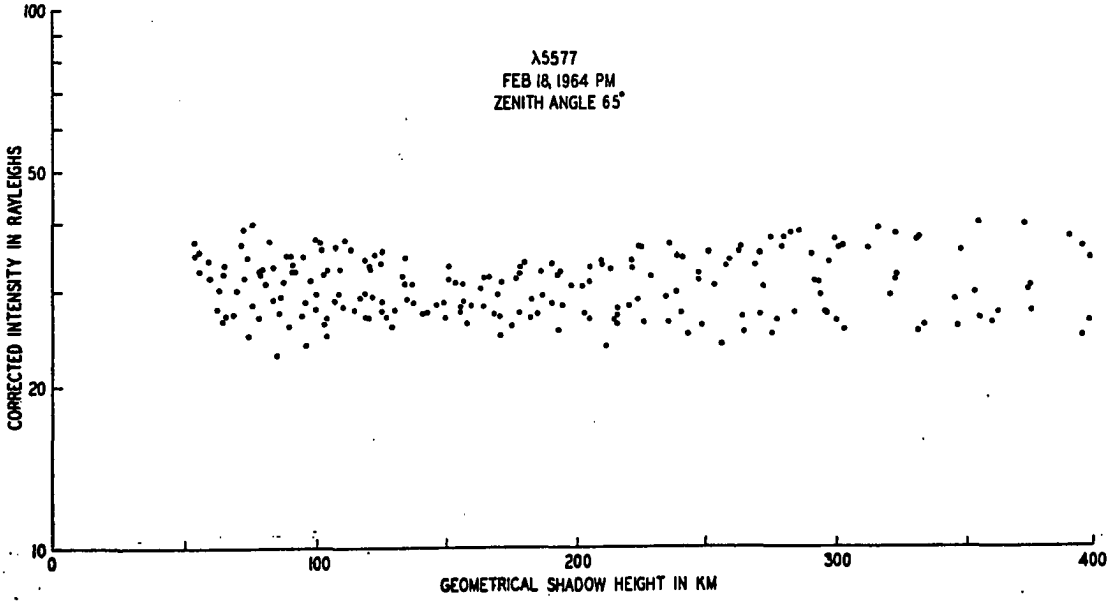

Fig. 3.2 Logarithmic plots of corrected intensity versus geometric shadow height.

Fig. 3.3 Local zenith intensities of 6300 A from azimuth sweeps as a function of geometric shadow height. The symbols denote the azimuth angle of each observation, every 22½° measured from the sun (S is the sun; ■, toward the sun; ϕ, +, toward the south; Δ, Y, toward the north; Z, away from the sun). The symbols comprising a single azimuth sweep are joined by a line. The zenith angle for all the sweeps on this graph was 65°. The data are from the morning twilight of 21 January 1964 at College, Alaska.

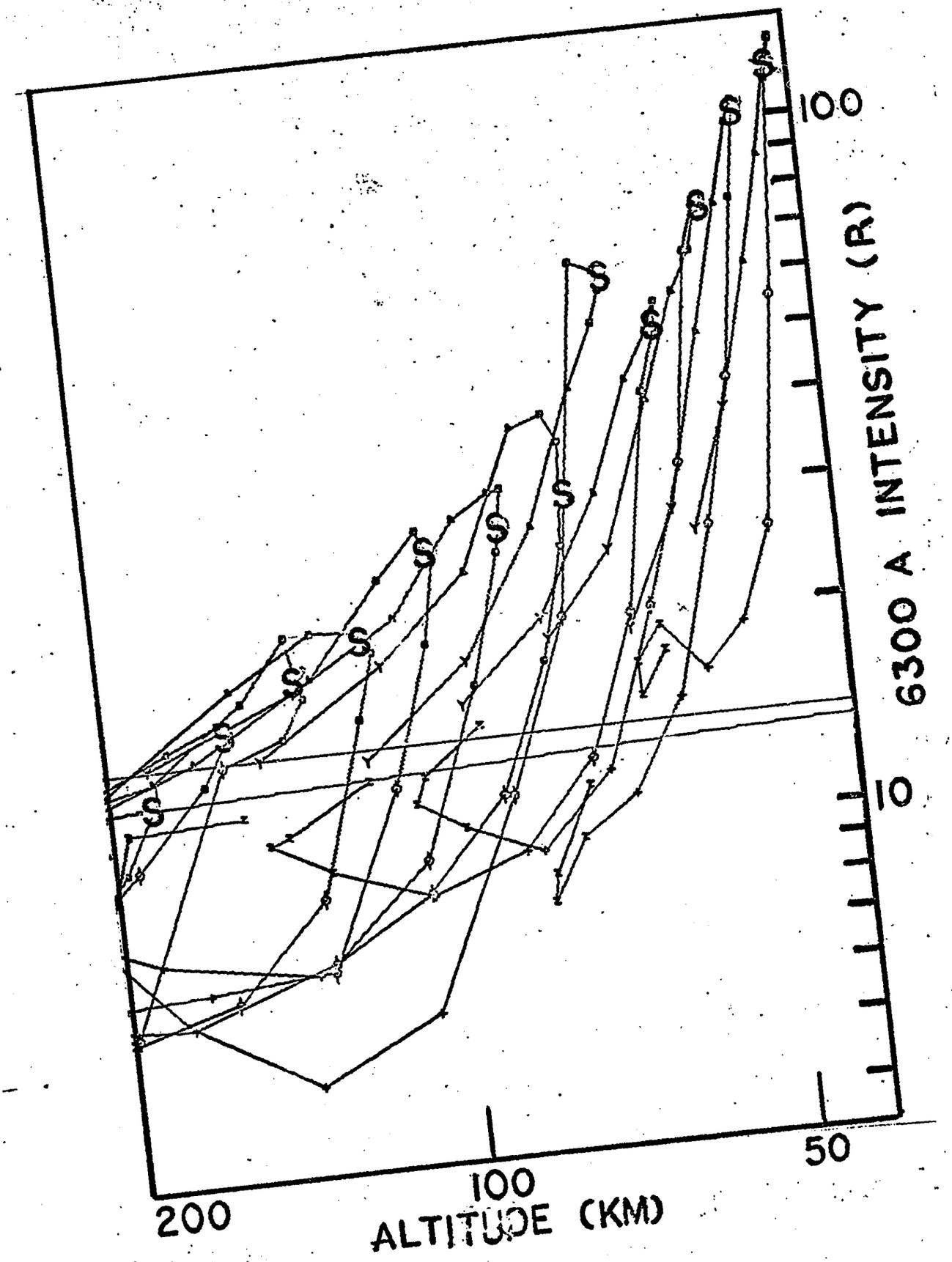

CHAPTER IV

THE PREDAWN ENHANCEMENT OF 6300 A [OI]

4.1 Introduction

An enhancement of the oxygen red line was noted by Elvey and Farnsworth (1942) to occur before the solar rays were low enough to excite a sufficient number of oxygen atoms to produce the observed intensity by any known process. The effect, which differed from the evening enhancement in magnitude and rate of change, was called the predawn enhancement and was observed to originate to the north of France by Dufay and Tcheng Mao-Lin (1946).

Barbier (1960) employed an azimuth-scanning photometer at 75°ZA (zenith angle) to observe the morphology of the predawn enhancement and to separate it from the true twilight effect. He found that the onset of the predawn enhancement at Haute Provence was long before twilight in winter, just before twilight at the equinoxes and continued with the twilight at the summer solstice. He interpreted it as a "sheet" of luminosity which advanced in the sky in a direction approximately 10° west of south in December. The 6300 A intensity of the sheet varied with the solar cycle. The average intensity over the cycle was about the same as that of the "western sheet" but the amplitude of the variation was less.

Cole (1965) drew a great deal of attention to Barbier's (1961) survey of the 6300 A airglow by proposing that this "subpolar sheet" was the airglow manifestation of the deposition of photoelectrons from

the conjugate hemisphere. Carlson (1967) has since shown that this effect is well correlated at Arecibo with the pre-sunrise electron temperature increase. This increase seemed to coincide with the sunrise in the magnetically conjugate ionosphere.

The possibility that electrons, released from atmospheric constituents by direct solar radiation, may escape from the ionosphere along lines of constant geomagnetic force was suggested on theoretical grounds by Hanson (1963). Roughly two-thirds of the solar EUV (1 to 1000 A wavelength) energy absorbed by the atmosphere is used in the process of ionization and the remaining one third is transferred to the ejected electrons (photoelectrons) as kinetic energy. It was thought that there would be little attenuation in the magnetosphere and the photoelectrons would be able to deposit an appreciable fraction of their energy in the conjugate ionosphere. This energy should then be transferred to local electrons and neutrals, creating a measurable increase in the electron temperature and raising oxygen atoms to the ^1D state. The electron temperature is not of concern in this study, because it does not exceed 1000°K (Carlson, 1967) during sunspot minimum and therefore would not be of importance to the production of [OI] (^1D) (Chamberlain, 1961, p. 533).

The morphology of the pre-dawn enhancement has not been described previously on a world-wide basis, and the published data of Barbier (1959, 1961) have not been fully developed; therefore a relatively

large amount of space will be devoted here, and in Chapter 5, to a new interpretation of his observations at Haute Provence. First, the relationship of the advancing airglow "sheet" to the solar radiation in the conjugate region will be established. Second, the change of the observed 6300 A emission with solar activity will be explained in terms of known changes in the atmosphere. Third, the resulting description of the 6300 A airglow emission produced by conjugate photoelectrons will be used to construct a world-wide map of photoelectron precipitation which will be applied, in particular, to the data taken from College. This precipitation will be shown to be negligible under quiet magnetic conditions poleward of L = 5, ("L" refers to the distance in earth radii in the equatorial plane from the center of the earth to a particular "shell", or envelope, defined by lines of constant geomagnetic force).

4.2 Morphology of Predawn Enhancement

The dynamic relationship of conjugate photoelectron precipitation to an observer anywhere in the world is not known because the precipitation pattern has not been completely described. The description of that relationship should be consistent with existing observations and

should enable the prediction of time and direction of onset and recession. It is useful to develop a model giving the morphology of the conjugate photoelectron precipitation for use with the data aquired at College. Such a model can aid in detecting the effects of precipitation of photoelectrons arising in the conjugate area and be useful for correlation of expected precipitation with other geophysical phenomena. The model can also be helpful in the organization of observing programs and the selection of observing sites.

The 6300 A airglow data of Barbier furnish the best measurements for determining the relationship of the advance of the predawn enhancement with the sunlight line in the southern hemisphere. Barbier (1959, Fig. 15, p. 212) plotted the December 1956 intensity of 6300 A emission at 75°ZA as a function of time for several azimuths. A singular point on the curve for each azimuth is the point at which the slope (dI/dt) is a maximum. Because we do not know the vertical profile of the emitting layer, this point affords the most accurate determination of the relative position of the layer as it advances across the Haute Provence observatory. The time at which this point occurred at each azimuth was scaled from Barbier's (1959) Fig. 15 and its position was plotted on a map, Fig. 4.1, assuming an emitting layer height of 300 km.

To relate the conjugate sunrise to the advancing layer along the magnetic field lines, a computer program which was developed and kindly lent by S.-I. Akasofu, was employed. This program allows determination of the longitude of the sunrise and sunset lines for each latitude at a

point in Universal Time. The longitude and latitude of the point conjugate to each sunrise and sunset point is calculated using a geomagnetic field line tracing program using the Hendricks and Cain coefficients of a spherical harmonic expansion of the geomagnetic field. The sunrise at 25 km altitude in the south was mapped through this field to the 300 km altitude region in the north for U.T. 00, 01, 02, 03 and 04 hours. These photoelectron onset times were plotted on the map of the advancing airglow layer (Fig. 4.1) and offer highly convincing evidence for the connection of the "subpolar sheet" through the geomagnetic field to the conjugate sunrise.

The time of onset of the photoelectron airglow at any particular observatory must be established next. This time should correspond to a solar depression angle in the conjugate region which is sufficiently small to produce enough photoelectrons so that some may escape to the magnetosphere. Carlson and Weill (1968) showed that the onset time at Haute Provence changed during the solar cycle by approximately fifteen minutes per year. The solar zenith angle (SZA) at the conjugate point corresponding to each onset time can be calculated for the December period of each year. A plot of the conjugate SZA at onset versus the 10.7 cm solar flux averaged over December for the appropriate years is shown in Fig. 4.2. The resulting smooth curve suggested the addition of several other points from the literature (Megill, 1960; Carman and Gibson-Wilde, 1964; Carlson, 1966; Yao, 1962). There are other observations, of course, but the 10.7 cm flux, which was taken from "Solar Geophysical Data" (ITS-ESSA, Boulder), was not always available and the effect not generally obvious at other stations.

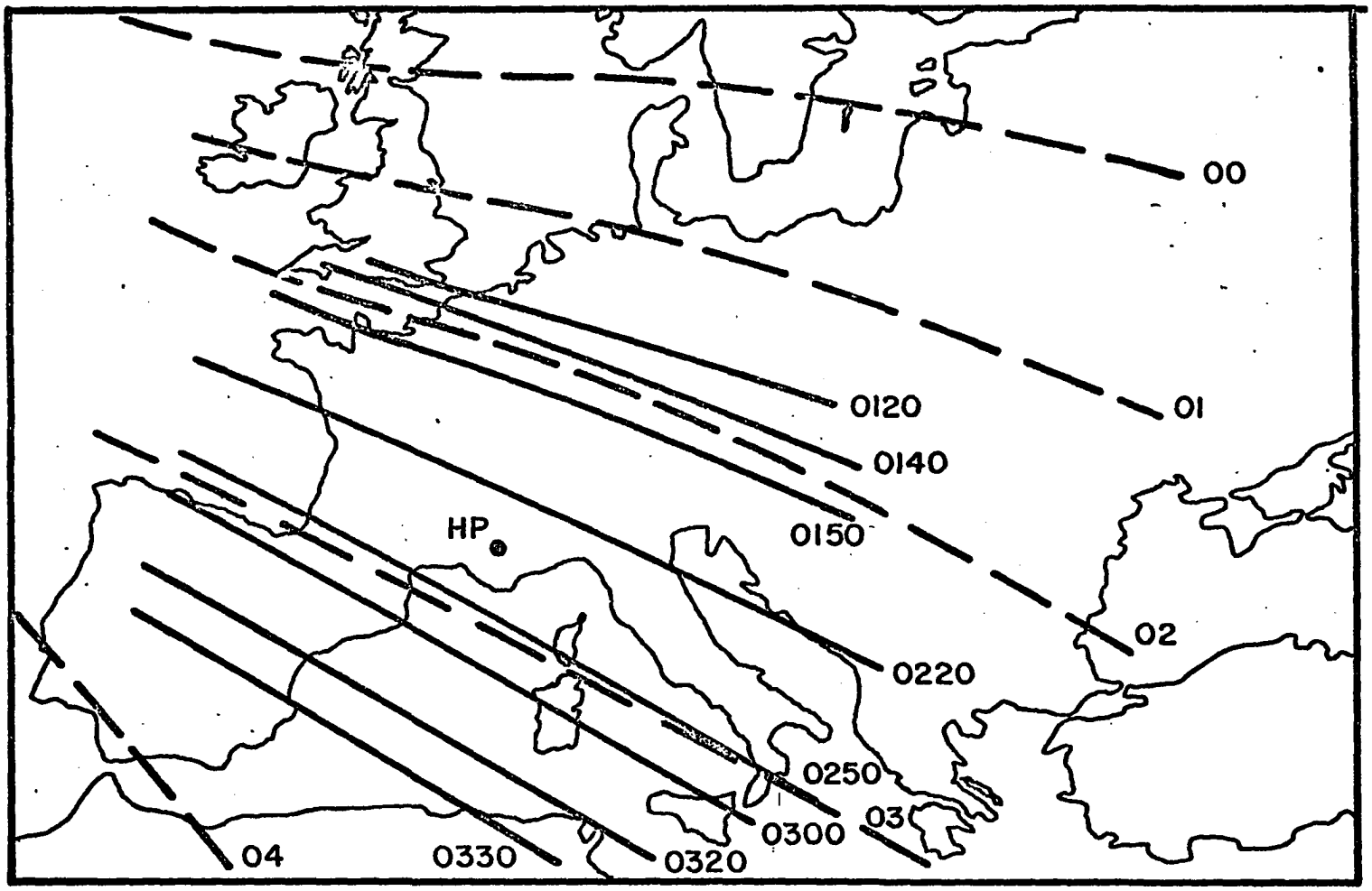

Fig. 4.1 Advance of 6300 A [OI] airglow sheet as seen from Haute Provence in December, 1956 (solid lines). The dashed lines are the sunrise lines at the geomagnetically conjugate points. Times are U.T.

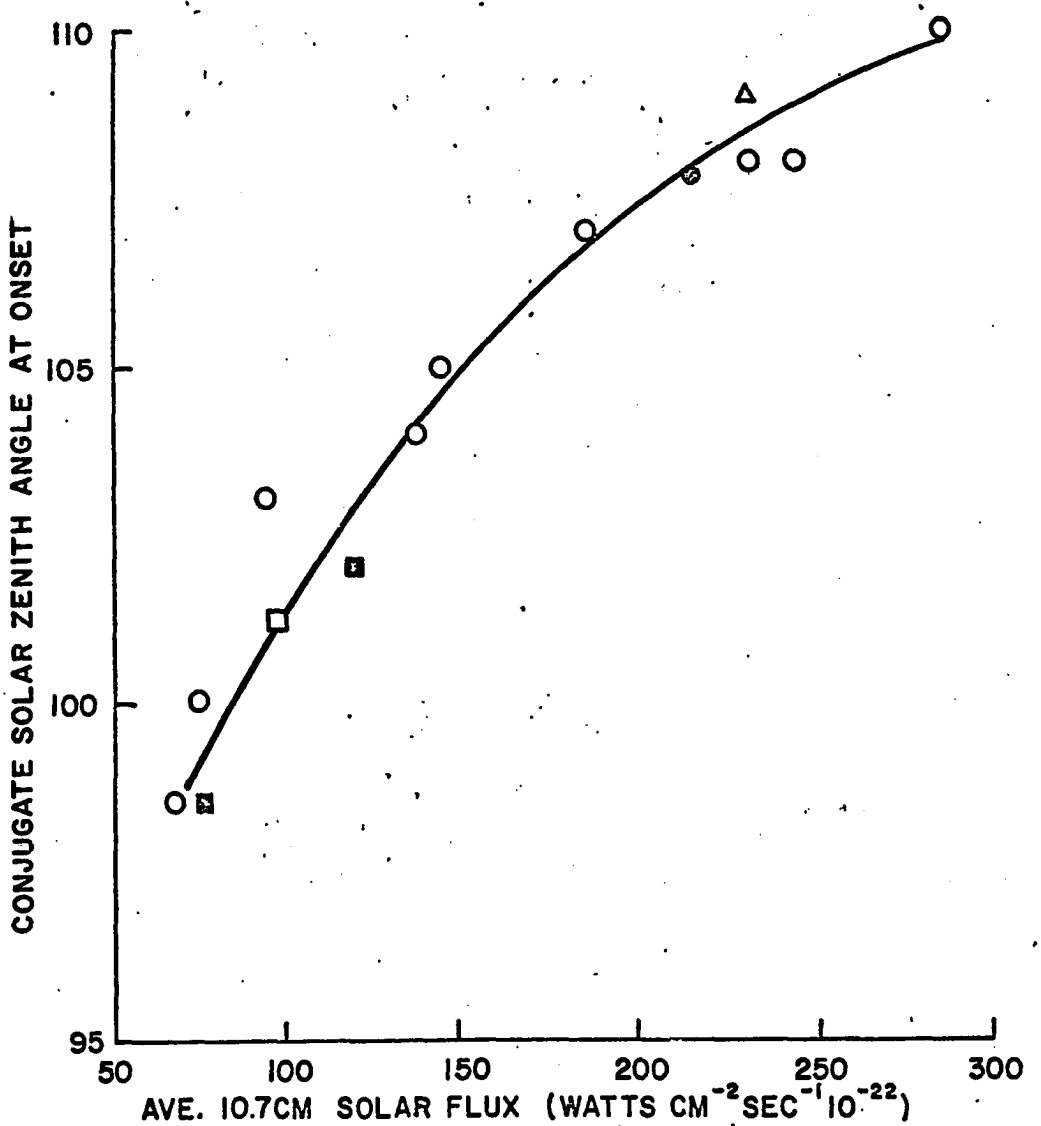

Fig. 4.2 The relationship of the 10.7 cm solar flux (Ottowa) to the conjugate solar zenith angle at the time of photoelectron onset at several stations: ○ Haute Provence, □ Townsville, △ Fritz Peak, ● Camden, and ■ Arecibo.

The final zenith intensity of 6300 A emission (plateau intensity), which is reached when the layer fully enters the instrumental field of view, is not evident from any data except the observations at Haute Provence. Barbier (1961) has tabulated these values for a solar cycle; they are plotted against the 10.7 cm solar flux in Fig. 4.3. This plot also shows a smooth relationship between the 6300 A plateau intensity and the 10.7 cm solar flux.

Two effects combine to prevent the plateau from being reached at other stations. Firstly, the inclination of the field line to the terminator is such that the local twilight occurs before the plateau is reached. Secondly, the time rate of increase at higher latitudes is less, owing to the slower change of solar zenith angle with time. The rate of increase of 6300 A intensity can be seen to be roughly constant over the solar cycle (Barbier, 1959, Fig. 5). The rate is about 6 Rayleighs/degree of solar zenith angle at the conjugate point. This value seems to hold for the other stations also. Thus, while the plateau intensity changes with the solar cycle, the onset time change and the rate of increase remain constant; consequently, the time at which the plateau is reached also remains roughly constant.

It can be shown that the travel time of the photoelectron from the conjugate hemisphere is less than several minutes. The speed of an electron of energy between 5 and 30 ev is from 1 to 3 x 10^8 cm sec^{-1}. This is equivalent to about ten earth radii per minute. In the extreme case of electrons in L-shells larger than 5 or 6, with highly distorted field lines extending quite far into the magnetospheric tail, one

might observe travel times of as much as four minutes. This value is certainly less than the time resolution of the calculations made here and of most airglow photometers.

Considering that nothing is known about the radiation-height profile of the photoelectron-induced 6300 A emission, one should not begin by attempting to predict the 6300 A intensity or of the number of photoelectrons involved. It is obvious that measurement of the volume emission profile by rocket-borne photometers or careful analysis of ground-based data from high resolution instrumentation is necessary. The existing data have not been fully exploited, however, and as has been shown earlier, many of the morphological details can be used in first-order descriptions of the physical processes involved.

Carlson and Weill (1968) explain the change of onset time with solar activity observed at Haute Provence in terms of a change in electron production rate in the conjugate region. Figure 4.4 shows the photoelectron production rate as a function of solar activity for several altitudes. It is apparent that the character of the curve is not the same as that relating the onset time to solar activity; nor is it the same as the change in plateau intensity of 6300 A emission as a function of solar activity plotted in Fig. 4.3. Some physical process must modify the photoelectron production so that curves of 10.7 cm solar flux versus the measures of photoelectron arrival at Haute Provence have a decreasing slope with increasing solar flux (Figs. 4.2 and 4.3) instead of the increasing slope that one would expect from the change in photoelectron production rate (Fig. 4.4).

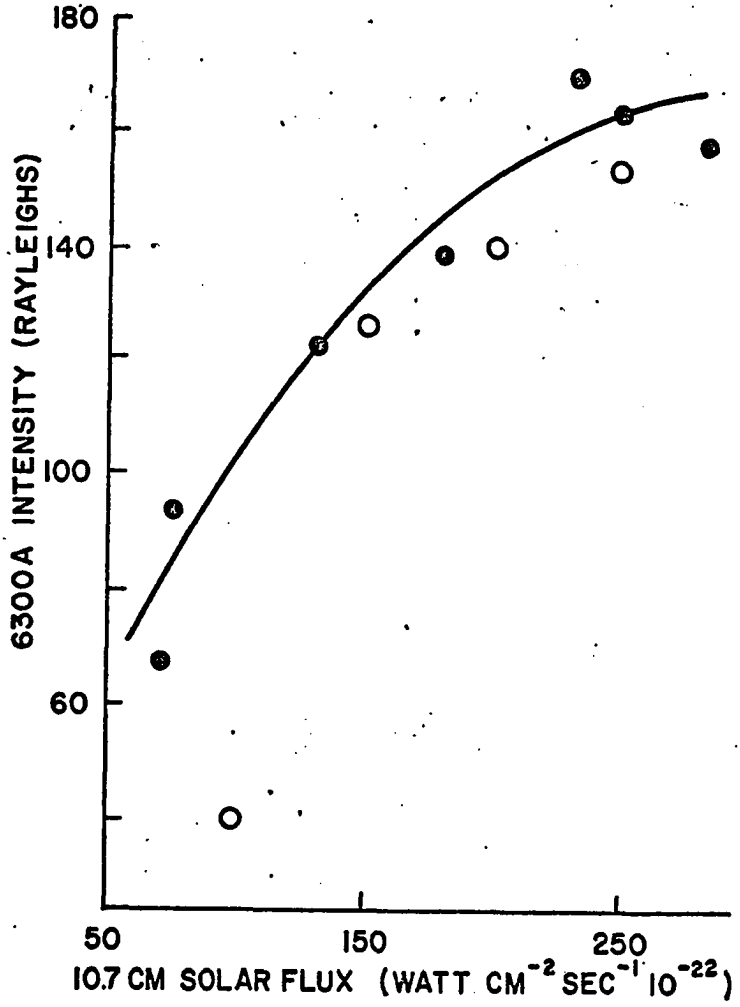

Fig. 4.3 The 6300 A plateau intensity observed towards the celestial pole from Haute Provence (dots) compared with the values calculated in this study (circles) as a function of solar activity.

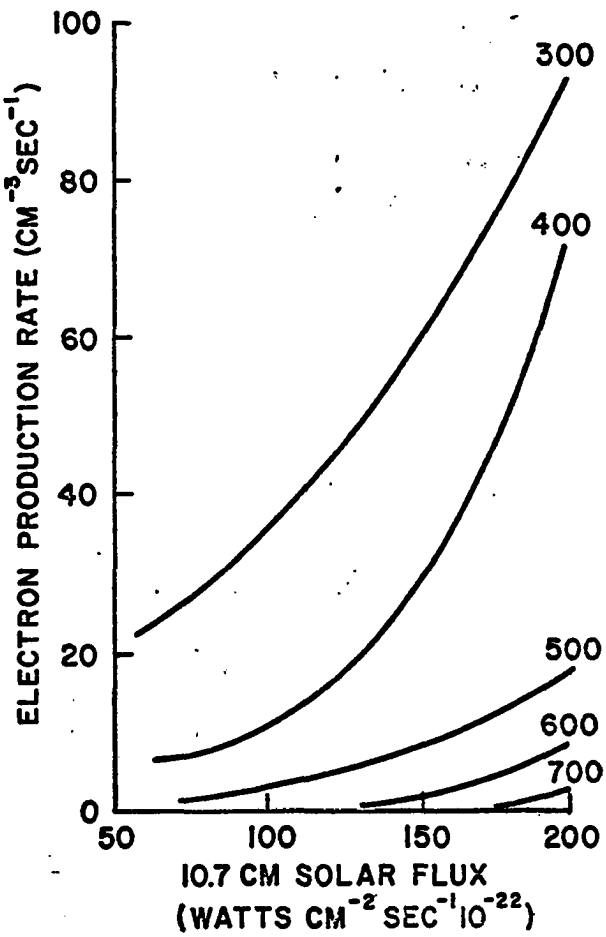

Fig. 4.4 Variation of photoelectron production rate at various altitudes as a function of solar activity near sunrise.

Using the dynamic relationship between the average 10.7 cm solar flux, the exospheric temperature, and the expansion of the atmosphere, the observed 6300 A plateau intensity (Fig. 4.3) can be related to the photoelectron production rate in terms of the differential transparency of the atmosphere to photoelectrons as a function of altitude. In order to do this, one must first consider the change of photoelectron production rate with solar activity as a function of altitude during twilight. Carlson and Weill (1968) have calculated several electron production rate altitude curves at several values of SZA and 10.7 cm flux. Using these curves and Fig. 4.2 above, the electron production rate-altitude profiles have been plotted in Fig. 4.5 for those SZA and solar flux values of interest to this study. The heavy, dashed line follows the maximum value of each photoelectron production rate profile which is sufficient for onset to be observed at Haute Provence at different levels of solar activity.

One must assume that the electron flux required at Haute Provence for onset is the same at all levels of solar activity, and that this flux originates, for the most part, in an altitude region about 100 km thick with a production rate characterized by the maximum value of the profile for the particular value of SZA and 10.7 cm solar flux represented by the heavy, dashed line in Fig. 4.5. Each altitude region along this line represents the onset flux at a different part of the solar cycle. As the solar activity increases, the average solar EUV flux and atmospheric density at high altitude increases also. As a consequence of these changes, the electron flux required for onset at Haute Provence is

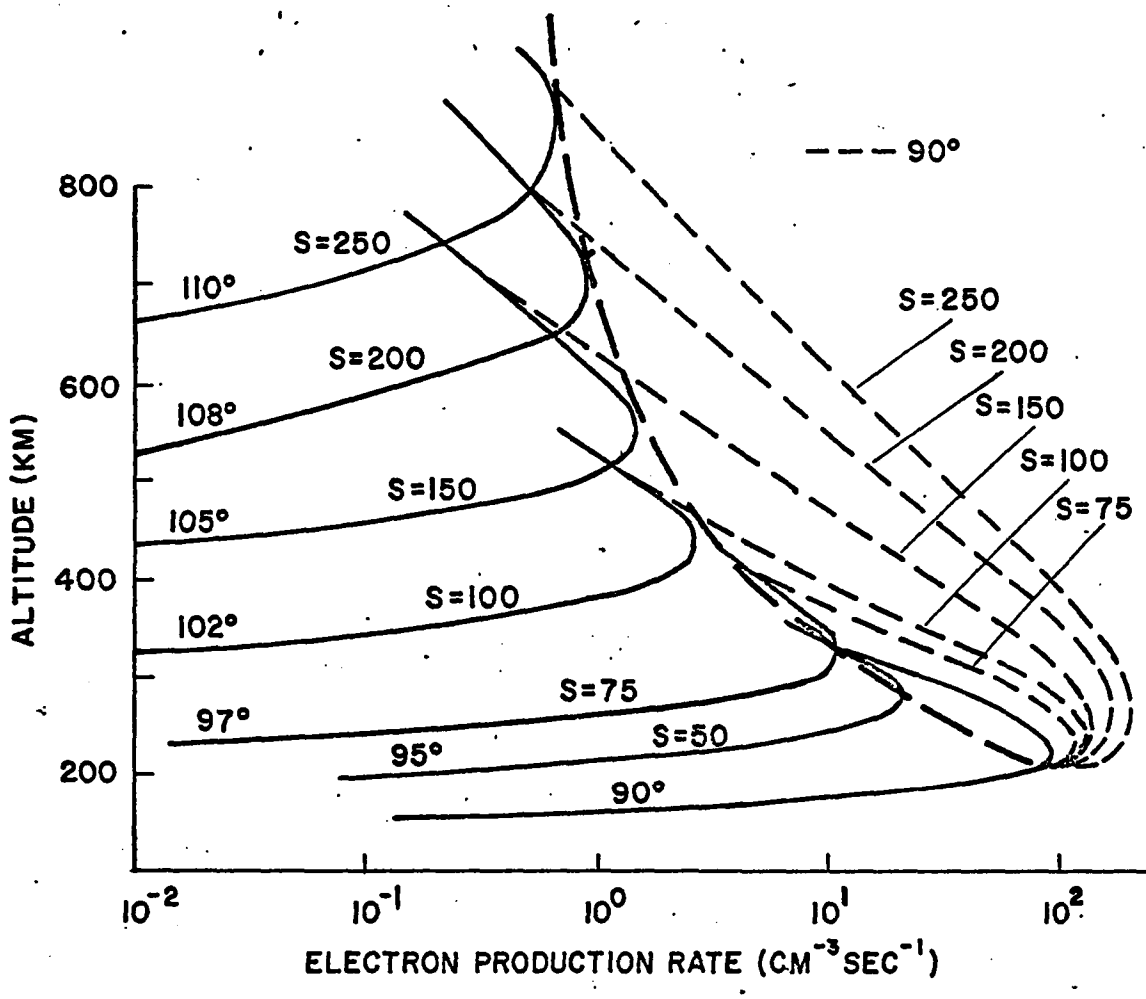

Fig. 4.5 Photoelectron production rate as a function of altitude for several values of solar zenith angle at different values of 10.7 cm solar flux, S. These values of solar zenith angle represent the various onset times for the observation of 6300 A emission at Haute Provence. The heavy dashed line represents the maxima of these curves at onset for differing solar flux and zenith angle. The 90° SZA curves to the right of the dashed line represent the production rate when the plateau intensity of 6300 A emission is observed at Haute Provence.

produced at higher altitudes and greater values of SZA in the conjugate region. The electron flux originating along the dashed line in Fig. 4.5 will be attenuated by collisions with other electrons and neutrals. If it is assumed that the electron flux arriving at Haute Provence is constant for each altitude region along the dashed line, then the change of electron production rate along this line is a measure of the attenuation of the escaping photoelectrons. Carrying this argument a step further, one may use the change in atmospheric pressure with solar cycle at each altitude to determine the total attenuation-height profile at all levels of solar activity.

The electron flux required for onset at Haute Provence is

$$F_e = 10^7 P_{ab} A_{ab} = K \tag{4.1}$$

where the altitude region is taken as 100 km (10^7 cm), P_{ab} is the photoelectron production rate, and A_{ab} is the attenuation factor for altitude region, a, and solar activity level, b. When a=b, P_{ab} corresponds to the values along the heavy dashed line in Fig. 4.5. The attenuation at different levels of solar activity is changed by the varying atmospheric pressure, ρ_{ab}. Thus A_{11} is related to A_{12} in this way:

$$A_{11} \frac{\rho_{11}}{\rho_{12}} = A_{12} \tag{4.2}$$

The definitions of the indices a and b are given in Table 4.1. The values of ρ_{ab} are given as a matrix in Table 4.2. This matrix is normalized to the diagonal in Table 4.3. The attenuation is then

normalized by assuming that there is no attenuation at a=6, b=1 (A_{61} = 1 corresponding to the highest altitude and lowest activity). Table 4.3 shows that the atmospheric pressure at a=6, b=6 is 20 times greater. Thus, A_{66} = 0.05 and the rest of the attenuation factors for a=b are calculated using Eq. (4.1), e.g.:

$$A_{55} = \frac{P_{66}}{P_{55}} A_{66} \tag{4.3}$$

The diagonal values of A_{ab} then operate on the matrix in Table 4.3 to establish their values off the diagonal, i.e.

$$A_{nn}\, \rho_{ni} = A_{ni} \quad \text{for } i=1 \ldots 6$$

TABLE 4.1

Definition of Index Numbers a and b

a	Altitude region	b	CIRA Atmo. number	Representative 10.7 cm solar flux	Exoxpheric Temperature
1	300 km	1	1	60 x 10^{-22} watts cm^{-2} sec^{-1}	705°K
2	400	2	2	75	731
3	500	3	3	100	804
4	600	4	5	150	979
5	700	5	7	200	1159
6	800	6	9	250	1317

TABLE 4.2

Atmospheric Pressure (dynes cm^{-2}) from the hour 04 1965 COSPAR International Reference Atmospheres, listed according to the altitude region and atmospheric gradient indicated by a and b (defined in Table 4.1).

a\b	1	2	3	4	5	6
1	2.0E-5	2.4E-5	3.6E-5	7.6E-5	1.4E-4	2.1E-4
2	2.0E-6	2.5E-6	4.4E-6	1.2E-5	2.7E-5	4.8E-5
3	3.2E-7	4.0E-7	7.4E-7	2.5E-6	6.7E-6	1.3E-5
4	1.0E-7	1.2E-7	2.0E-7	6.6E-7	1.9E-6	4.2E-6
5	5.3E-8	6.0E-8	8.7E-8	2.3E-7	6.5E-7	1.5E-6
6	3.2E-8	3.6E-8	5.0E-8	1.1E-7	2.8E-7	6.0E-7

$3.\overline{2E}\text{-}\overline{8} = 3.2 \times 10^{-8}$

TABLE 4.3

Matrix of Atmospheric Pressure from Table 4.2 normalized to the diagonal

a\b	1	2	3	4	5	6
1	1	1.2	1.8	3.8	7	10
2	0.8	1	1.8	4.8	11	19
3	0.43	0.54	1	3.4	9.1	18
4	0.15	0.18	0.30	1	2.9	6.4
5	0.08	0.09	0.13	0.35	1	2.3
6	0.05	0.06	0.08	0.18	0.5	1

The resulting values of the attenaution factor, relative to $A_{61} = 1$ must be normalized to a region which attenuates 100% of the electrons escaping in a vertical direction. The minimum conditions for onset are probably SZA=95°, S=50 (see Fig. 4.2); the difference of production rate at onset and plateau (SZA=90°) is negligible, according to Fig. 4.5. Thus, one would expect the 100% attenuation of vertically moving electrons to occur at about 280 km for S=75. The 100% attenuation for other values of S is then set according to the relationship of each curve relative to S=75. The plots of percent attenuation versus altitude are shown in Fig. 4.6 for several values of solar flux.

Having determined the electron production rate necessary for 6300 A emission onset at Haute Provence and also the electron attenaution, both as a function of altitude and solar activity, one is now in a position to explain the observed variation of plateau intensity as a function of solar activity. That a "plateau" is reached is easily explained by noting that the electron production rate above 250 km does not appreciably increase once the SZA is less than approximately 90° (Tohmatsu, et al, 1965, Fig. 4) for any given solar activity level. The variation in intensity of the plateau is more difficult to explain, however. It cannot be due to the increase with solar activity of the oxygen atom population at higher altitudes above Haute Provence because this increase would vary as the increase in electron production shown in Fig. 4.4. The latter curve has already been shown to be of the wrong slope to explain the change of 6300 A emission with solar activity. Thus, the variation is not a function of total production rate, but

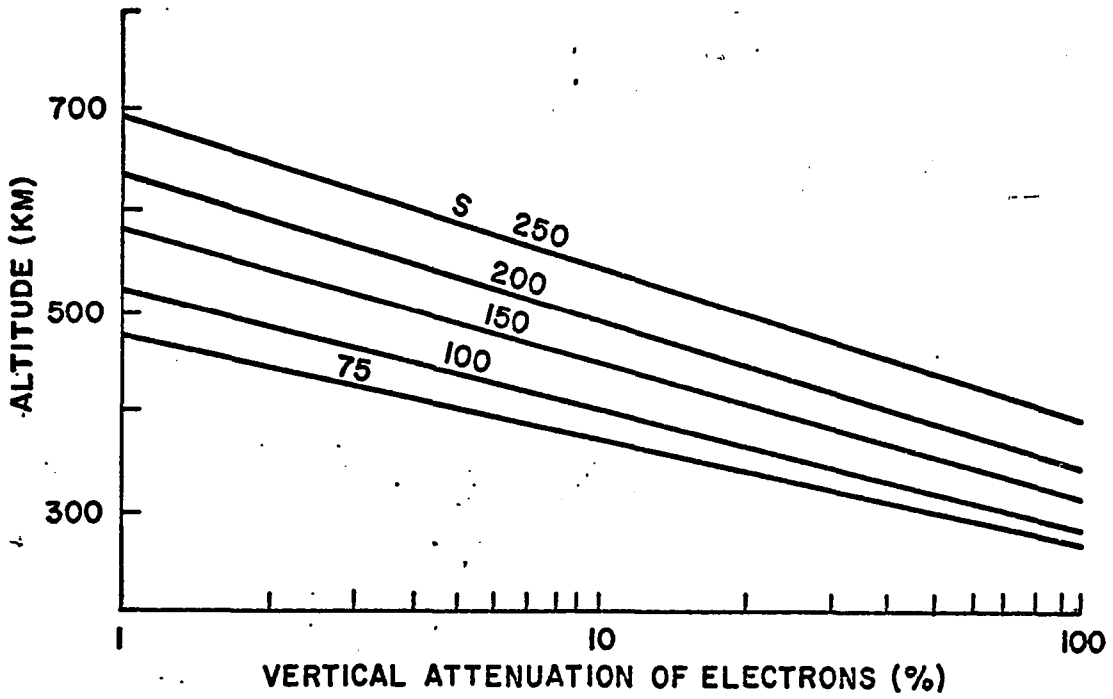

Fig. 4.6 Percent attenuation of electrons in a vertical direction as a function of altitude for several values of the 10.7 cm solar flux, S.

it may be a function of the change in the rate of electron escape from the conjugate ionosphere. This rate may be found by subtracting the electron production rate at onset from the production rate at an SZA of 90° (Fig. 4.5) for several values of solar activity. The rates must be corrected for atmospheric attenuation with values from Fig. 4.7. The difference between the corrected rate corresponds to the change in electron flux between 6300 A onset and the 6300 A plateau intensity. It is thus the effective electron production rate needed to produce the 6300 A emission observed at Haute Provence. Because the attenuation has been calculated on the basis of an observed effect at the opposite end of the field line, the non-radiative losses due to direction and collision are automatically included. In order to find the effective rate of escape, one must multiply the effective production rate in each altitude range by that range in centimeters (10^7) and add it to the contribution from the other ranges. This is done for several values of 10.7 cm solar flux and the result plotted in Fig. 4.7. The character of this curve is very much the same as that of Fig. 4.3. This similarity suggests very strongly that the variation of plateau intensity with solar cycle results from a change of effective electron escape rate in the conjugate region. This change of escape rate is due to the changing attenuation of the upward moving photoelectrons and to variation in the effective production altitude.

As was stated in section 4.1, the heating of local electrons by the incoming photoelectrons does not appreciably contribute to the red line intensity under normal conditions. The incoming particles

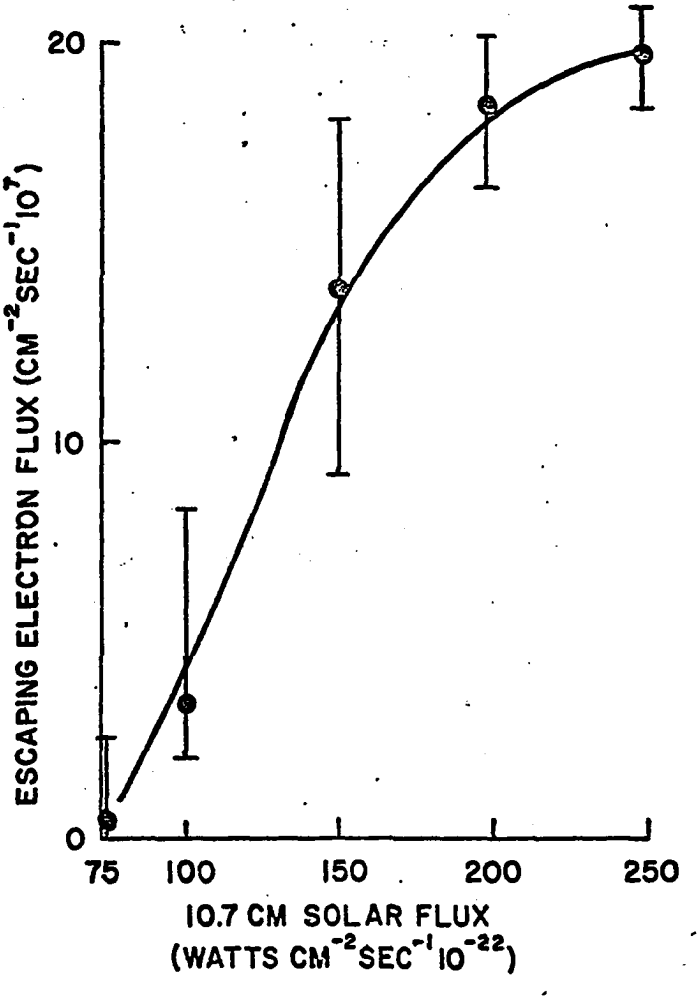

Fig. 4.7 Flux of photoelectrons from the conjugate ionosphere as a function of solar activity near sunrise.

have sufficient energy to excite the red line by inelastic collisions with oxygen atoms. Quenching can be neglected because the emitting altitudes are all above 300 km. Following Chamberlain (1961), the reactions per unit volume are given by

$$F_{21} = N(O)\ N_e\ S_{12} \qquad (4.4)$$

for two-body collisions. $N(O)$ and N_e are the atomic oxygen and electron densities, respectively. S_{12} is the rate coefficient for emission. The average electron energy is approximately 20 ev, corresponding to an average velocity, $\bar{v}$, of approximately 3×10^8 cm sec^{-1}. If the collision cross section, $Q_{12}(v)$ does not vary much over this range, then

$$S_{12}\ Q_{12}(\bar{v})\ \bar{v} = 6 \times 10^{-9}\ cm^3\ sec^{-1} \qquad (4.5)$$

Here, $3/4\ F_{21}$ is used to allow for branching into the 6364 A line.

Assuming that the photoelectrons escaping from the sunlit region arrive above Haute Provence and are absorbed by the atmosphere according to the attenuation factors calculated from their release, the volume emission rate-height profile can be computed. The COSPAR 1965 Model Atmospheres are used. The 04 hour models corresponding to four values of 10.7 cm solar flux result in the four volume emission rate-height profiles shown in Fig. 4.8. The zenith intensity corresponding to the respective curves is plotted in Fig. 4.3. These calculated values nearly match the observed values plotted in the same figure.

In order to assess the value and the accuracy of this calculation, the assumptions and procedures involved in the calculation can be

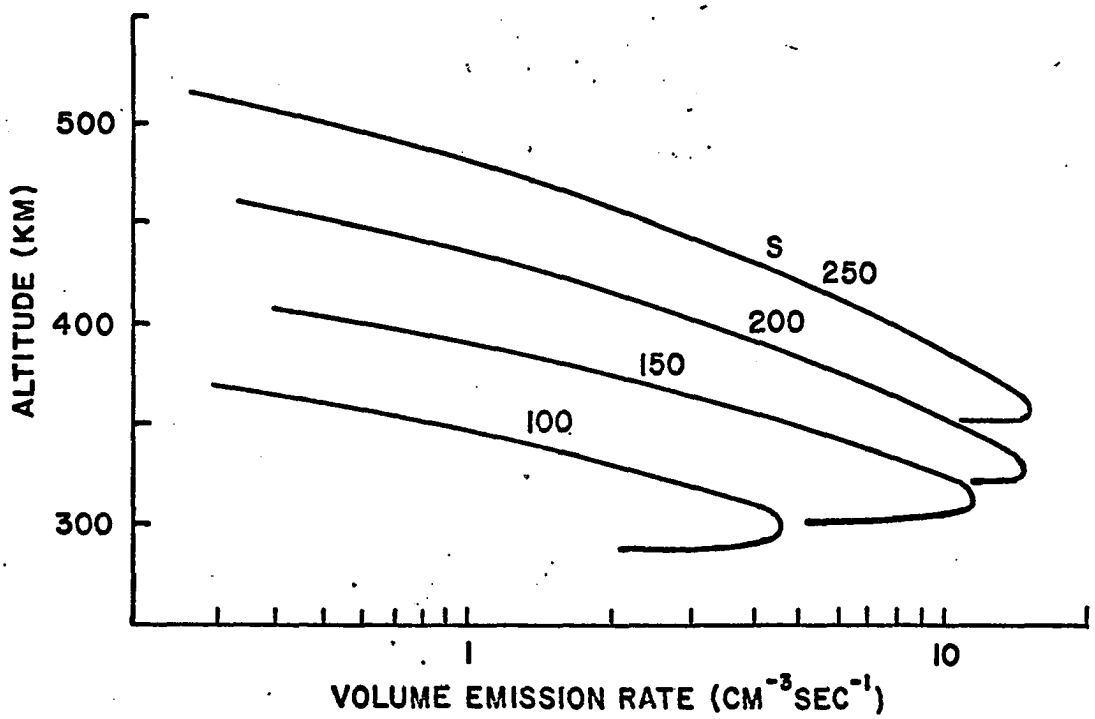

Fig. 4.8 The 6300 A [OI] volume emission rate calculated from the photoelectron flux in Fig. 4.4 and the attenuation in Fig. 4.7, for several values of the 10.7 cm solar flux, S.

reviewed. Beginning with a curve relating the onset of red line emission due to photoelectron precipitation at Haute Provence with the solar zenith angle at the geomagnetically conjugate ionosphere (Fig. 4.2), the altitude dependence of the electron production rate necessary for onset as a function of solar activity was found. It was assumed that onset of the red line emission at Haute Provence requires roughly equal incident electron flux over the solar cycle, and that the main contribution to onset at Haute Provence originates in a relatively narrow altitude range (100 km) at the conjugate point. The photoelectron production rate in each altitude range at onset is a measure of the attenuation when it is compared to the production rate in another range. The relation of the attenuation factor for other values of the solar flux was found by relating the attenuation to the change in atmospheric pressure as a function of solar activity. The red line reached a plateau at Haute Provence when the southern conjugate SZA was 90°. Referring again to Fig. 4.5, the total electron flux arriving at Haute Provence can be obtained by applying the attenuation factor to the electron production rate at SZA 90°. The effective electron flux which produces the difference in 6300 A emission between onset and plateau at Haute Provence is obtained by subtracting the electron flux calculation for onset from the total calculated at the plateau. Assuming the attenuation factors calculated at the conjugate region indicated the relative absorption of energy from the electrons by oxygen atoms, the volume emission rate of 6300 A at Haute Provence was calculated. The zenith intensity from these curves compared favorably with the observations,

not only with the shape of the curve, but with the observed intensities as well.

The errors in this calculation, which involves so many variables, cannot be well estimated. It can probably be said that convincing arguments have been raised which present a physical description of the 6300 A "subpolar sheet" consistent with the available observations. In brief, the "subpolar sheet" is a result of the precipitation in the atmosphere of low energy electrons (probably 5 to 50 ev) released from the magnetically conjugate ionosphere by solar EUV radiation. The emitting layer probably varies in altitude between 300 and 350 km and changes intensity between 50 and 200 Rayleighs. These variables, along with the time of onset, vary in a similar manner: smoothly proportional to the average 10.7 cm solar flux. The physical relation of the varying observables to the average 10.7 cm solar flux is through the relationship of this flux to the average solar EUV radiation which, in turn, determines the exospheric temperature of the atmosphere and hence its density gradient. It is the change of the density gradient which affects the production and attenuation of the photoelectrons and hence the onset time, plateau intensity, and the height profile of the conjugate 6300 A emission.

4.3 World-wide Maps of Conjugate Photoelectron Precipitation

Now that the factors governing the morphology of the photoelectron problem have been assembled, the world-wide distribution of photoelectron conjugate precipitation can be calculated. Using the program described

in section 4.2 for tracing the conjugate sunrise-sunset line, the positions of the onset and recession photoelectron precipitation have been plotted at intervals of two hours throughout a Universal day at all latitudes for both solstices and an equinox. The height of the sunlight line was taken as 25 km or approximately 95° SZA. This value was chosen because it corresponds to the latest onset time during a period of minimum solar activity.

In order to visualize the geometric relationships more easily, consider Fig. 4.9. This figure illustrates the global picture of the photoelectron precipitation for only one time (02^h U.T.) at the northern winter solstice. The S-shaped central region (lightest shading) divides the earth surface into the sunlit (unshaded) and nighttime (shaded) areas. The width of the S-shaped region indicates that portion of the world which is between civil and astronomical twilight. Of the three remaining shaded areas, the black regions are completely dark, the other two regions are experiencing photoelectron precipitation. The lighter area is always subject to photoelectron precipitation independent of solar activity. The narrow shaded region adjacent to the black region receives photoelectron precipitation only during the maximum of solar activity. The actual width of this region at any time in the solar cycle can be estimated with the help of Fig. 4.2. The white areas are sunlit and the effects of the conjugate electrons on the 6300 A dayglow are probably negligible. Figures 4.10, 4.11 and 4.12 show both the photoelectron onset and recession lines at intervals of two hours and the sunrise-sunset lines

Fig. 4.9 A world map of photoelectron precipitation at 02^h U.T. for the northern winter solstice. Thin dashed lines are sunset lines while thin, solid lines denote sunrise. The shaded area bounded by sunrise-sunset lines, and an S shaped curve across the maps, is the twilight region between 95° SZA and 108° SZA. The darkest shading represents night with no photoelectron precipitation from the conjugate sunrise. The heavy, dashed lines represent the recession of photoelectron precipitation corresponding to conjugate sunset, and the heavy, solid lines are the onset lines at conjugate sunrise. The grey area bounded on the north by the L=5 line and on the south by the photoelectron onset-recession lines is the area of conjugate photoelectron precipitation. The shading between 02 min and 02 max represents the possible expansion of the area of photoelectron precipitation between minimum solar activity and maximum solar activity.

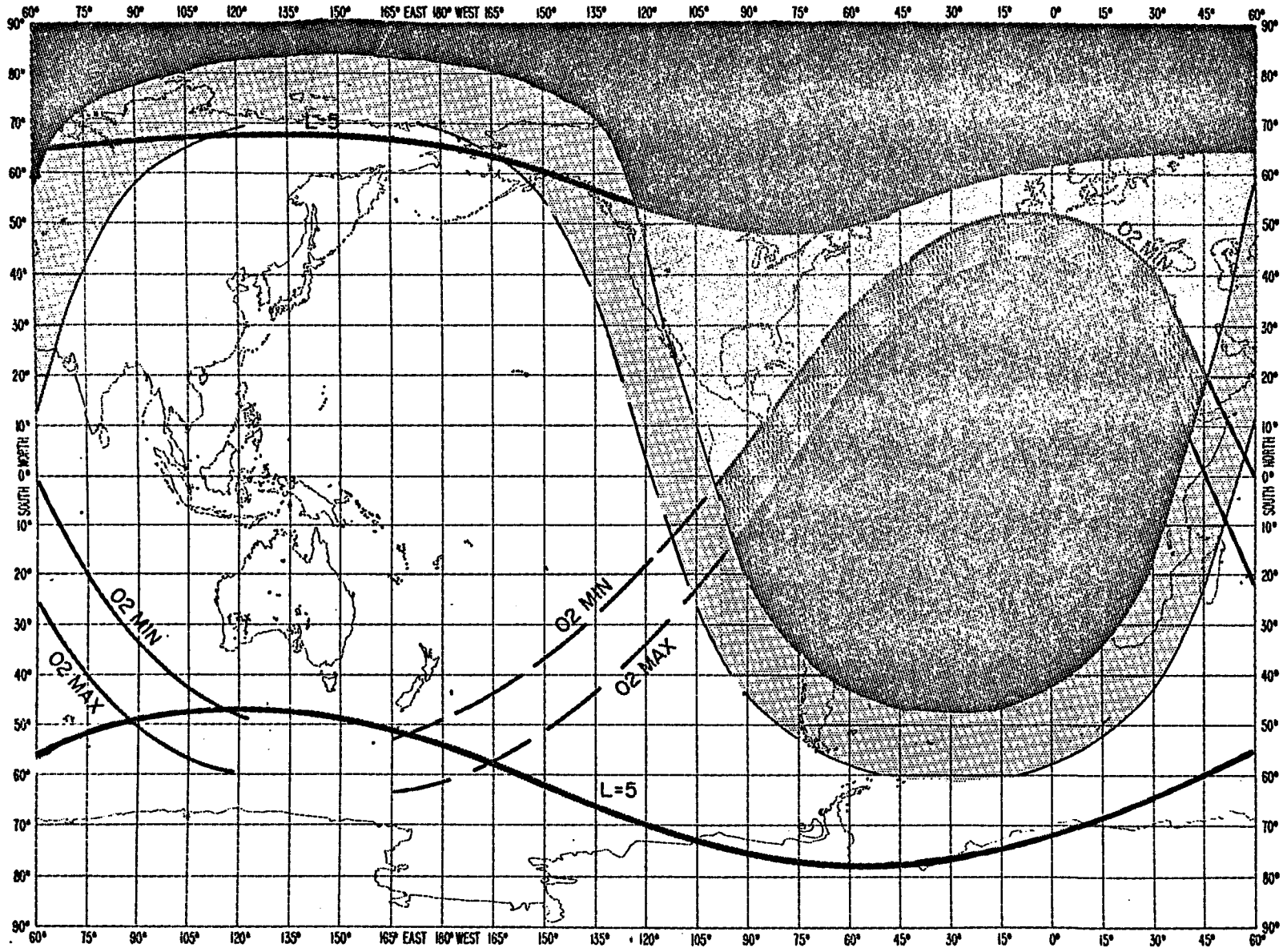

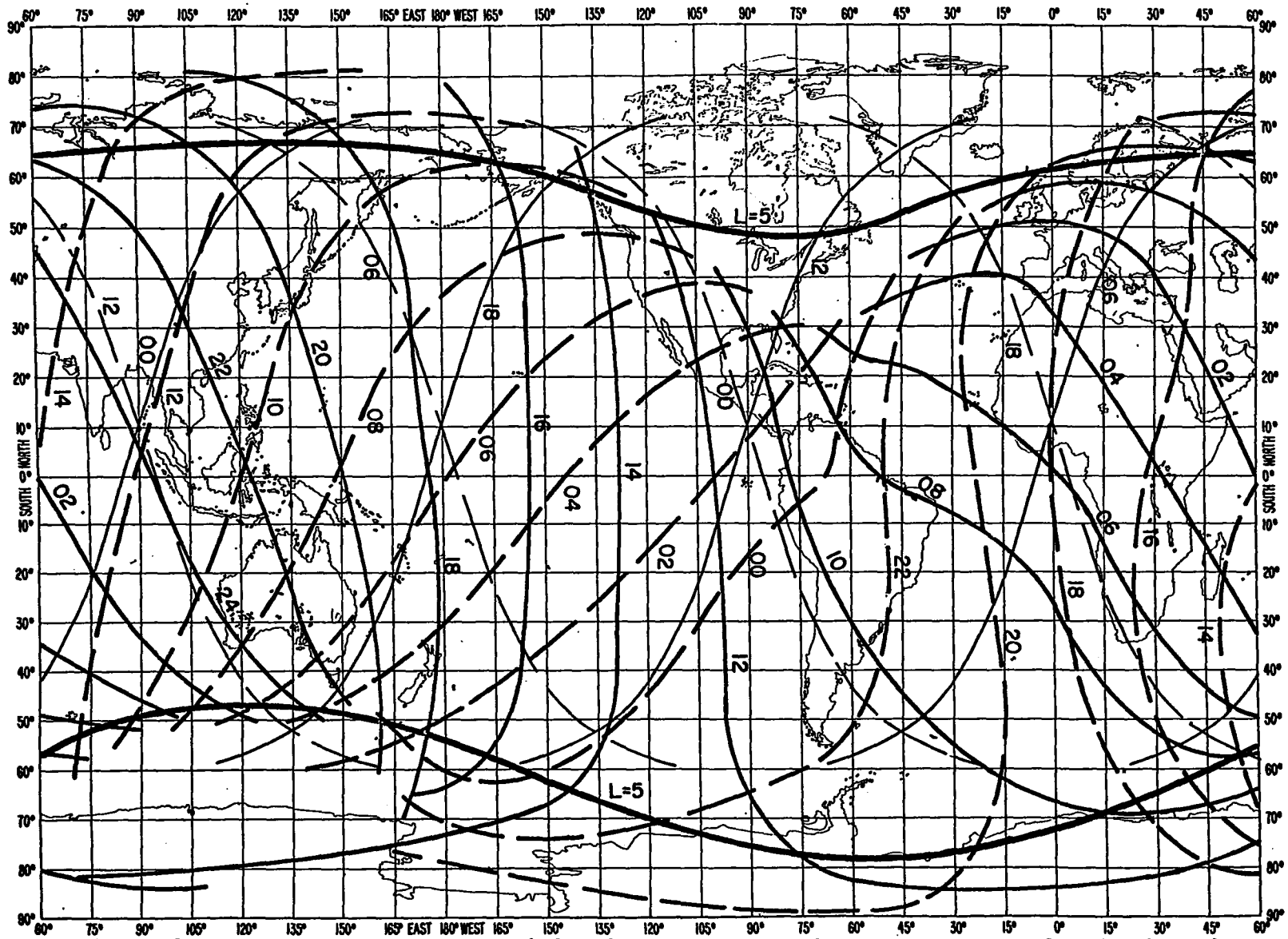

Fig. 4.10 A world map of photoelectron precipitation for every 2 hours of a solar day for December. The heavy, dashed lines represent the recession of photoelectron precipitation corresponding to conjugate sunset, and the similar heavy, solid lines are the onset lines at conjugate sunrise. The thin, dashed lines and the thin solid lines respectively denote sunrise and sunset, plotted every 6 hours so that one can determine by interpolation where the night-time effects of photoelectron precipitation can be observed. The heaviest solid lines are the L=5 limits to the poleward extent of the photoelectron precipitation.

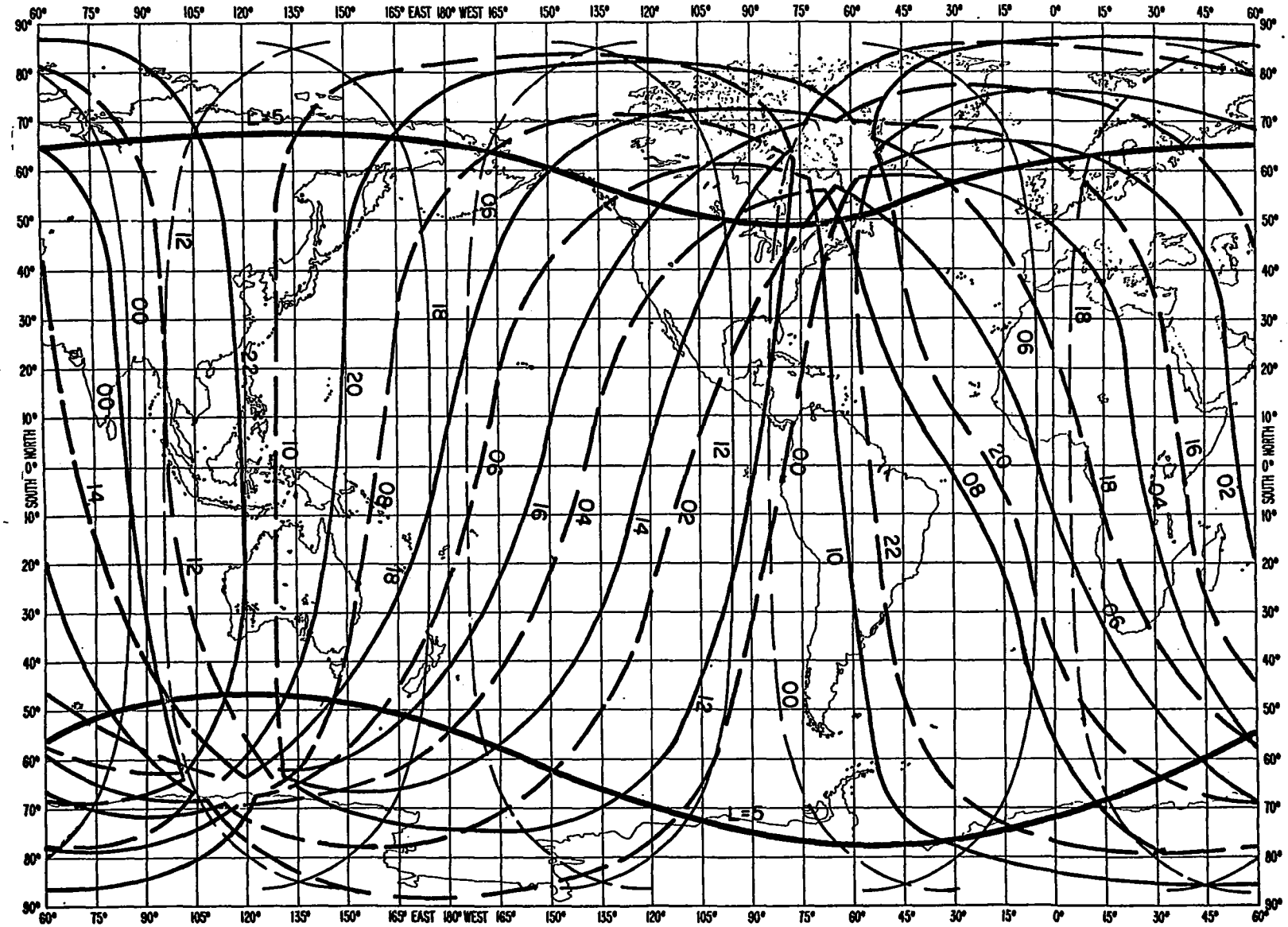

Fig. 4.11 A world map of photoelectron precipitation for every 2 hours of a solar day for March. The heavy, dashed lines represent the recession of photoelectron precipitation corresponding to conjugate sunset, and the similar heavy, solid lines are the onset lines at conjugate sunrise. The thin, dashed lines and the thin solid lines respectively denote sunrise and sunset, plotted every 6 hours so that one can determine by interpolation where the night-time effects of photoelectron precipitation can be observed. The heaviest solid lines are the L=5 limits to the poleward extent of the photoelectron precipitation.

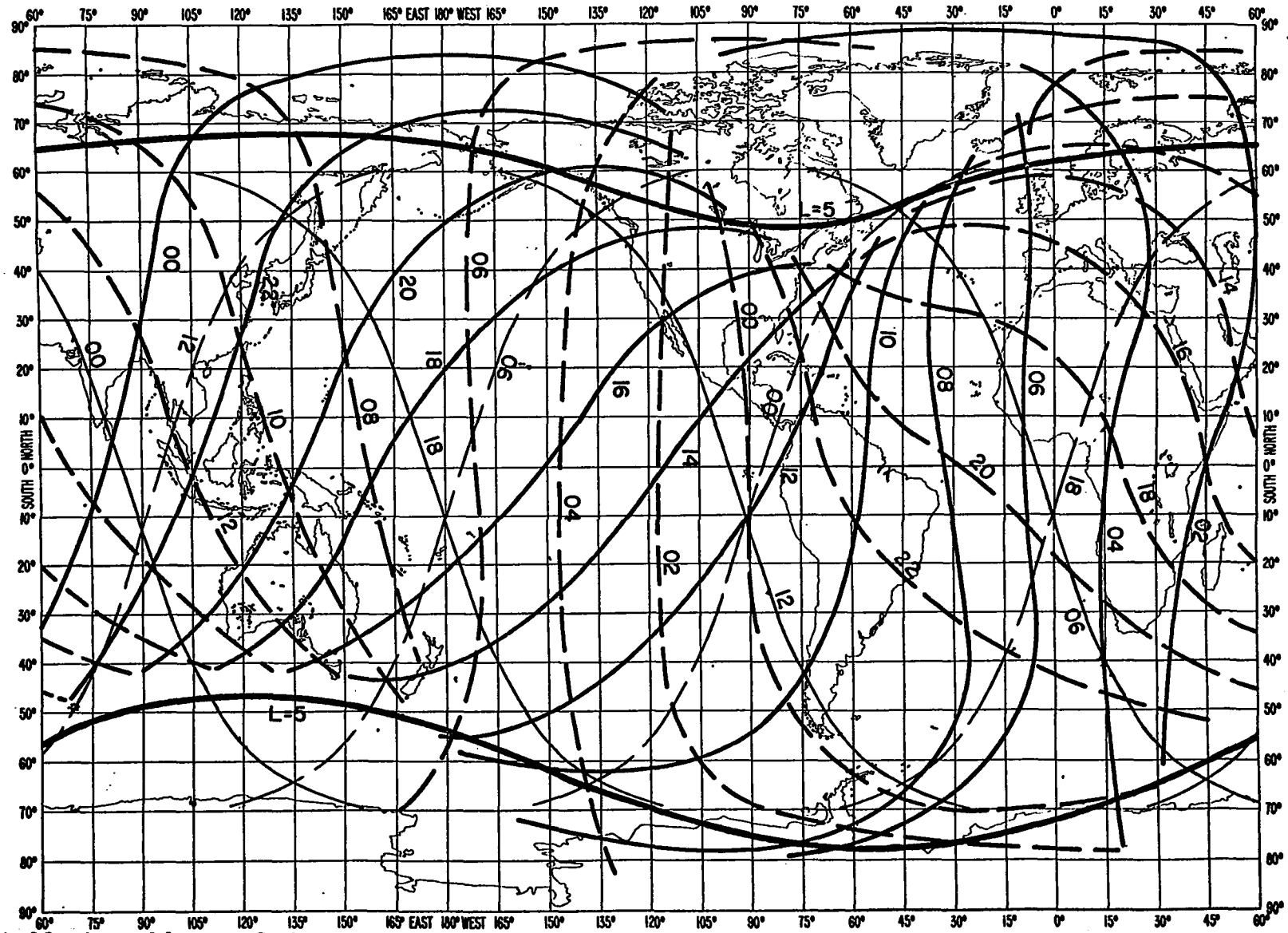

Fig. 4.12 A world map of photoelectron precipitation for every 2 hours of a solar day for June. The heavy, dashed lines represent the recession of photoelectron precipitation corresponding to conjugate sunset, and the similar heavy, solid lines are the onset lines at conjugate sunrise. The thin, dashed lines and the thin solid lines respectively denote sunrise and sunset, plotted every 6 hours so that one can determine by interpolation where the night-time effects of photoelectron precipitation can be observed. The heaviest solid lines are the L=5 limits to the poleward extent of the photoelectron precipitation.

at intervals of six hours for the winter solstice, spring equinox, and summer solstice, respectively.

In order to use the maps to arrive at information on a specific day of the year, interpolation is necessary. The direction of approach for the date of interest can be interpolated between the maps for equinox and solstice. The time of approach must be extrapolated from the onset and recession lines which are plotted for a SZA of 95° in the conjugate region. This geometry corresponds to solar minimum conditions. The correct conjugate SZA may be found from Fig. 4.2 by applying the monthly average of the 10.7 cm solar flux for the period of interest to the graph. The approximate change with solar activity in the position of the onset or recession line can be estimated by interpolating between the onset and recession lines of Fig. 4.10 which correspond to conjugate solar zenith angles of 95° and 108° at 02^h U.T. at the December solstice.

As an example, consider the 6300 A intensity in the direction of the pole at Haute Provence. The average 10.7 cm solar flux for, say, December 1955 was 130×10^{-22} watts cm^{-2} sec^{-1}. According to Fig. 4.2, the conjugate SZA at onset was 104°. This value would be approximately half way between the onset lines corresponding to 95° and 108° in Fig. 4.9. Looking at the world map in Fig. 4.10, it is seen that the Haute Provence observations were made roughly where the 104° SZA line would fall with respect to the 95° SZA line at 02^h U.T. Consulting Barbier (1959, p. 192) the onset time is found to be 01^h50^m U.T. which is quite close to the 2^h value for which the map is plotted. Extrapolations from the 95° line in Figs. 4.10, 4.11 and 4.12 are more difficult

at later hours and higher latitudes, but the calculations are more approximate in these regions.

It is evident that the onset or recession line for the photoelectrons is of the same type as that for the sun: i.e. it is a "U" shape which moves from east to west. The "U" is distorted in the former case, though, and the locus of points forming the line moves in longitude and latitude, rather than simply moving straight westward as is the case with the sunlight line. This motion is obviously the result of the angle between the geographic pole and the geomagnetic pole. The effects of this difference are numerous, but generally speaking, the direction of approach of the photoelectron onset time is not the same as that of the recession line (as it is with the sunrise and sunset lines). The change in direction of the onset-recession line with the change of solar declination is also very difficult to visualize. Nevertheless, it is very important to the interpretation of twilight phenomena in the summer because the expected direction is usually determined in the winter when the effect is more apparent. Another effect, not generally realized, is a direct result of the inclination of the magnetic pole: poleward of a certain latitude at the solstices, the atmosphere is continually sunlit; the result is that a large area in a ring about the opposite pole is continually bombarded by the photoelectrons. Obviously, there is a geomagnetic latitude which represents the poleward limit of conjugate electron precipitation. If the field lines extend farther than about 5 earth radii in the earth's equatorial plane, then external sources (ring-currents, currents in the magnetopause and in the neutral

sheet of the geomagnetic tail) probably exert more influence on the local field lines and cause large asymmetries. A high latitude is finally reached at which the field lines do not connect and a conjugate event is, by definition, impossible. It is reasonable to assume that the auroral oval forms a poleward boundary for the precipitation of conjugate photoelectrons. The equatorward boundary is formed by the conjugate sunlight line. The most interesting point, however, is that there are field lines along which there should be continuous photoelectron precipitation; these field lines correspond to L-values as small as 3 during solar minimum and 2 during years of maximum activity. This situation occurs in local winter only in areas of Northeastern North America during sunspot minimum. However, during maximum activity only the extreme southwestern part of the United States would be shaded from the photoelectrons. They reach the south coast of Australia and southwest of Australia during solar maximum. During the equinoxes, the effect is more difficult to visualize. Both poles, instead of only one receive continuous precipitation, as is the case at the solstices. The lowest latitude of continuous precipitation is higher at the equinoxes; it is safe to say that at solar minimum it is poleward of the closed field lines. During solar maximum, however, continuous precipitation could occur in the northeastern United States. Considerations of this "anomaly" are even more intriguing than the advance and retreat of the photoelectrons due to the changing sunlight line, primarily because the area of continuous precipitation should provide a more static picture of the variation with latitude of the escaping

photoelectron flux and of the magnetic field lines capable of supporting the photoelectron flow from the conjugate hemisphere. The extent of conjugate photoelectron precipitation could be mapped much more easily from such a stable pattern. The only changes in the 6300 A emission would be due to the decay of intensity in local time due to dissociative recombination in the F region and shifts in the photoelectron precipitation pattern due to changes in the geomagnetic field.

4.4 Predawn Enhancement at College

Close examination of the map for the northern winter solstice (Fig. 4.10) reveals that morning twilight observations at College in November, December, and January could record the onset of photoelectron precipitation before astronomical twilight. Moreover, the direction (east) from which the "subpolar sheet" advances would differ from that of the twilight in the southeast and that of the aurora in the northeast.

Because the direction of onset is important, the data format as it was plotted in Chapter III was only used as a guide in the selection of data. In order to locate the precipitation onset more easily, the local zenith intensity and direction of observation from the 45°ZA and 65°ZA azimuth sweeps has been plotted in geographic coordinates, assuming an emitting layer height of 250 to 300 km. Isophots, or lines of constant intensity, are drawn on the maps. The result is a first approximation to the geographic distribution of 6300 A [OI]. Figure 4.13 shows the maps at 15-minute intervals during the morning of 21 January 1964. This was one of the geomagnetically quietest periods of the IQSY. The aurora occurred to the north of 70° geomagnetic latitude that night,

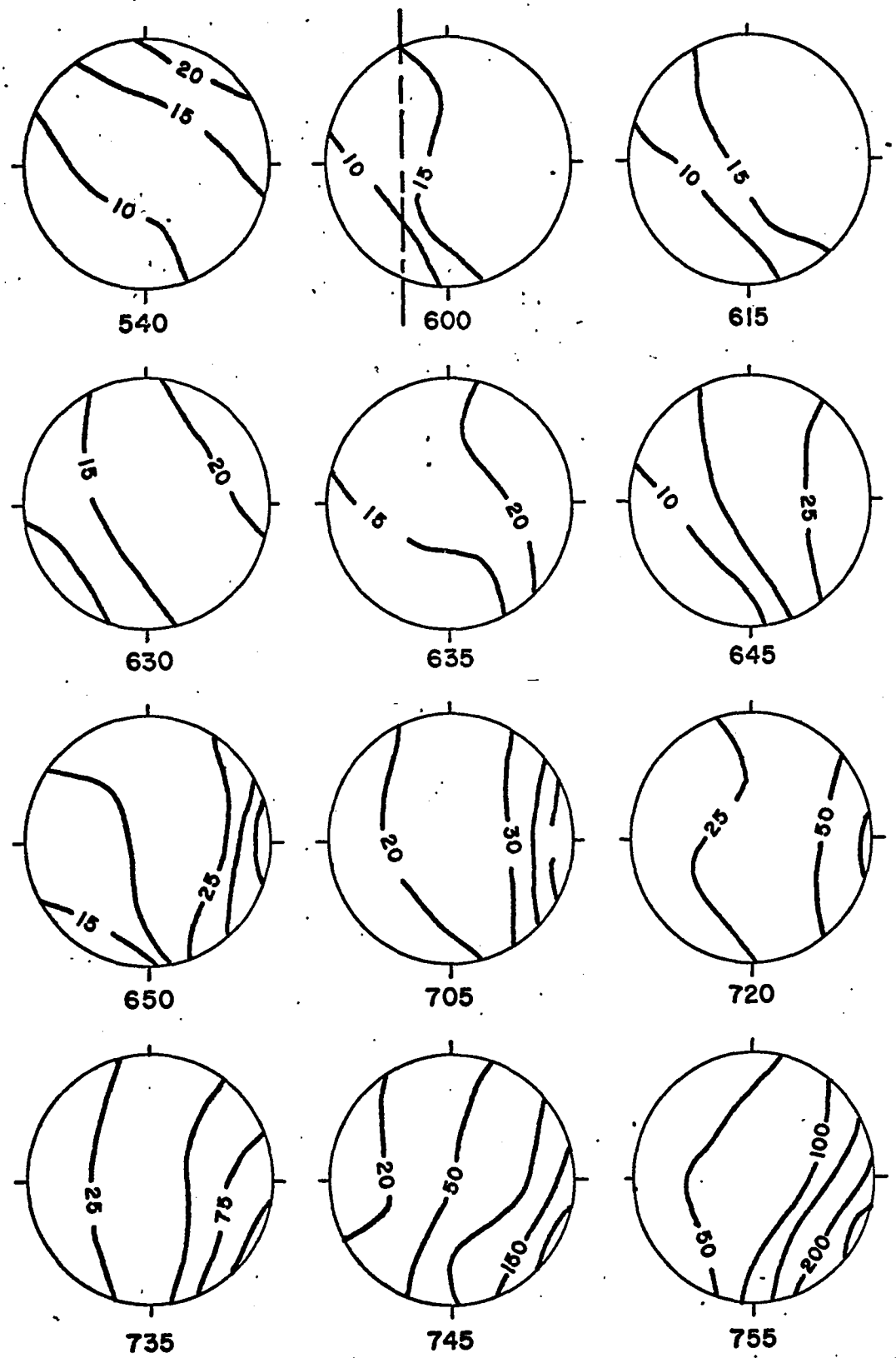

Fig. 4.13 Circular plots of the sky showing the approximate intensity distribution of 6300 A zenith emission (Rayleighs) over Alaska on 21 January 1964 (150° WMT). The top is north; east is to the right.

and the field of view intercepted the aurora at such a high altitude that 5577 A [OI] << 6300 A [OI] (Fig. 4.14). The earliest maps show an obvious 6300 A enhancement in the geomagnetic north. This enhancement was probably due to aurora but it could have been produced by photoelectrons from the conjugate region, which is continually sunlit at that time of year. (The important difference between the two cases is not the excitation mechanism, which is probably the same, but the origin of the particles.) If it were produced by the latter particles, one would expect to see the onset of photoelectrons in the east at a time corresponding to 25 km sunrise in the region conjugate to College and at other latitudes equatorward of the continuously sunlit region in the south. The intensity should be about 50R, which is the value observed at Haute Provence at a corresponding period of solar activity (Fig. 4.2). First, particles traveling field lines at L=2, 2.5, and 3 (Haute Provence and Camden) should suffer no less attenuation than those at L=5 or 5.5, if the field line can support the transport of the particles. Second, if the enhancement to the north is related to photoelectron precipitation, one might expect 50R enhancement in the onset from the east. Examination of the relationship of the isophots to the expected onset line (dotted lines at 0600) reveals that no enhancement greater than 5R could have occurred, even though the isophots began to tilt to the east after 06^h owing to enhancement by morning twilight (see Chapter V). The same conclusion was reached upon examination of the 19 November 1963 morning twilight. These two nights were the only ones occurring in the entire observing program which were quiet enough to

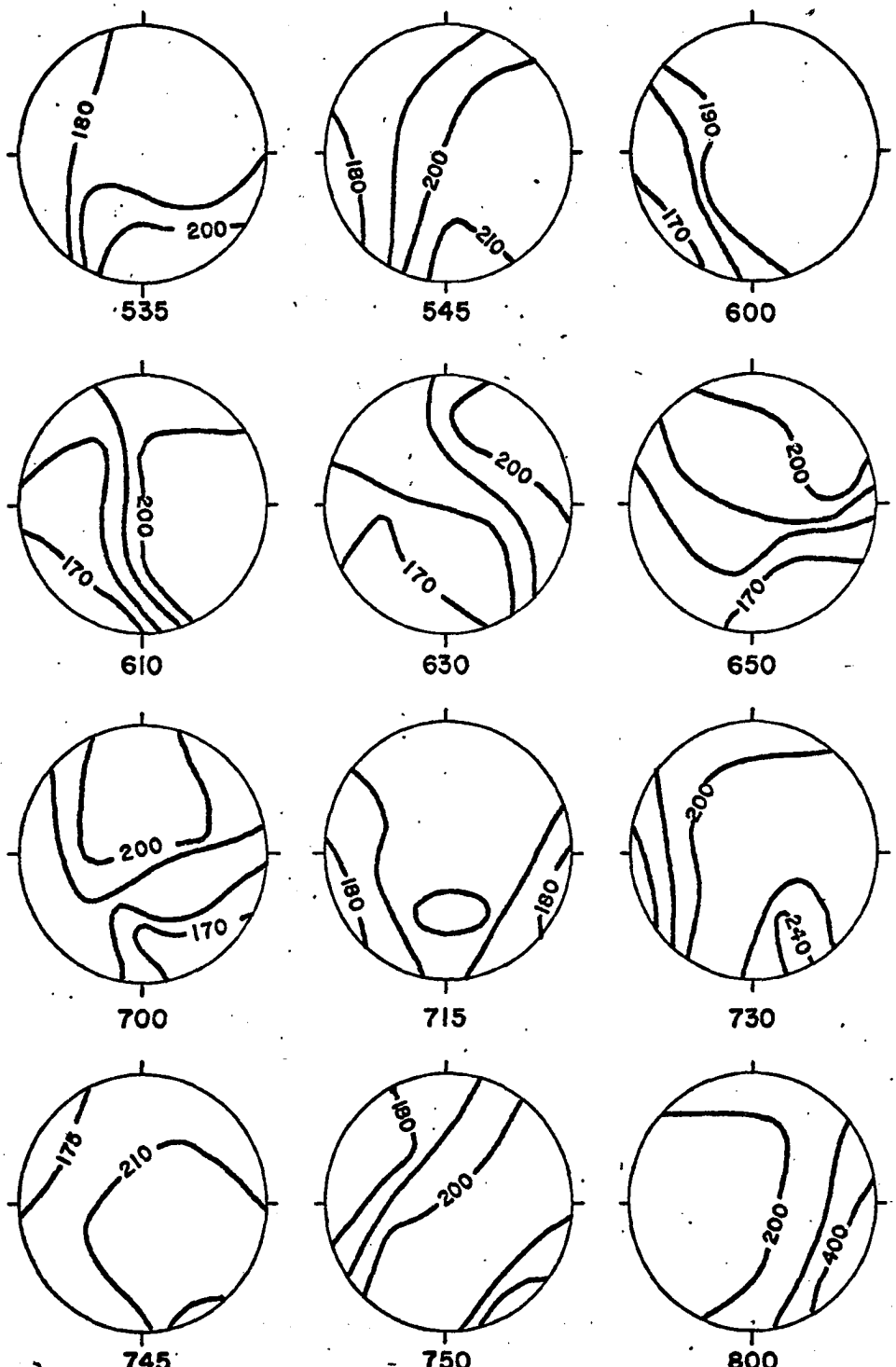

Fig. 4.14 Circular plots of the sky showing the approximate intensity distribution of 5577 A zenith emission (Rayleighs) over Alaska on 21 January 1964 (150° WMT). The top is north; east is to the right.

allow the detection of any photoelectron produced enhancement above 5R. Because of the geographic extent of the observations in Fig. 4.13, it can be said that the transport of photoelectrons from the conjugate region is probably very small, if there is any at all, poleward of L=5. The L=5 contour is indicated on the maps of world-wide conjugate photoelectron precipitation as a tentative poleward boundary under quiet magnetic conditions (Figs. 4.10, 4.11, 4.12). This is not an unexpected result, but it would be interesting to learn where the closed field lines do occur and what is the relationship of this point to the auroral oval under various conditions of magnetic disturbance.

4.5 Evidence for Conjugate Photoelectrons in Other Observations

It is rewarding to qualitatively consider some ramifications of the conjugate photoelectron precipitation found in observations of other geophysical phenomena. The more obvious cases are those in which the writer has already suggested that they are strongly affected by photoelectrons from the conjugate region. It is hoped that the present study will at least indicate new methods to be applied to other data in order to confirm the possibility of photoelectron effects.

In this regard, another twilight observation which seems to be affected by photoelectron precipitation is that of resonant scattered N_2^+ emission. Broadfoot and Hunten (1966) have documented a winter maximum in the evening twilight N_2^+ emission. They suggested that the resulting morning-evening asymmetry was due to conjugate photoelectron precipitation. The onset of photoelectron precipitation seems to occur when the solar zenith angle at the conjugate point is 90° or less.

At the longitude of Kitt Peak, the effect is difficult to observe in the morning owing to the declination of the magnetic field lines. However, the evening enhancement has been well documented. If some directional data were available, the effect could be more directly linked to conjugate photoelectron precipitation. However, even if this were impossible, a dependence of intensity or onset time on solar activity should be evident. On the basis of the present study, not only is the evening twilight enhancement substantiated, but one would also predict that the detection of photoelectron enhancement of N_2^+ in the morning twilight from Kitt Peak should become possible as the sun becomes more active, and the conjugate solar zenith angle sufficient for onset becomes greater.

Another example of a major effect on twilight observations by conjugate photoelectrons is the case of the twilight Helium observations by Tinsley (1967). A dominant process for the production of He atoms in the metastable state, 2^3S, is bombardment by electrons precipitating into the atmosphere from above (Ferguson and Shulter, 1962). The twilight enhancement of the 10,830 A line is produced by resonant scattered sunlight from these metastable atoms. Tinsley points out that the observed winter maximum, the greater intensity in the north, and the suspected solar cycle dependence are strong indications of conjugate photoelectron excitation. His only objections to this mechanism to be discussed below can be qualitatively explained in terms of the analysis presented in section 4.2 above.

First of all, Tinsley observed no morning-evening asymmetry, as was found in the N_2^+ twilight data by Broadfoot and Hunten (1966). The

latter observations, however, were of a different altitude and require a different electron production at the conjugate region. The conjugate solar zenith angle required to produce enough electrons to result in He emission is probably much larger than that for N_2^+ because of the difference in excitation cross section and g factor. Supporting this contention is the relatively greater He enhancement observed to the north where the conjugate SZA would be less. The observations were made during January 1967, when the average 10.7 cm solar flux, was approximately 130 x 10^{-22} watts cm^{-2} sec^{-1}. Figure 4.2 indicates that one would expect an onset of 6300 A emission enhancement when the conjugate SZA was 100° to 105°. Thus, if the solar depression angle for onset is approximately the same for both the case of 6300 A and 10,830 A, the He observations made to the north were all in the zone of continuous precipitation. Hence, the relatively greater He intensities to the north would be expected during each twilight. The effective electron precipitation must take place over Texas for some time after sunset and begin again long before dawn. Because the observed He emission is resonant scattered sunlight by He atoms, which were excited to the 2^3S state by the conjugate precipitation, the time of photoelectron onset or recession is of no consequence so long as it occurs before 10,830 A sunrise at 500 km altitude. Therefore, one would not expect to see a consistent morning-evening asymmetry in the observed He enhancement, even though the electrons are responsible for the enhancement.

Tinsley's second concern was that the Loparskaya results of Federova (1961) were obtained at L=15 where one would not expect photoelectron

precipitation. The difference between the enhancement at L=15 and L=2.5 is probably only in the origin of the particles. Federova found an intensity dependence on auroral "activity". In line with this, a relatively continuous precipitation of low energy electrons from the outer magnetosphere at L=15 during the years of high solar activity is not an unreasonable explanation for Federova's observation. Thus it seems that, not only can the directional dependence of twilight He observations be explained (at least at larger solar depression angles) by electron excitation, but they provide evidence for the zone of continuous precipitation of photoelectrons predicted in section 4.3.

Chapter V

TWILIGHT ENHANCEMENT OF THE RED AND GREEN LINES OF ATOMIC OXYGEN

5.1 The True Twilight Enhancement of 6300 A [OI]

From his observations of the enhancement of the red line by the direct action of sunlight, Barbier (1959) showed that the excitation mechanism was probably photodissociation of O_2 by sunlight in the Schumann-Runge continuum between 1750 and 1350 A:

$$O_2 + h\upsilon_{1750A} \rightarrow O(^3P) + O(^1D)$$

There were, however, a number of unexplained difficulties, the most notable of which was that of assigning a scale height to the emitting species.

Before beginning an analysis of the twilight phenomena observed at College, one may first consider the characteristics of Barbier's observations and compare them with the College data. The following is a list of the major points to be considered.

1) At Haute Provence, in winter, the true twilight phenomenon was observed to be superimposed on the "subpolar sheet' which came in from the north in the early morning and covered the sky by dawn. The arrival of the "subpolar sheet" in summer coincided with local twilight and the effects could not be separated easily. At the equinoxes, this northern maximum was more easily separable from the true twilight effect.

2) Abnormal twilights were observed ($\leq$ 2X normal intensity) but they were still closely allied with the "normal" values. The scatter of intensity values was attributed to changes in the diffusion properties of the atmosphere.

3) There were strongly abnormal twilights (> 2X normal) which were obviously dependent on magnetic activity but were not directly connected with aurora. When the twilight phenomena could be separated from the aurora, it kept the same pattern of intensity increase as a funcstion of solar depression angle.

4) Observed intensities in the solar meridian were larger than those observed 30° in azimuth to either side. Thus, the scale height of the emitting layer, measured from the series of sweeps making up a twilight run, was found to be approximately 70 km; the scale height observed from any one sweep was approximately 40 km.

5) The true twilight enhancement was not observed to occur more than 90° from the sun.

6) The normal intensity of the true twilight enhancements did not seem to change with solar activity.

Consider now the relationship between the data from College and that from Haute Provence

(1) Among the differences one finds most obvious is the lack of the "subpolar sheet" at College.

(2) The normal intensity at College is rather constant (although abnormal values of the twilight intensity are observed).

(3) The scale height determined from a number of sweeps in a single direction is large, and that from a single sweep in a number of directions is much smaller.

(4) The true twilight effect is observed at all azimuths (this is simply because the College data extend farther into twilight).

(5) There are no summer observations from College, but the lack of a "subpolar sheet" during the winter allows a fairly detailed study of the true twilight enhancement.

(6) One peculiarity of the College data is the relatively greater intensity of the enhancement to the north of the sun. This occurs on virtually all of the twilight observing runs and varies in magnitude.

The morning twilights at College are nearly always accompanied by an auroral display. During the years of minimum solar activity, however, some mornings are relatively free of auroral activity. It will be shown that the spatial resolution afforded by the almucantar sky survey allows the separation of the aurora and the true twilight effect, provided, of course, that the aurora does not change in a period of an hour or so and that it is not appreciably brighter than the twilight enhancement. These are fairly stringent requirements, unfortunately.

5.2 6300 A Intensity by Radiative Dissociation of O_2

The true twilight enhancement may result from two processes: resonance scattering by O atoms and photodissociation of O_2. Barbier's (1959) analysis of his true twilight enhancement data found the latter mechanism to best fit his observations. Although he was correct in

choosing this mechanism, several morphological details have not yet been explained. Hunten (1967) suggested that the use of a large quenching coefficient for N_2 (Hunten and McElroy, 1966) would remove these difficulties. The main feature of Hunten's analysis is in pointing out that the changing intensity during twilight comes from above 300 km because quenching by N_2 below that altitude results in little change of 6300 A emission with altitude. Hunten's analysis seemed to account for the large scale heights measured by Barbier, but it did not account for the small ones. It may be anticipated that the remaining problems can be explained by combining the effects due to a large screening height, quenching by N_2 and absorption of the exciting radiation by the emitting species. These effects are taken into account here in a calculation of the 6300 A emission intensities due to Schuman-Runge dissociation of O_2 in the twilight. The development of the analytical expressions used in the computations follows in some detail.

The twilight geometry is given in Fig. 5.1. The symbols used here are generally accepted (Chamberlain, 1961),but the previous developments have been extended enough to necessitate a list of definitions:

$\zeta \equiv$ zenith angle of observation at observer

$\Phi \equiv$ azimuth angle from solar meridian at observer

$\theta_o \equiv$ zenith angle of observation at Z_o

$Z_o \equiv$ altitude of intersection of field of view with screened shadow

$\beta_o \equiv$ solar depression angle at Z_o

$\alpha \equiv$ solar depression angle at observer

$\gamma_o \equiv$ angle between observer and Z_o (vertex at center of earth)

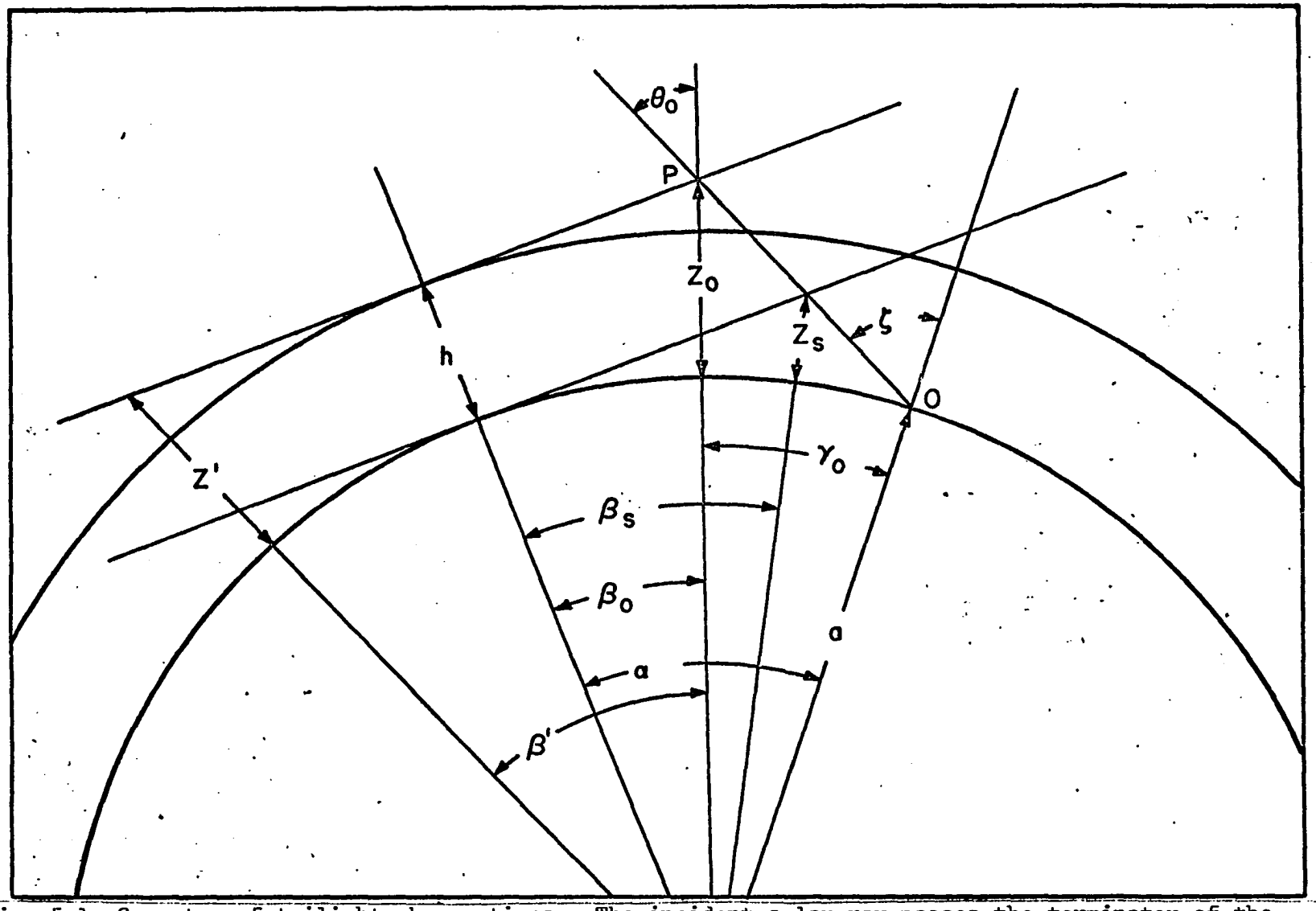

Fig. 5.1 Geometry of twilight observations. The incident solar ray passes the terminator of the screening height, h and intersects the line of sight at Z_o. For values of the observer's azimuth, $\phi > 0$, β_o and γ_o are not in the same plane and $\alpha \neq \beta_o + \gamma_o$. (see text for definition of symbols)

$\beta_s \equiv$ solar depression angle at Z_s

$a \equiv$ radius of earth

$h \equiv$ altitude of screened shadow at terminator

$Z' \equiv$ altitude of screened shadow at points toward the sun

$\beta' \equiv$ angle between the terminator and Z'.

For each observation in a given direction, determined by ζ and ϕ, the local solar depression angle α, is calculated, using the usual method involving the solar declination and hour angle along with the longitude and latitude of the station (See Chamberlain, 1961, p. 400). There are four other unknowns (γ_o, β_o, Z_o and θ_o)and they are calculated using Chamberlain's (1961, p. 595) general solutions for the apparent height:

$$a + Z_o = \sec \beta_o (a + h) \tag{5.2}$$

$$\sin \theta_o = \sin \zeta \, [a/(a + Z_o) \tag{5.3}$$

$$\gamma_o = \zeta - \theta_o \tag{5.4}$$

$$\sin \beta_o = \cos \gamma_o \sin \alpha - \sin \gamma_o \cos \alpha \cos \Delta\phi \tag{5.5}$$

The quantities of interest are β_o and Z_o, which are calculated for an observation in a single direction (constant α, ζ, ϕ) for h varying in 20 km increments between 120 and 300 km. The volume emission rate p, is then calculated at Z_o for each h. The result is then integrated between values of Z_o approximating the effective local zenith intensity of the emission.

The volume emission rate at Z_o is given by

$$p = n(O_2, Z_o) \int_{1350}^{1750} \pi F(\lambda) \, T_\lambda(Z_o) \, \sigma_\lambda (O_2) \, d\lambda \tag{5.6}$$

Wallace and McElroy (1966) point this out as being an assumption because of the possible continuum absorption associated with the $^3\pi_u$--$^3\Sigma_u^-$ transition. The situation is illustrated in Fig. 5.2. The $^3\pi_u$ curve has been extended to intersect the left branch of the $B^3\Sigma_u^-$ curve at v=4 in order to account for the effects of predissociation observed by Carroll (1959). If the $^3\pi_u$ curve extends farther up, then the left branch of the $B^3\Sigma_u^-$ curve, representing the Schumann-Runge continuum absorption transitions, may not account for all the absorption observed by Metzger and Cook (1964). Thus, some percentage of the molecules dissociated by wavelengths near 1700 A may produce two oxygen atoms in the ^3P state.

Another source of error in the use of dissociation cross sections around 1700 A is that the solar flux is increasing rapidly and the cross section is decreasing even more rapidly in this wavelength region. As a result, the product of these two quantities is not well known at the longer wavelengths in the Schumann-Runge continuum. This product is called the g-factor (for resonant scattering) or the d-factor (in fluorescent scattering). The factor is basically a measure of the efficiency of conversion of solar flux into the observed scattered radiation in terms of the population of the scattering particles: photons sec^{-1} $atom^{-1}$ (or $molecule^{-1}$). The d-factor for the production of 6300 A emission, by photodissociation of O_2, calculated using values for the solar flux from Detwiler, et al (1961) and Schumann-Runge continuum absorption cross sections from Metzger and Cook (1964), is 4.4×10^{-6} photons sec^{-1} $molecule^{-1}$. The values used in the volume emission rate calculation and for the d-factor are listed in Table 5.1.

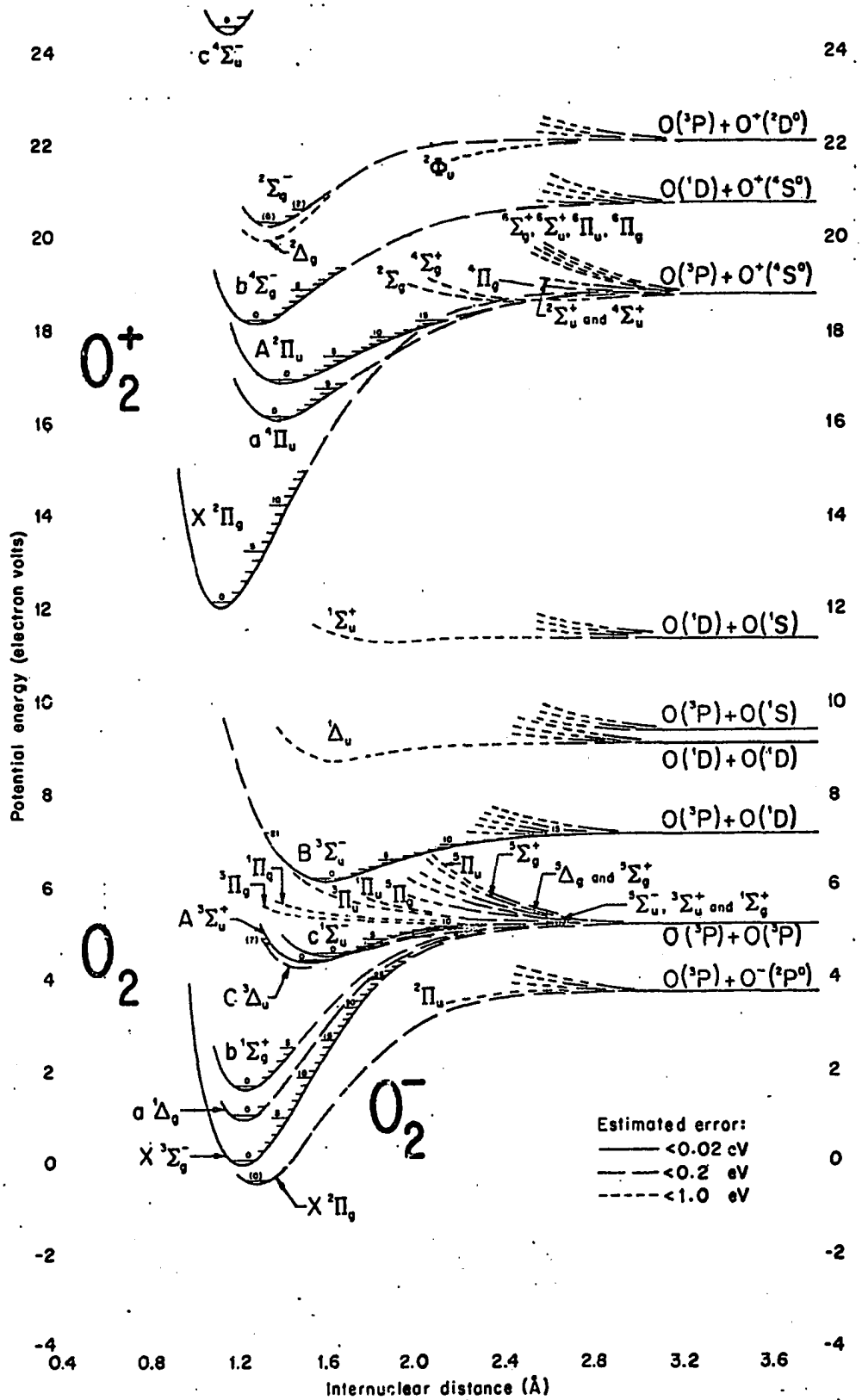

Fig. 5.2 Potential-energy curves for O_2^-, O_2, and O_2^+. From Gilmore (1965).

Table 5.1

The Solar Flux and Dissociation Cross Section in the Schumann-Runge Continuum

Wavelength Region (A)	Solar Flux $\left(\frac{\text{Photons}}{\text{cm}^2 \text{ sec}}\right)$	Cross Section $\left(\frac{\text{cm}^2}{\text{molecule}}\right)$	d-factor for $O(^1D)$ $\left(\frac{\text{Photons}}{\text{sec molecule}}\right)$
1700-1750	910×10^{9}	0.35×10^{-18}	0.318×10^{-6}
1650-1700	575	1.65	0.948
1600-1650	328	3.9	1.280
1550-1600	190	7.5	1.425
1500-1550	91	11.0	1.000
1450-1500	56	13.0	0.728
1350-1400	17	11.0	0.187
1325-1350	9	2.25	0.020
Total d-factor for 6300 A and 6364 A emission =			5.9
Multiply by 0.75 for 6300 A emission alone.			

The value of the d-factor quoted by Hunten (1967) as calculated from Hinteregger et al. (1965) is 4.5×10^{-6} sec^{-1}. The value used in this study in Table 5.1 is 4.4×10^{-6} sec^{01}. While this difference is negligible, it is important to consider that Hinteregger, et al. used values of solar flux and cross section out to 1775 A. This was done simply because they were interested in the total dissociation, not only that which leads to $O(^1D)$ (wavelengths < 1750 A). The cross section values used by Hinteregger et al. (1965) were reduced from the values given by Metzger and Cook (1964) but the d-factors are different from the ones used in this study. The important difference between the results from each study is not when the emission rate is calculated, but it appears when one allows for absorption by the atmosphere. The expression for the excitation rate takes the form:

$$P_\lambda = \pi F_\lambda \sigma_\lambda (O_2) N(O_2, Z_o) \exp-[\sigma_\lambda(O_2) n(O_2, h) H] \qquad (5.7)$$

$\pi F(\lambda)$ and $\sigma_\lambda(O_2)$ are the values of the solar flux (photons cm^{-2} sec^{-1} A^{-1}) and the cross section for emission (cm^2). Thus, P_λ is directly proportional to the d-factor but the transmission of the atmosphere involves the absorption cross section in an exponent. Because small changes in this cross section affect P_λ considerably and for values of h approximately equal to Z_o, the absorption cross section near 1700 A controls the emission rate almost exclusively.

The arguments of the preceding paragraphs indicate that there are some qualifications to the statement that one ^1D atom results from each photodissociation. Apart from predissociation, the effect of the atmosphere and the absorption cross section tend to affect the calculated volume emission rate near 1700 A. The method of allowing for predissociation would be to use the larger cross section values for absorption of the incoming solar ray and the reduced values for emission cross section in the field of view. This was not done here, however. The point to be made here is not that the difference in d-factors is very large, but that the emission is more sensitive to the value of the d-factor when used with an absorption calculation and therefore some basis for taking predissociation into account should be established. Unfortunately, this would involve accurate intensity measurements of 6300 A [OI] in the laboratory, which are presently very difficult. Because the O_2 population and the effect due to quenching are not well known in the upper atmosphere, the values of the d-factors given here will be accepted as correct and used to determine values for these less well known parameters.

$T_\lambda(Z_o)$ is the transmission function; it represents the fraction of the sunlight which reaches the point Z_o. It is a function of solar depression

angle, α, screening height, h, and wavelength, λ. The expression derived here is due to Chamberlain and Sagan (1960). It is based on a function obtained by Hunten (1954) to relate the number of absorbing particles between the sun and Z_o to the density at a height, h, at the terminator, or point of closest approach. From Chamberlain (1961)

$$T_\lambda(Z_o) = \exp\,[-N(h)\sigma_\lambda(O_2)] \tag{5.8}$$

where N(h) is the total number of particles in a column of unit cross section tangent to the earth at the terminator at a height, h.

$$N(h) = \int_{-\infty}^{\infty} n(O_2,Z')dS \approx \int_{-\infty}^{\infty} n(O_2,h)\,\exp - [(Z'-h)/H]\,ad\beta' \tag{5.9}$$

where H is the scale height of O_2 at h, and

because $n(O_2,Z') = n(O_2,0)\exp - [Z'/H]$ and $ds \approx ad\beta'$

Then $\cos\beta' \approx 1- (\beta'^{\,2}/2)$ and $(a+h)/(a+Z) \approx 1 -(Z'-h)/a$

but $\cos\beta' = (a+h)/(a+Z')$ implying $Z'-h = a\beta'^{\,2}/2$.

$$N(h) = a\, n(O_2,h)\int_{\infty}^{\infty} \exp -[a\beta'^{\,2}/2H]d\beta'. \tag{5.10}$$

Solving this integral according to the limits stated,

$$N(h) = n(O_2,h)\,\sqrt{2\pi aH}\ , \tag{5.11}$$

leads to Hunten's (1954) transmission function:

$$T_\lambda(Z) = \exp\,[-n(O_2,h)\,\sigma_\lambda\,(O_2)\,\sqrt{2\pi aH}\ ]. \tag{5.12}$$

As Chamberlain and Sagan point out, this expression is valid only for Z_o not approximately equal to h. Physically, it is simply that the observer's field of view toward the sun (see Fig. 5.1) intercepts the screened shadow line at a point (Z_o) near the terminator (h) where only roughly half of the absorption accounted for in Eq. (5.12) has taken place. Chamberlain and Sagan (1960) replaced the $+\infty$ limit in

Eq. (5.12) with β_o, which is the angle between the terminator and the point of observation at Z_o. Then

$$T_\lambda(Z_o) = \exp\left[-\sigma\lambda(O_2)\ a\ n(O_2,h) \int_{-\infty}^{\beta_o} \exp -[a\beta'^2/2H]\ d\beta'\right] \quad (5.13)$$

Separating into two integrals and solving the first ($-\infty$ to 0) yields

$$T_\lambda(Z_o) = \exp\left[-\sigma_\lambda(O_2)\ a\ n(O_2,h)\ [\pi aH/2]^{\frac{1}{2}} + \int_0^{\beta_o} \exp\ [-a\beta'^2/2H] d\beta'\right] \quad (5.14)$$

$N(O_2,h)$ and $n(O_2,Z_o)$ are the O_2 number densities at the respective altitudes h and Z_o. The densities and scale heights are taken from several model atmospheres in order to determine the effects of changing parameters and to find the best fit for the data. The boundary conditions for the models used are listed in Table 5.2 to facilitate intercomparison.

Table 5.2

Boundary Values of Model Atmospheres

	$n(0,120\ km)$ $(\times 10^{11}\ cm^{-3})$	$n(O_2,120\ km)$ $(\times 10^{11}\ cm^{-3})$	$n(N_2,120\ km)$ $(\times 10^{11}\ cm^{-3})$	$T(120\ km)$ (^oK)
CIRA (1965)	0.76	0.75	4.0	355
McElroy (1964) Model B	2.0	0.2	5.0	350
McElroy (1964) Model C	0.76	1.18	5.8	324

Exospheric temperatures are chosen in accordance with the time of day magnetic activity, and average 10.7 cm solar flux (CIRA, 1965).

The $O(^1D)$ state is metastable with a lifetime of approximately 110 seconds. It is collisionally de-excited or quenched in the laboratory by the walls of the container and in the upper atmosphere by other particles. Observations of the atmospheric emission show marked effects, so there is no question as to the existence of the process as a major condition in the upper atmosphere. The concern at this point is the quantitative evaluation of its occurrence.

The quenching factor, Q, is defined as the ratio of the observed intensity, I, to its value I_o in the absence of quenching:

$$Q = \frac{I}{I_o} = \frac{A}{A + d_i(X)n(X,Z_o)} \tag{5.15}$$

where $d_i(X)$ is the quenching rate coefficient of the state i by particle X with number density at Z_o, $N(X,Z_o)$. A is the sum of the radiative transition probabilities. If there is reasonable competition between different particles to quench the state of interest, more terms of the same form appear in the denominator.

Hunten and McElroy (1966) recently reviewed the laboratory and dayglow observations of the metastable oxygen emissions (among others) and concluded that the normally inert N_2 molecule quenches the ^1D state rather than the more active O_2 molecules. The reason for this is that DeMore and Raper (1964) found that the quenching seems to follow a chemical reaction.

$$N_2 + O(^1D) \rightarrow N_2O \rightarrow N_2 + O(^3P) \tag{5.16}$$

Because the quenching species was previously thought to be O_2 some difficulty was encountered in assigning a rate coefficient to match the observations. Values ranged from the gas-kinetic value of 3×10^{-10} cm^3

sec^{-1}, or larger, to 10^{-19} cm^3 sec^{-1} for O_2. Assuming N_2 to be the quenching species, Wallace and McElroy arrived at 9×10^{-11} cm^3 sec^{-1}, while Hunten and McElroy (1967) find 5×10^{-11} cm^3 sec^{-1}. Values representative of all these ranges were used to match the observations reported here (see pg. 80).

Briefly, the analysis of the dayglow rocket data proceeded as follows. The excitation rate was calculated for the ^1S and ^1D states of O. The quenching of the former state does not occur in the altitude region of interest to the latter because of a factor of 100 difference in lifetimes. Comparison of the calculated emission rates using several values of the quenching coefficient with the observations has indicated coefficients between 1 and 10×10^{-11} cm^3 sec^{-1}. There are numerous sources of error in this type of analysis, not the least of which are in the observations themselves. It is therefore with some justification that one applies the same type of analysis to the twilight data in hopes of achieving some closer estimate of the quenching coefficient.

As it was pointed out in Chapter I, the twilight observation is somewhat akin to a rocket flight and it therefore is subject to the same sources of error: lack of a suitable model atmosphere, calibration inaccuracies, and lack of knowledge of the observational geometry. There is one exception: the number of possible processes leading to the ^1D state is more limited in twilight. Thus, on a winter morning, and in the absence of electron precipitation, one really must deal only with radiative dissociation of O_2.

Proceeding with the calculation of the expected intensity due to this process, the correction to the volume emission rate, $P(Z_o)$, is applied according to Eq. (5.15). Values of the rate coefficient used in the

present calculation were 10^{-10}, 5×10^{-11} and 10^{-11}(cm^3 sec^{-1}) for N_2 and 1×10^{-11} (cm^3 sec^{-1}) for O_2 as the quenching species. The O_2 and N_2 number densities were taken from the model atmosphere appropriate to the particular calculation. (See Table 5.2).

After the quenching corrections were applied to the volume emission rate, P(Z), it was integrated between values of Z_o (for each h at one ζ and ϕ) approximating a local zenith intensity. The calculation was then repeated every 22 1/2 degrees in azimuth (ϕ) at constant altitude (ζ) from toward the sun, through 90° from the sun to 180° from the sun. The nine readings were then plotted versus the geometric shadow height, Z_s, in order to facilitate intercomparison with the observations.

Figs. 5.3, 5.4, and 5.5 are examples of the expected zenith intensity versus shadow height plots for one azimuth sweep. They have been calculated using the model atmospheres listed in Table 5.1, with the exospheric temperatures and quenching coefficients labeled on the figures. There are several general points which can be used in the analysis of the observed emissions: 1) varying the solar flux produces a proportional change in the intensity at all shadow heights. 2) Fig. 5.3 shows that quenching by O_2 is ten times less effective than by N_2 at the same rate (due to difference in number density), and 3) even if the rate were adjusted to make O_2 roughly as effective as N_2, the slope of the curve for O_2 is much less (more negative) than that for N_2. 4) Effectively increasing the total amount of O_2 in the atmosphere, as in McElroy's Model B and Model C plotted in Fig. 5.4 produces a relatively greater intensity at smaller solar zenith angles. That is, the slope of the curve (negative) changes in a negative direction

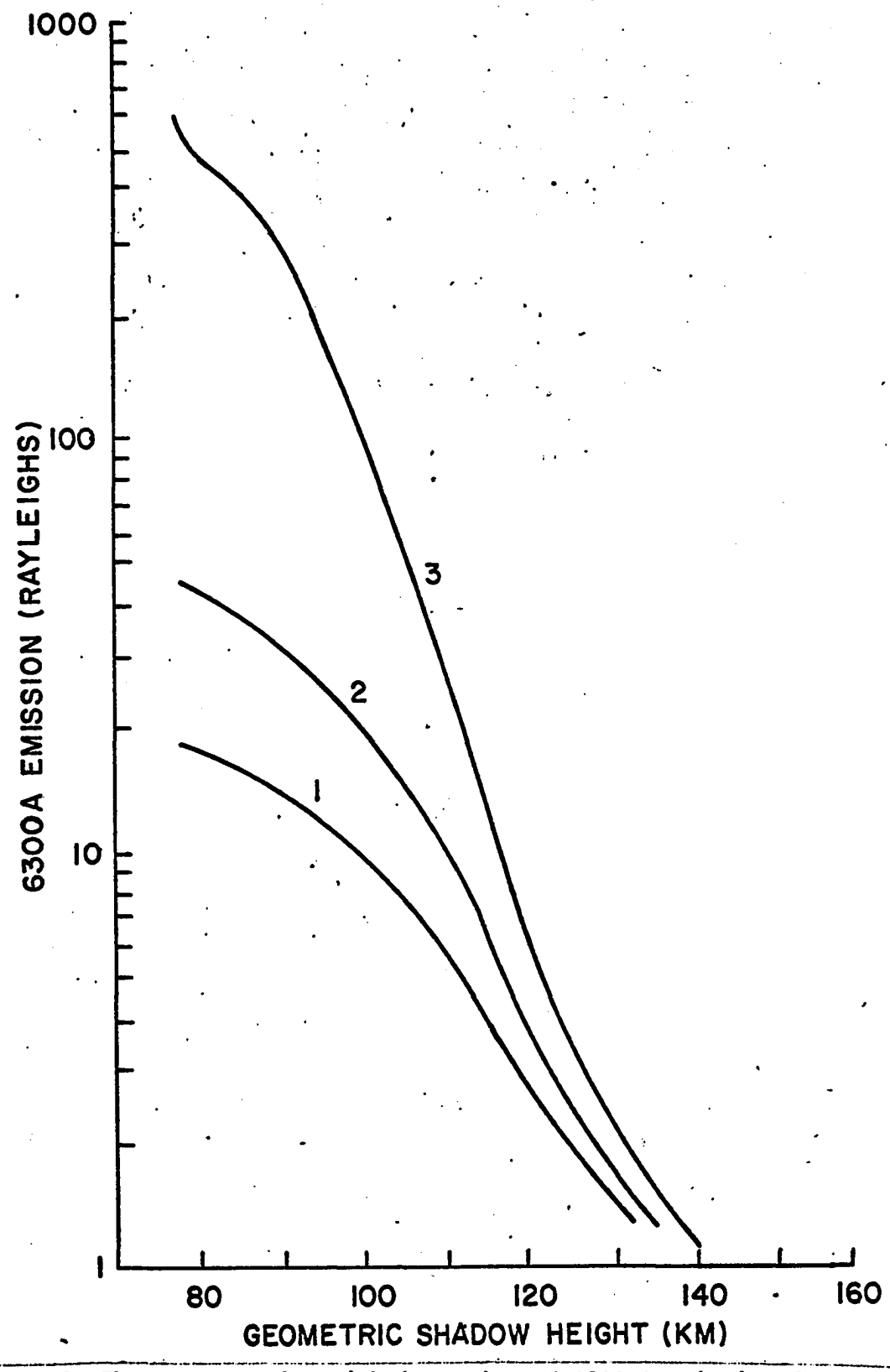

Fig. 5.3 The calculated zenith intensity of 6300 A emission due to photodissociation of O_2 sunlight in the Schumann-Runge continuum versus the height of the earth's geometric shadow at 100.5° SZA. The CIRA 1965 atmosphere Model 1, hour 4 (T_∞ = 705°K) was used. The quenching rate was varied as follows: 1) by N_2 at 5×10^{-11} cm^3 sec^{-1}, 2) by N_2 at 10^{-11} cm^3 sec^{-1} and 3) by O_2 at 10^{-11} cm^3 sec^{-1}.

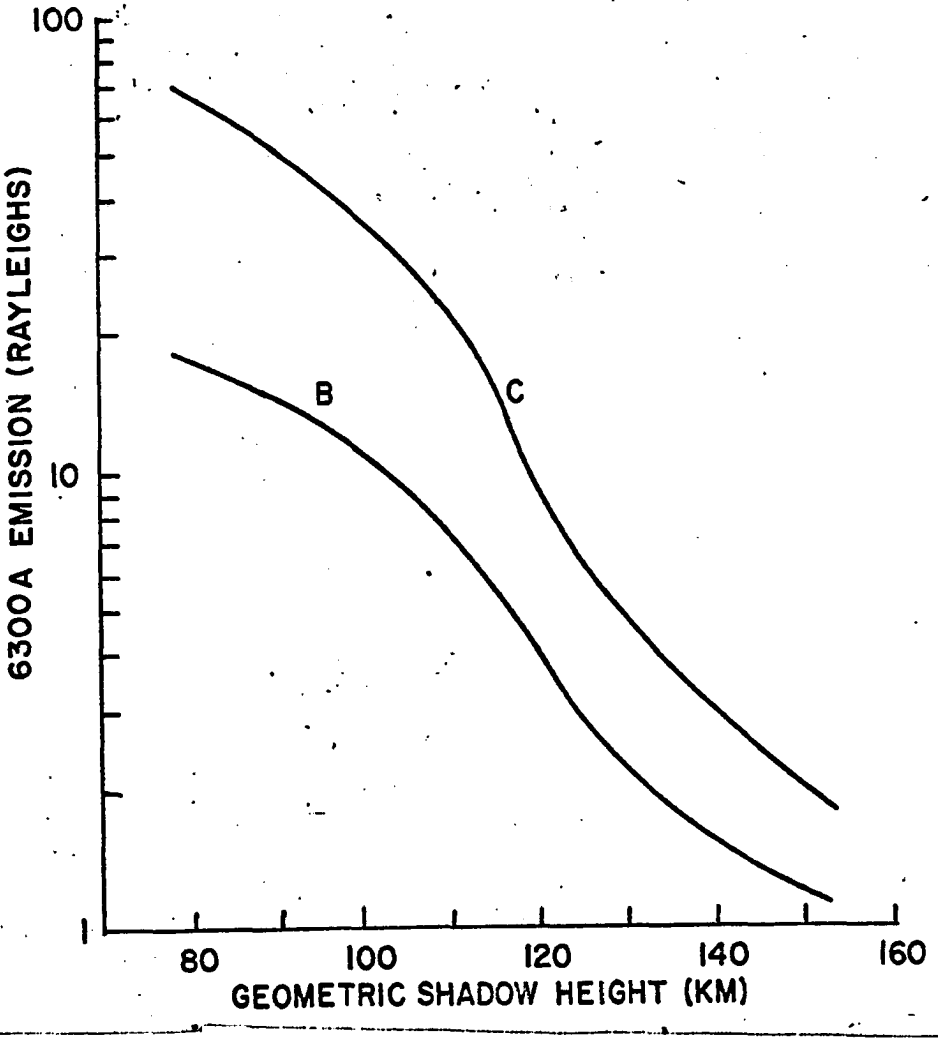

Fig. 5.4 The calculated zenith intensity of 6300 A emission due to photodissociation of O_2 by sunlight in the Schumann-Runge continuum versus the height of the earth's geometric shadow at SZA = 100.5°. The atmospheres used were the McElroy models B and C at T_∞ = 750°K and quenching by N_2 at 10^{-11} cm^3 sec^{-1}.

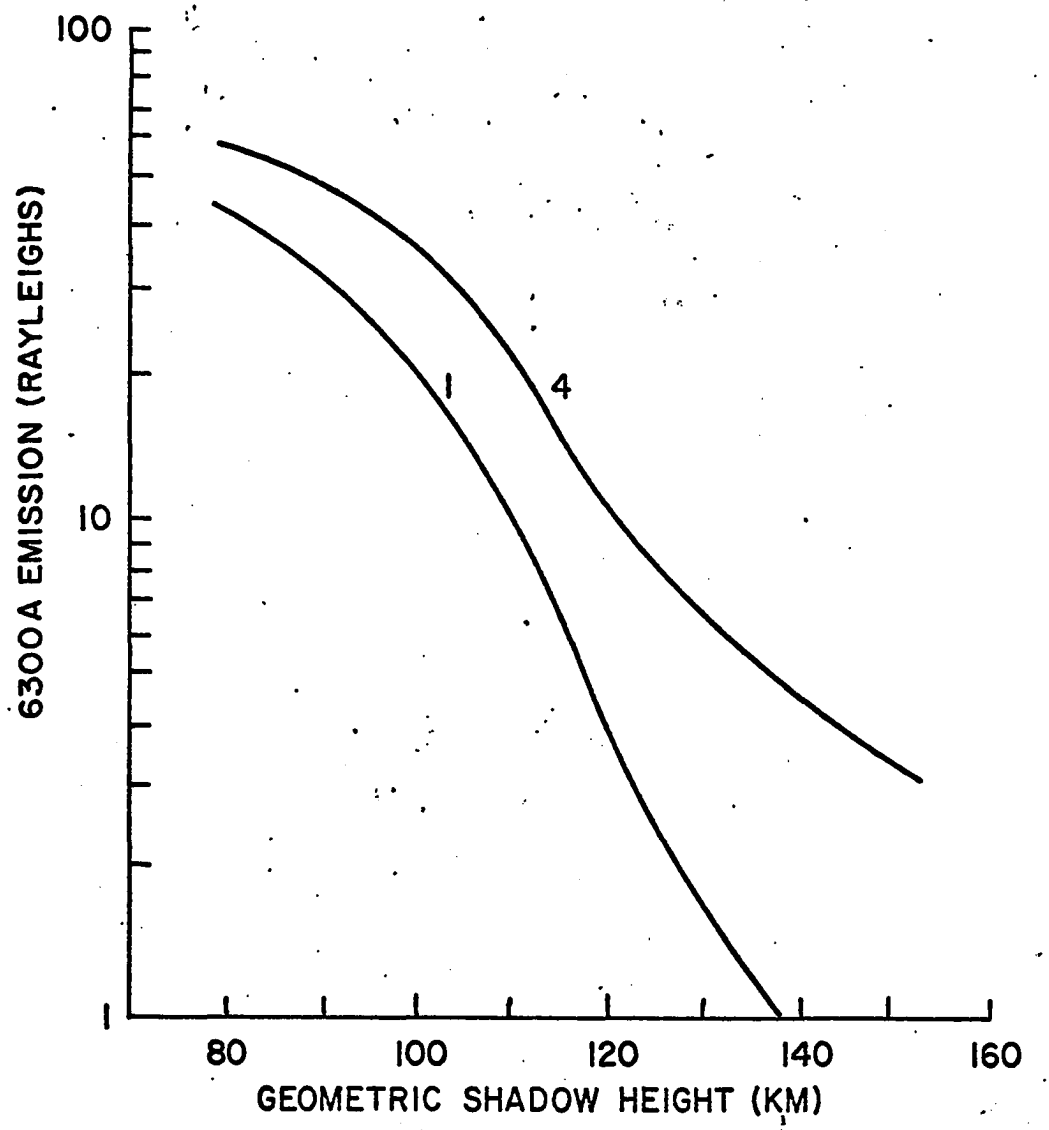

Fig. 5.5 The calculated zenith intensity of 6300 A emission due to photodissociation of O_2 by sunlight in the Schumann-Runge continuum versus the height of the earth's geometric shadow at 100.5° SZA. The atmospheres used were the CIRA 1965 models 1 and 4, hour 04 with T_∞ = 705°K and 883°K respectively. The quenching was by N_2 at 10^{-11} cm^3 sec^{-1}.

(more negative). 5) decreasing the quenching coefficient for a single quenching species changes the curve in the same manner as 4) above. 6) increasing the temperature, on the other hand, produces the opposite effect: intensities at larger solar zenith angles are relatively greater (see Fig. 5.5). That is, the slope (negative) increases (less negative).

Figs. 5.3, 5.4, and 5.5 are thus the best means of illustrating the usefulness of the red line observations. Because there is thought to be only one major process contributing to the production of $O(^1D)$ the number of variables is reduced to a minimum. Solar flux in the Schumann-Runge region is thought to change very little during the solar cycle; it is quoted to be within $\pm$ 15%. The Schumann-Runge absorption coefficients are well-known and the actual production efficiency of ^1D in this wavelength region should not be far from the values used here. While some improvements can be made in the analytical expressions for the twilight geometry, it is not a major source of error. What remains to be determined from a comparison with observations is a model atmosphere; which after all is one of the main purposes of the observations in the first place.

It is indeed fortunate that the O_2 population, and the number density gradient affect the intensity versus shadow height curves in different ways (see points 4) and 5) above). There is, therefore, some hope that enough observations can be made under favorable conditions, to allow determination of the O_2 population and its distribution with altitude.

It is unfortunate that the quenching factor and even the quenching species are still debated. Even if the coefficient were known, the role of N_2 as the quenching species requires assumptions which weaken the final purpose: determination of O_2 density with altitude. As mentioned above, one method

of correcting for this effect is to monitor the $O(^1S)$ emission, which is not quenched appreciably above 120 km. There are difficulties with this which will be pointed out later.

Up to this point, only one sweep has been considered. One of the major characteristics of the true twilight enhancement is the change in character and the separation of the intensity versus shadow height curves generated by each azimuth sweep as the sun comes up. This characteristic led to Barbier's puzzlement as to the actual scale height of the emitting layer, because one sweep indicated a small scale height (40 km) and the collection of sweeps indicated a larger one (70 km). Fig. 5.6 is a plot of the volume emission rate with altitude toward the sun for two values of the solar depression angle. It shows that neither of the scale height observations were correct and that they were the result of an apparent change in the altitude of the maximum emission region. The effect is caused by the changing absorption of the sunlight which reaches any point as the sun rises. That is, because the absorbing species is also the emitting species, and the absorbing and emitting wavelength are different, the relative amount of effective radiation ($\lambda < 1750$) towards the sun and away from the sun increases as the sun comes up because the absorbing path becomes shorter. This can be seen in Fig. 5.1 by imagining the change in β_o as α becomes smaller: the point of observation approaches the terminator where the absorbing path is half the amount traversed by sunlight acting on the atmosphere on the night side of the observer. The effects of changing such parameters as the exospheric temperature are much more apparent at smaller solar zenith angles because of the large absorption effects combined with the relatively small scale height of O_2.

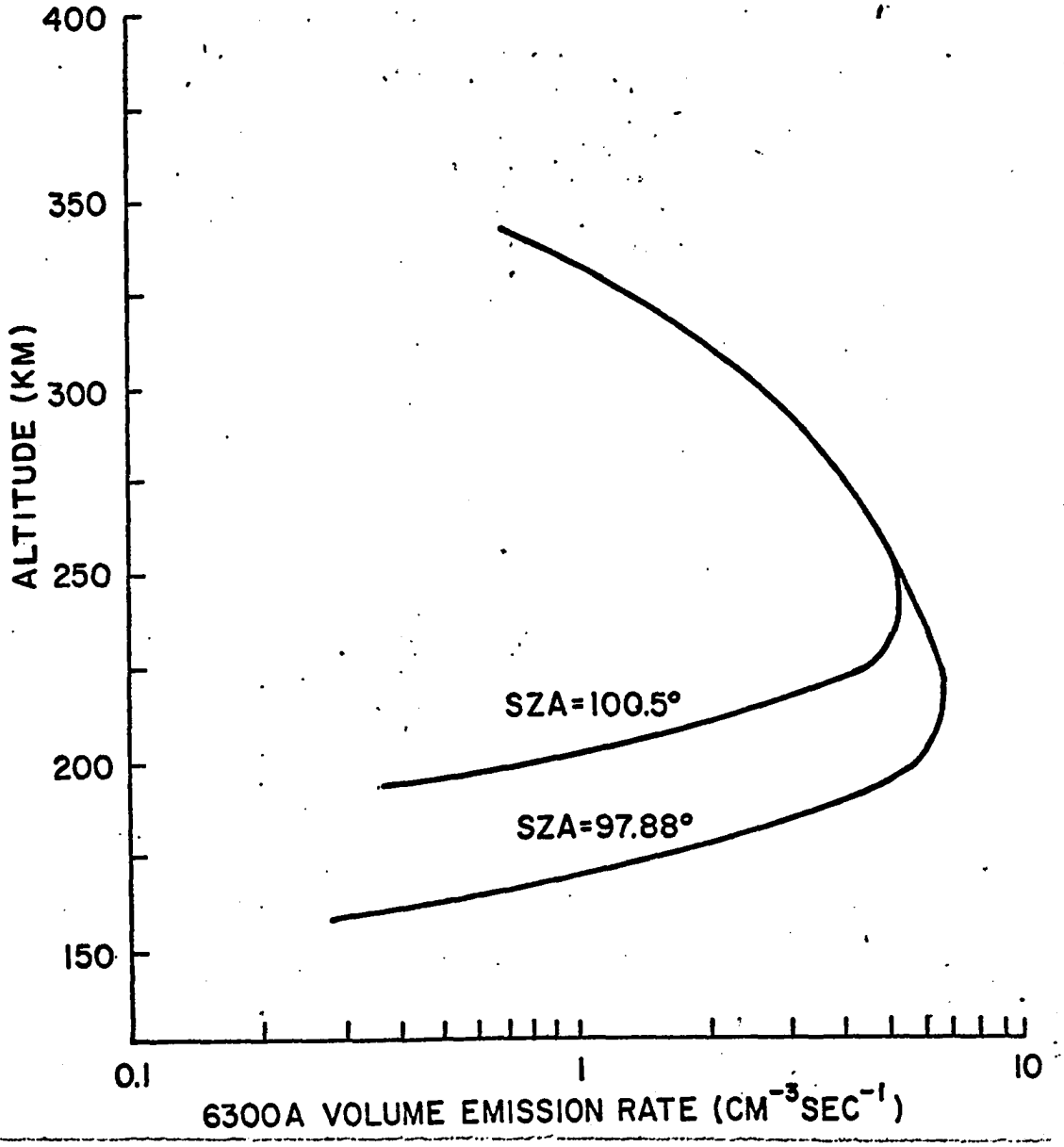

Fig. 5.6 The calculated volume emission rate of 6300 A emission due to photodissociation of O_2 by sunlight in the Schumann-Runge continuum versus altitude for observations toward the sun at 65° ZA. The atmosphere used was the CIRA 1965 Model 1 hour 04 (T_∞ = 705°K).

5.3 The 6300 A Observations

Of the ten morning twilights scaled for this study, seven were suitable for some kind of analysis. The dates and some pertinent information about magnetic activity and relative enhancement are given in Table 5.2. Auroral activity was present to a varying degree in all the twilights. Those with a very low K sum showed 6300 A enhancement in the geomagnetic north, with little or no associated green line. The morning twilight on 21 January 1964 is a good example of this situation (see Fig. 4.14); for this period the K_p sum was 02. An example showing the difference between auroral and twilight enhancement in both red and green lines is shown in Figs. 5.7 and 5.8. In this case, 31 October 1963, the K sum was 09, and the shift of the red line maximum to the azimuth of the sun is easily seen. Not so obvious, however, is the 5577A twilight enhancement; it is merely indicated by a general shift of isophotes to the southeast as the sun rises.

In order to compare realistically the observed twilight enhancements with the results calculated in the previous section, the auroral component must be removed from the observed intensity. This is accomplished by subtracting from the observed twilight intensity an amount corresponding to the auroral intensity at that particular azimuth observed before the twilight set in. This method is crude, and the results depend on the stability of the aurora over a period of about one half hour. Figures 5.9, 5.10, and 5.11 show that the correlation leaves something to be desired, but the general trend is quite obvious.

The most obvious aspect of the morphology of the 6300 A twilight enhancement is the separation of the azimuth sweeps on the curve of

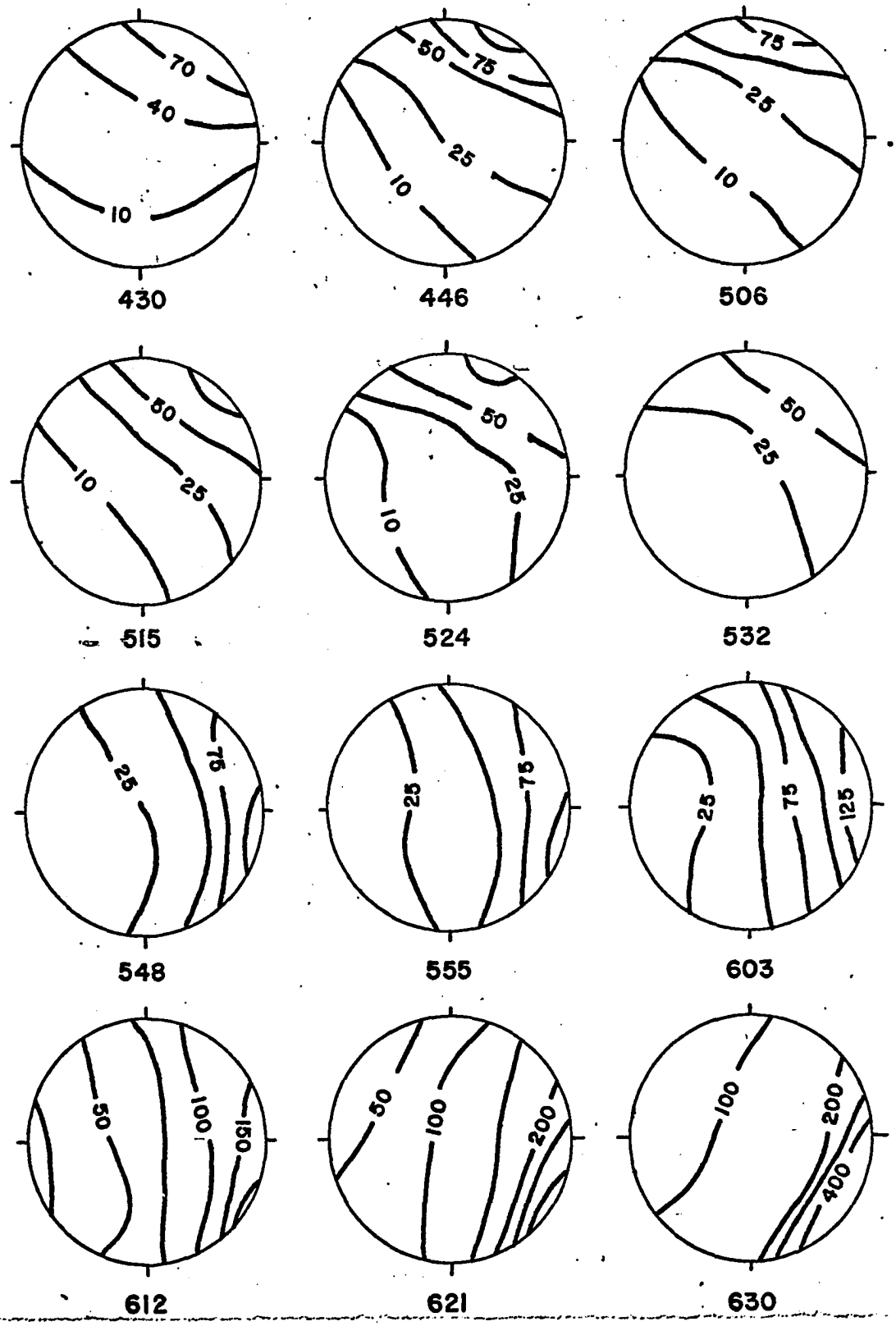

Fig. 5.7 Circular plots of the sky showing the approximate intensity distribution of 6300 A zenith emission (Rayleighs) over Alaska on 31 October 1964 (150° WMT). The top is north; east is to the right.

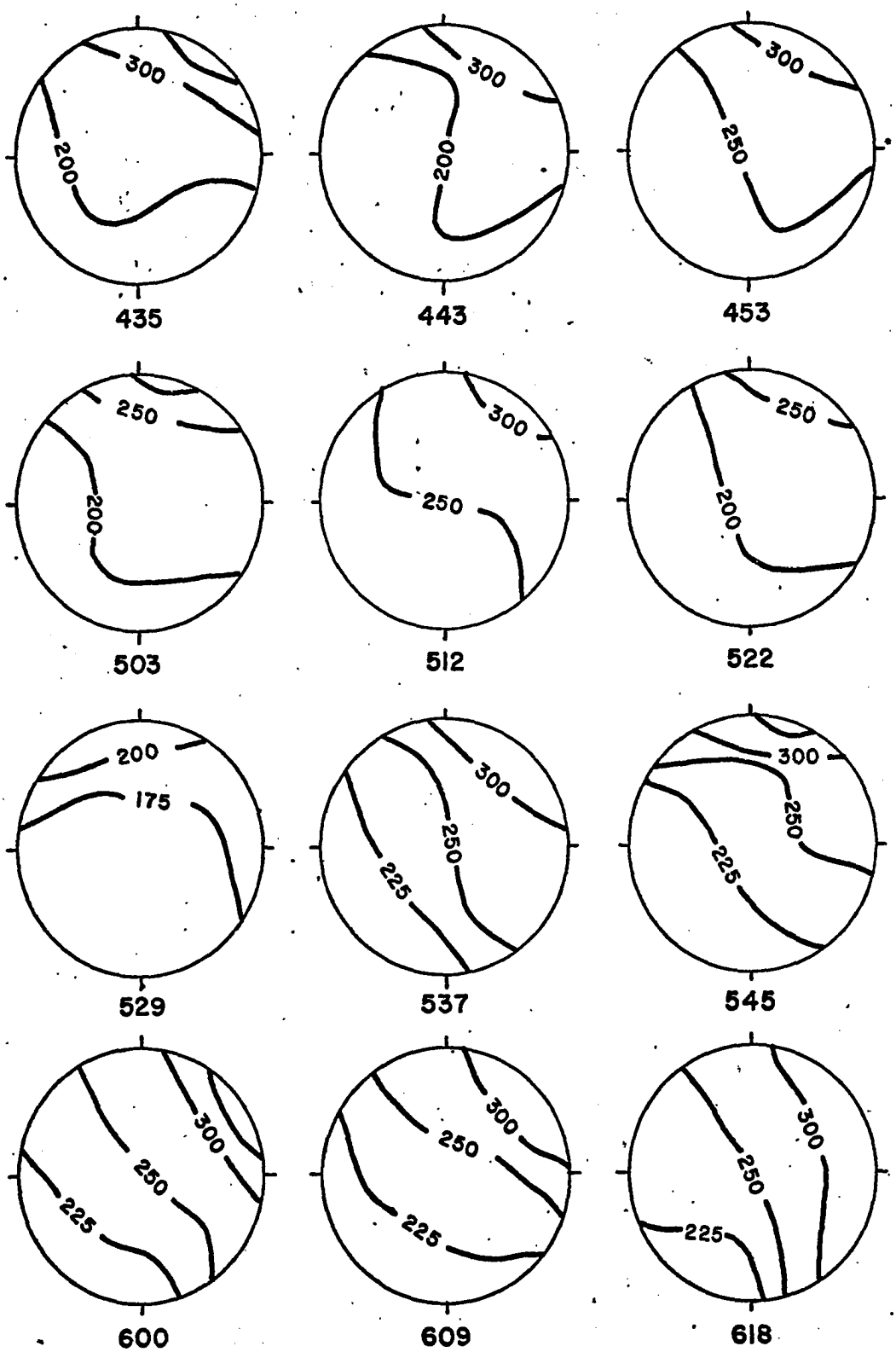

Fig. 5.8 Circular plots of the sky showing the approximate intensity distribution of 5577 A zenith emission (Rayleighs) over Alaska on 31 October 1964 (150° WMT). The top is north; east is to the right.

log intensity versus shadow height. Figure 5.9 shows a clear example of this effect in both the calculated and observed sweeps at solar depression angles 7.88 and 10.5 degrees. The explanation of this effect appeared in section 5.2 above and was illustrated in Fig. 5.6.

Ideally, the calculated curves could be adjusted to meet the observed curves by using different values of exospheric temperature for the model atmosphere. One should then find the number density and height distribution of the O_2 molecules. As is obvious from Figs. 5.9, 5.10, and 5.11, the amount of O_2, the quenching coefficient and the quenching species can be adjusted to fit the data.

The data are best fit by using the CIRA atmosphere corresponding to an exospheric temperature between 705° and 885°; the quenching species seems to be N_2 with a rate coefficient of approximately 1 to 3 x 10^{-11} cm^3 sec^{-1}. This value is quite sensitive to the density ratio $n(O_2)/n(N_2)$. The value found by Wallace and McElroy (1966) was at least 7 x 10^{-11} cm^3 sec^{-1}, which is higher than the value found here, but the density ratio $n(O_2)/n(N_2)$ differed by a factor of two. Thus the difference between the values is small, but the value derived here is more in agreement with the results of Hunten and McElroy (1966).

Although the errors involved in the intensity calculation and in the photometer calibration could combine to introduce some ambiguity as to the species of the quenching agent, the number density of O_2 produces a steeper curve. Considering both the curves in Fig. 5.9, the data seem to fit the N_2 curves somewhat better. Unfortunately, the last three or four azimuth values looking away from the sun produce

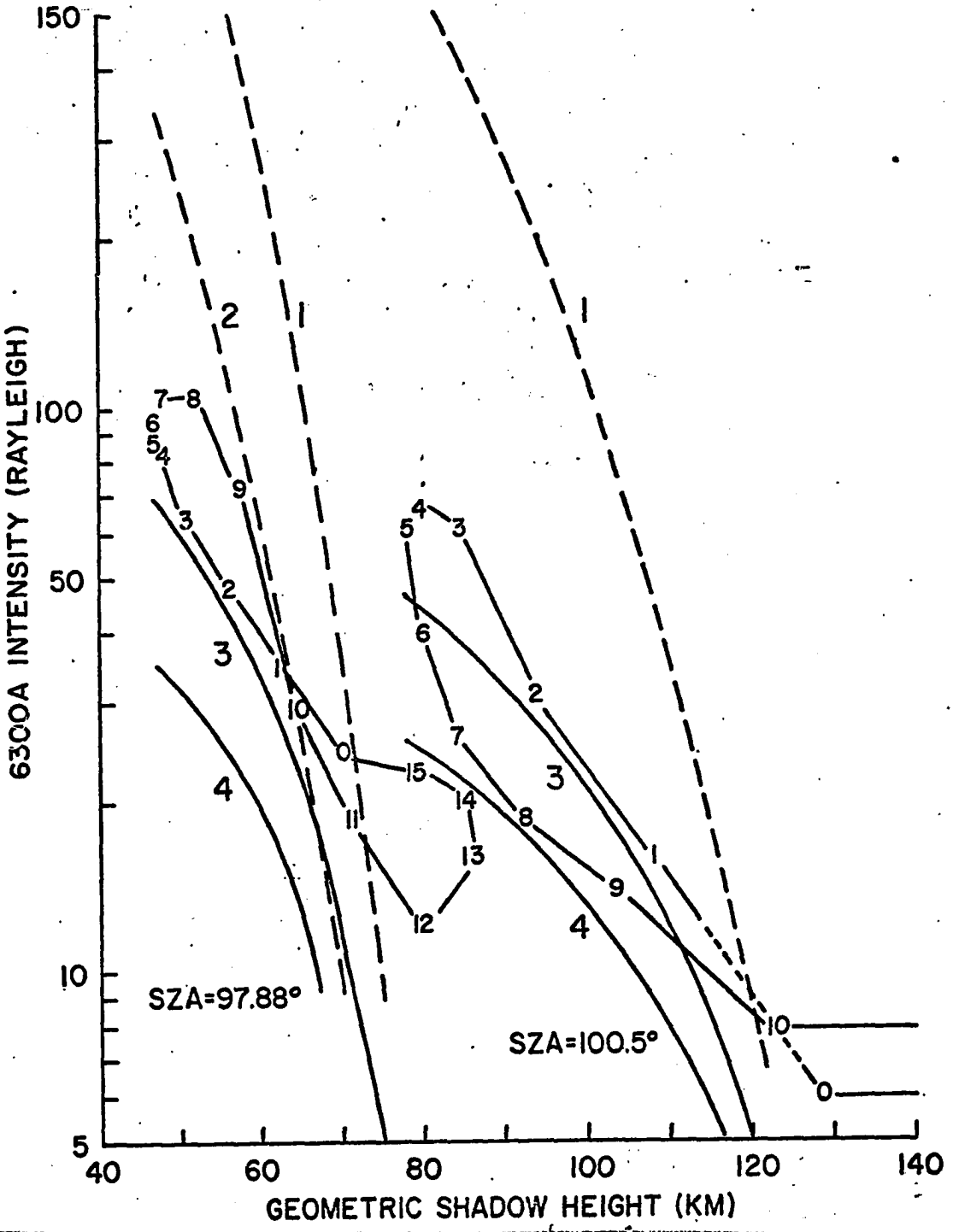

Fig. 5.9 The calculated (lines) and observed (closed loops) zenith intensity of 6300 A emission due to photodissociation of O_2 by sunlight in the Schumann-Runge continuum versus the height of the earth's geometric shadow, for 97.88° SZA and 100.5° SZA. The quenching is: 1) by O_2 at 10^{-11} cm^3 sec^{-1}, 2) by O_2 at 10^{-10} cm^3 sec^{-1}, 3) by N_2 at 10^{-11} cm^3 sec^{-1}, 4) by N_2 at 5×10^{-11} cm^3 sec^{-1}. The CIRA 1965 Model 1, hour 04 was used for a model atmosphere. The numbers on the observed curves refer to the directions in azimuth every 22½° clockwise from north. The azimuth sweep was at 65° ZA on 21 January 1964.

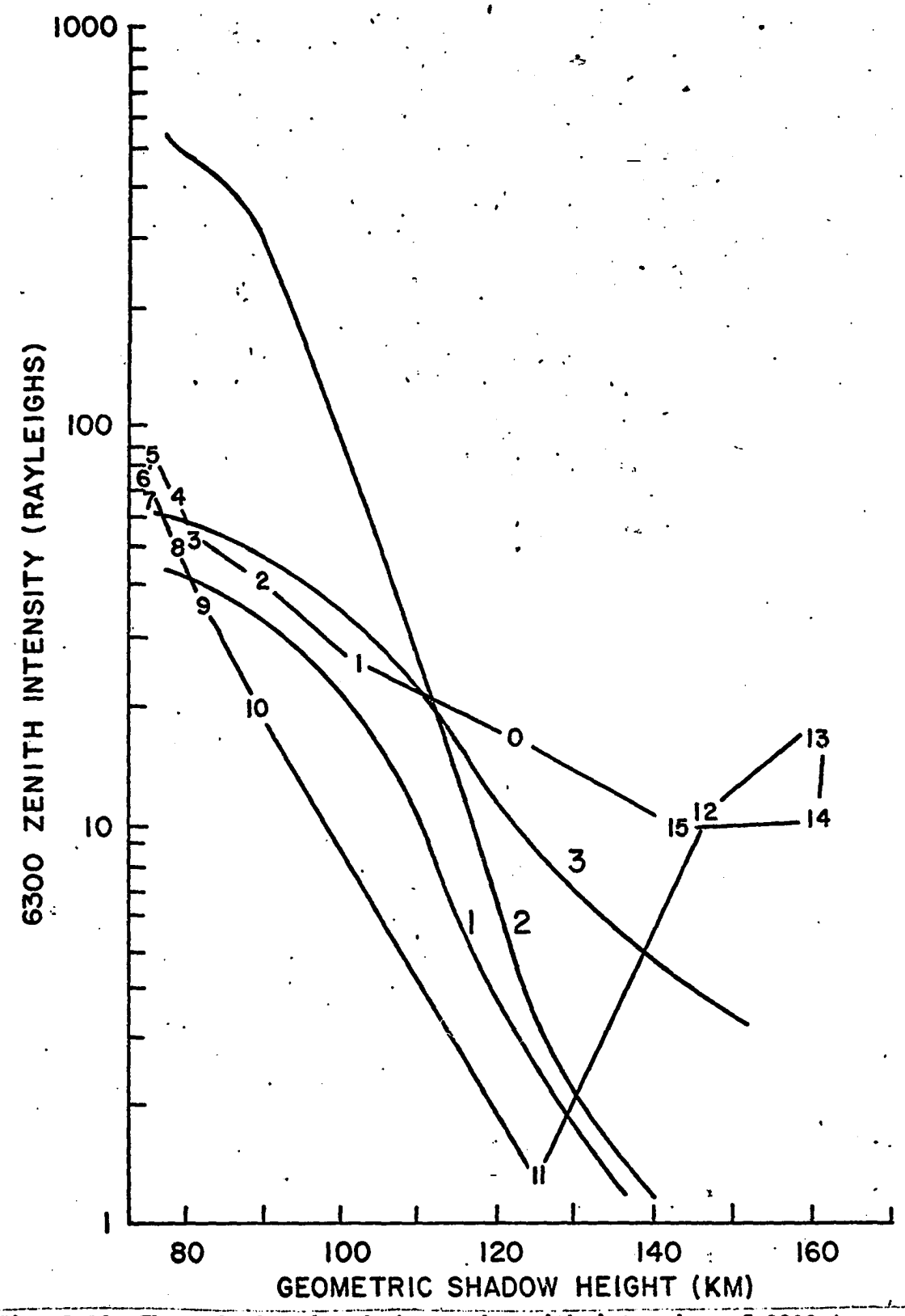

Fig. 5.11 The calculated and observed zenith intensity of 6300 A emission due to photodissociation of O_2 by sunlight in the Schumann-Runge continuum versus the height of the earth's geometric shadow at 100.5° SZA. Curve 1) CIRA 1965 Model 1, T_∞ = 705°K quenching by N_2 at 10^{-11} cm^3 sec^{-1}. Curve 2) CIRA 1965 Model 1, quenching by O_2 at 10^{-11} cm^3 sec^{-1}. Curve 3) CIRA 1965 Model 4, T_∞ = 885°K, same quenching. The numbers on the observed curve refer to the direction of the observation in azimuth every 22½° clockwise from north. The azimuth sweep was at 65° ZA on 21 January 1964.

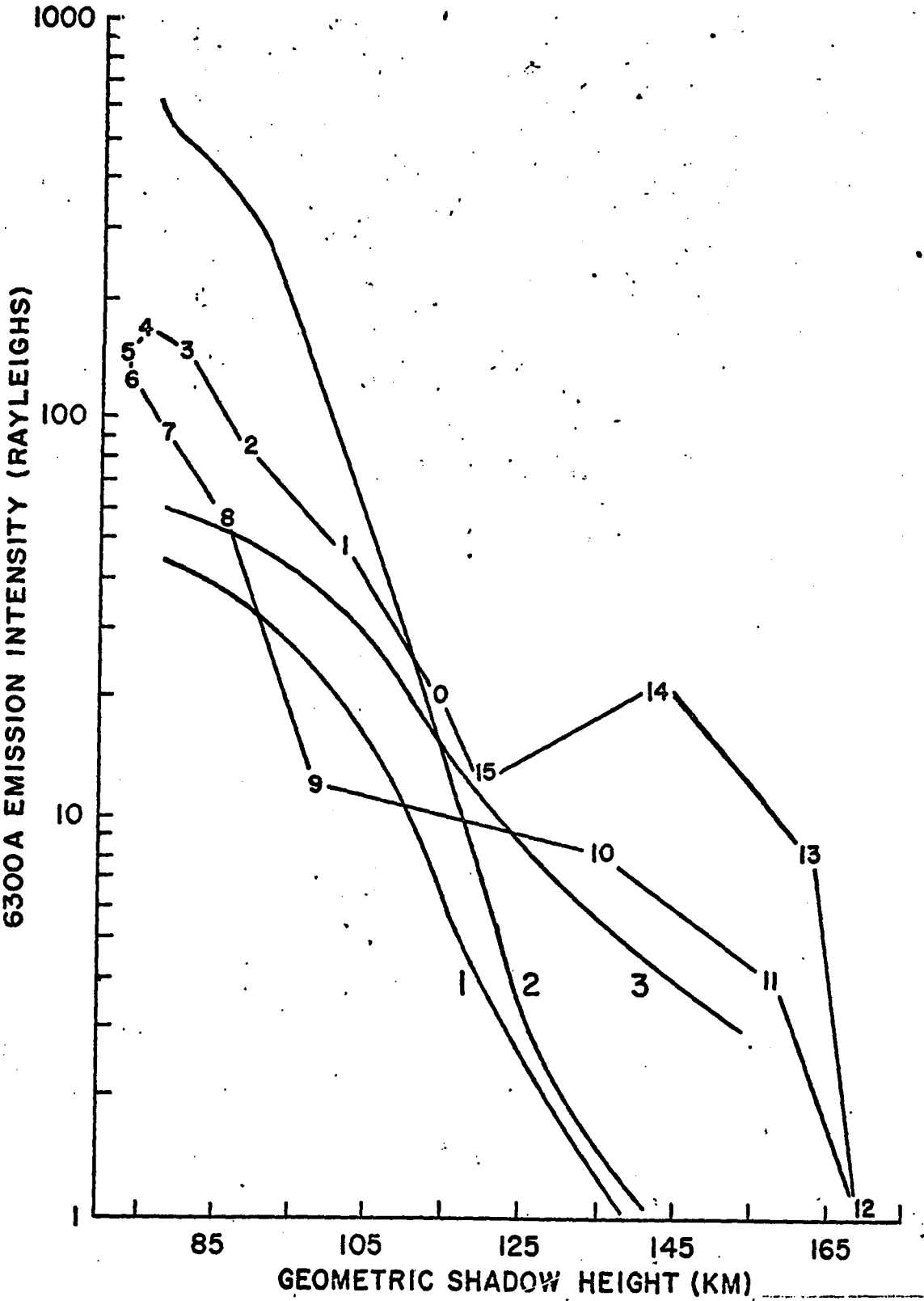

Fig. 5.10 The calculated and observed zenith intensity of 6300 A emission due to photodissociation of O_2 by sunlight in the Schumann-Runge continuum versus the height of the earth's geometric shadow at 100.5° SZA. Curve 1) CIRA 1965 Model 1, T_∞ = 705°K quenching by N_2 at 10^{-11} cm^3 sec^{-1}. Curve 2) CIRA 1965 Model 1, quenching by O_2 at 10^{-11} cm^3 sec^{-1}. Curve 3) CIRA 1965 Model 4, T_∞ = 885°K, same quenching. The numbers on the observed curve refer to the direction of the observation in azimuth every 22½° clockwise from north. The azimuth sweep was at 65° ZA on 31 October 1964.

values of $\beta_o \gtrsim 0.3$, which is larger than the approximation will allow (see section 5.2). Thus, the intensities calculated away from the sun may be low. However, this only makes it more conclusive that the quenching agent is N_2 and the rate coefficient is approximately 1 to 3 x 10^{-11} cm^3 sec^{-1}.

The range of intensities of the twilight 6300 A emission are shown by Fig. 5.12. The values at a shadow height of 50 km do not vary much, but two or three of the twilights would be listed by Barbier (1959) as 'abnormal'. The observations on 20 January 1964 have been plotted in Fig. 5.11. It is obvious that the increase in brightness takes place mainly at lower altitudes. Figures 5.13 and 5.14 indicate that in order to increase the intensity at lower altitudes, either the quenching rate is made smaller or the O_2 population increases. The latter process is the most probable and is illustrated by the volume emission rate curves in Fig. 5.13. The McElroy Model B and C atmospheres (see Table 5.2) were plotted using $T_\infty = 750°$ and N_2 quenching with a rate coefficient of 1 x 10^{-11} cm^3 sec^{-1}. The amount of O_2 in Model C is 10 times that in B, while the N_2 population remains roughly the same. A significant increase in emission rate at lower altitudes (250 km) is recognizable between B and C. It should be noted that although the Model C is considered to be rich in O_2, it is still not sufficient to account for the observed 6300 A intensity. Thus, the general conclusion is that the anomalous twilights are a result of horizontal and vertical transport of O_2 to the 250 km altitude region. Further confirmation of this result will be shown in a comparison with the 5577A twilight enhancement.

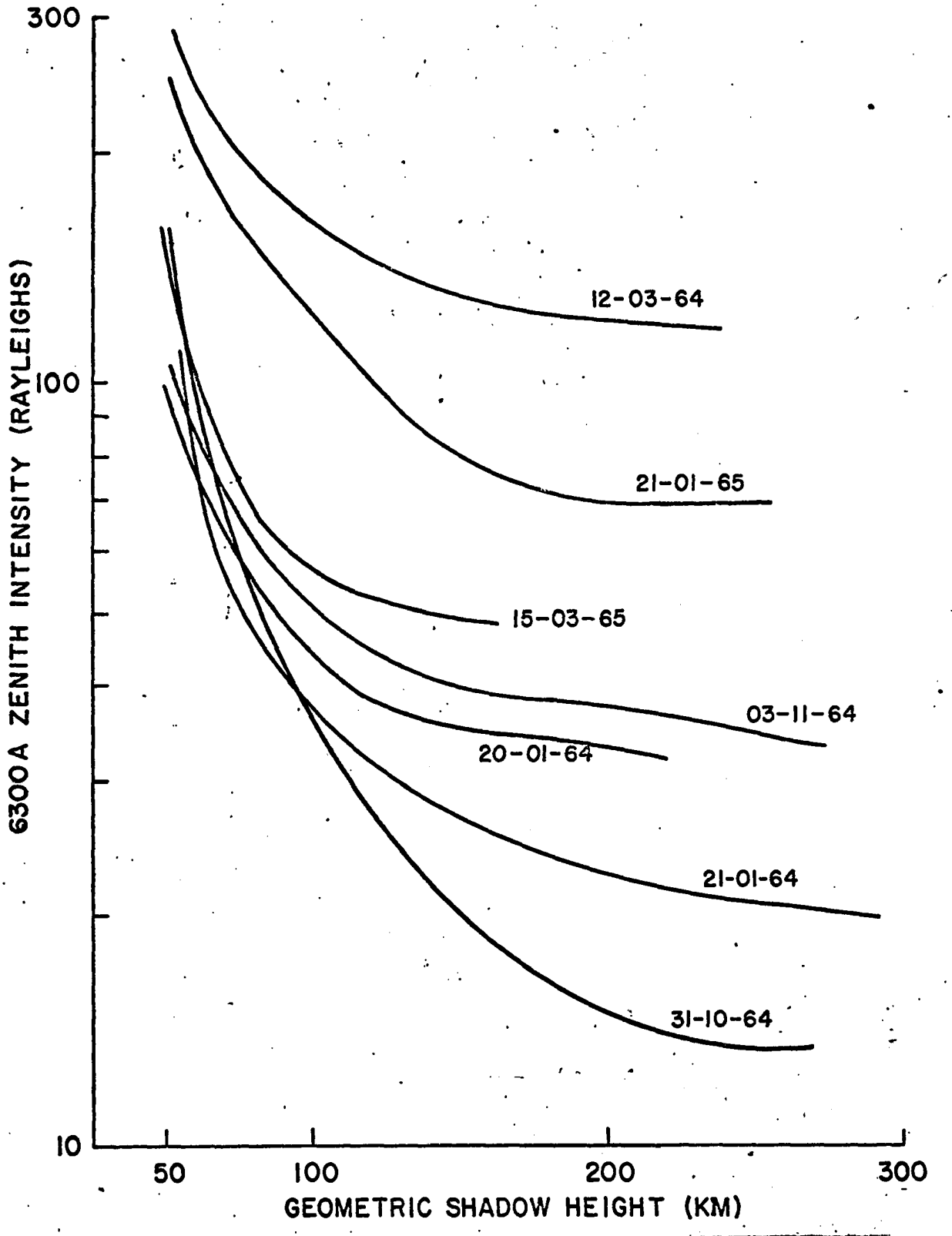

Fig. 5.12 Morning twilight observations of 6300 A emission in the zenith for various dates listed in Table 5.4.

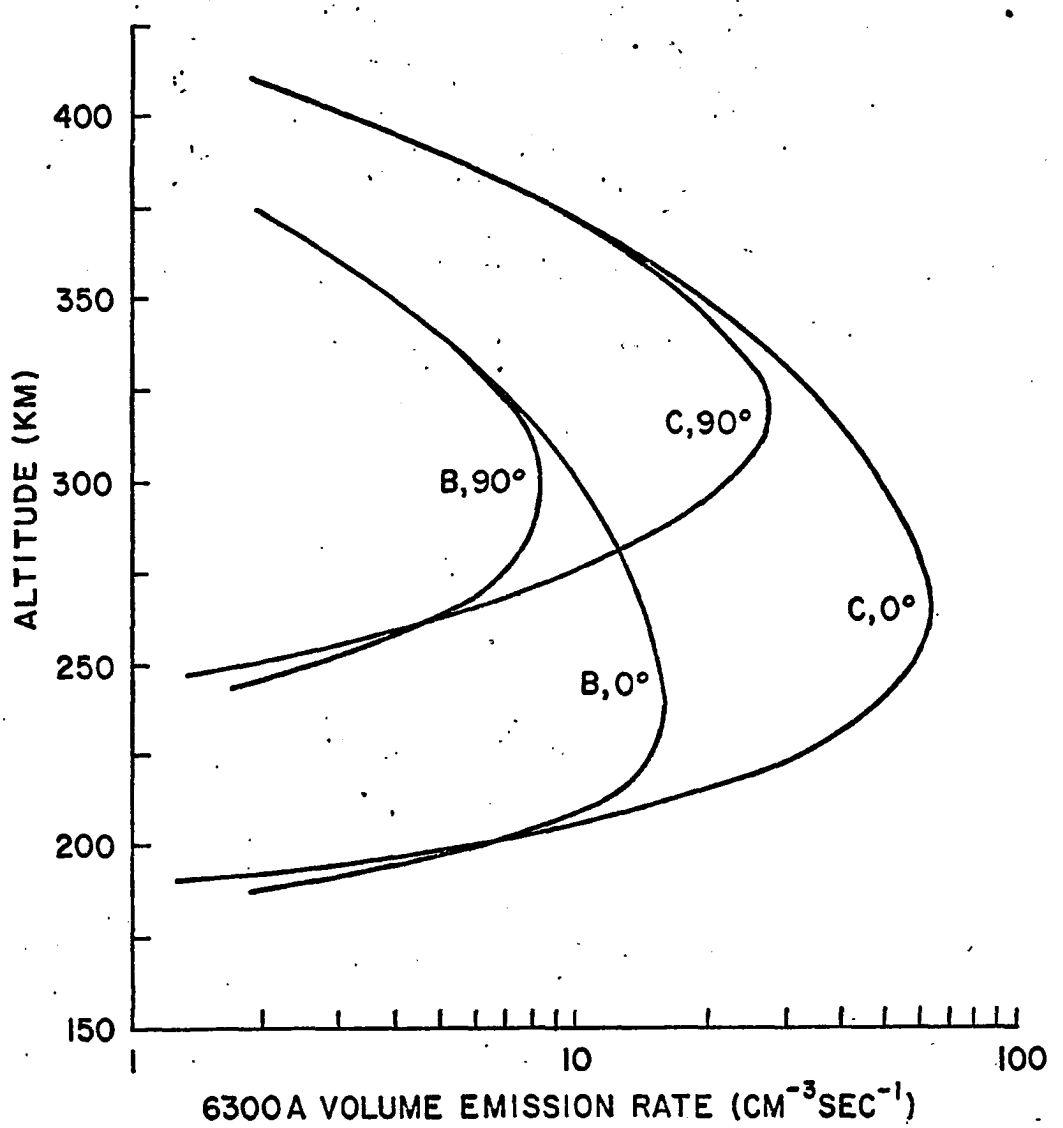

Fig. 5.13 The 6300 A [OI] emission rate quenched by N_2 with a rate coefficient of 10^{-11} cm^3 sec^{-1}, for McElroy atmospheres Models B and C, observed at 65° ZA toward the sun (0°) and at right angles to the sun (90°), all at 100.5° SZA.

The foregoing argument leads to one other direct conclusion. Figure 5.14 shows the volume emission rate versus altitude at two different values of T_∞, 750°K and 883°K for the same quenching rate and model atmosphere (CIRA, models 1 and 4). The increase in T_∞ results in an increase of the emission at high altitudes. One can conclude that abnormal twilights are not simply the result of an increase in the exosphere temperature. However, because T_∞ does affect the twilight intensity to a certain extent, one would expect to observe a dependence on solar activity. Barbier (1961) stated that he did not observe such a dependence. This could be explained by noting that his studies of the true twilight enhancement took place in the summer or at the equinoxes. During these periods, the position of the sub-polar sheet shifted from the north (where he mapped it during the winter) around towards the east where it would overwhelm whatever small variation there is in this true twilight enhancement.

5.4 The True Twilight Enhancement of 5577A[OI]

The green line was observed by Dufay and Dufay (1948) to show a small intermittent enhancement. Megill (1960) and Megill, Jamnick and Cruz (1960) found a morning and evening enhancement to occur sporadically during the IGY with an apparent winter maximum in intensity and occurrence. They found the effect to be present at 44°N, rare at 40°N and absent at 33°N. Negative results have been reported by Berthier (1956), Maartense and Hunten (1963), Koomen, Packer and Tousey (1956) and Manring and Pettit (1956). Although the observations of Megill were taken in the same manner as those reported here, the data handling

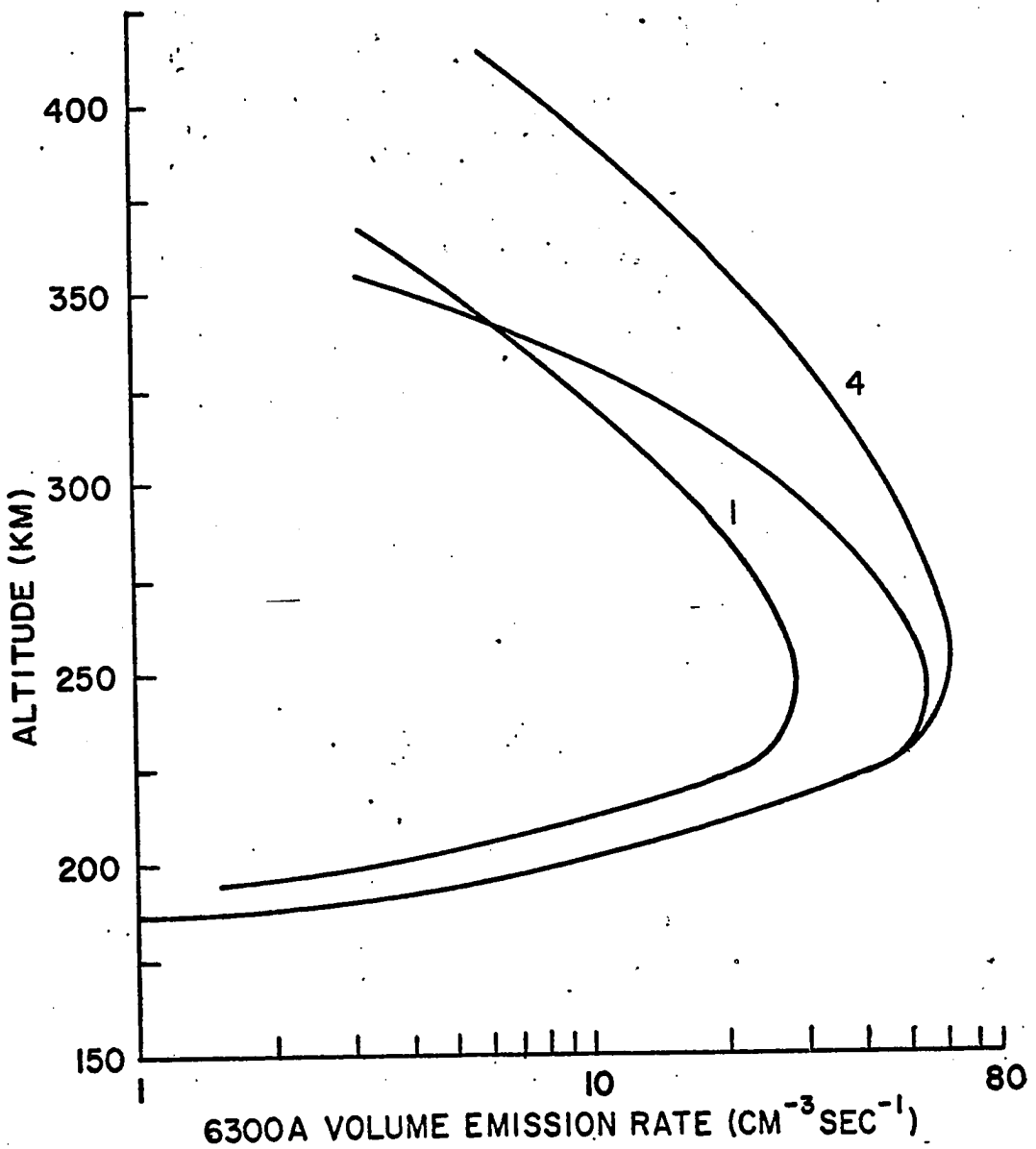

Fig. 5.14 The 6300 A [OI] emission rate versus altitude, Z_o. Curve 4 is calculated with CIRA 1965 Model 4, hour 04 at T_∞^o = 833°K quenched by N_2 at 10^{-11} cm^3 sec^{-1}. Curves 1 are calculated with CIRA 1965 Model 1, hour 04 at T_∞ = 705°K quenched by N_2 at 10^{-11} (middle curve) and 5 x 10^{-11} cm^3 sec^{-1}. The curves are calculated for observations toward the sun at 65° ZA for 100.5° SZA.

procedure was somewhat different.

Megill (1960) did not attempt to find the relationship of a single azimuth sweep to the general trend of sweeps. That is, the intensities observed in each altitude region were averaged through the whole twilight in an attempt to determine the scale height of the emitting species. The result, 30 km, did not appear to be the scale height of oxygen atoms in the region in which the suspected processes (fluoresence, resonance scattering) could take place. Figure 5.15 shows the green line observation by Megill on the morning of 7 January 1958. One of the most striking characteristics of this collection of points is that the intensity decays differently according to the direction in which the observation was made. This strongly suggests a mechanism like the one described for the red line in section 5.2 above.

Examination of the previous observations allows one to determine if the other characteristics of the enhancement can result from photodissociation of O_2. That the enhancement shows no morning-evening asymmetry would be expected of this mechanism. The sporadic appearance, the seasonal variation, the latitude dependence, and the association with solar maximum can all be explained from mass motion or diffusion of O_2. This might correspond to the "abnormal" twilights in the red line enhancement, observed by Barbier, which are associated with magnetic activity. The negative results reported by most searchers for the green line enhancement all occurred during minimum solar activity (with the exception of Elvey (1948) who was located at MacDonald Observatory, about ten degrees south of the latitude where Megill found

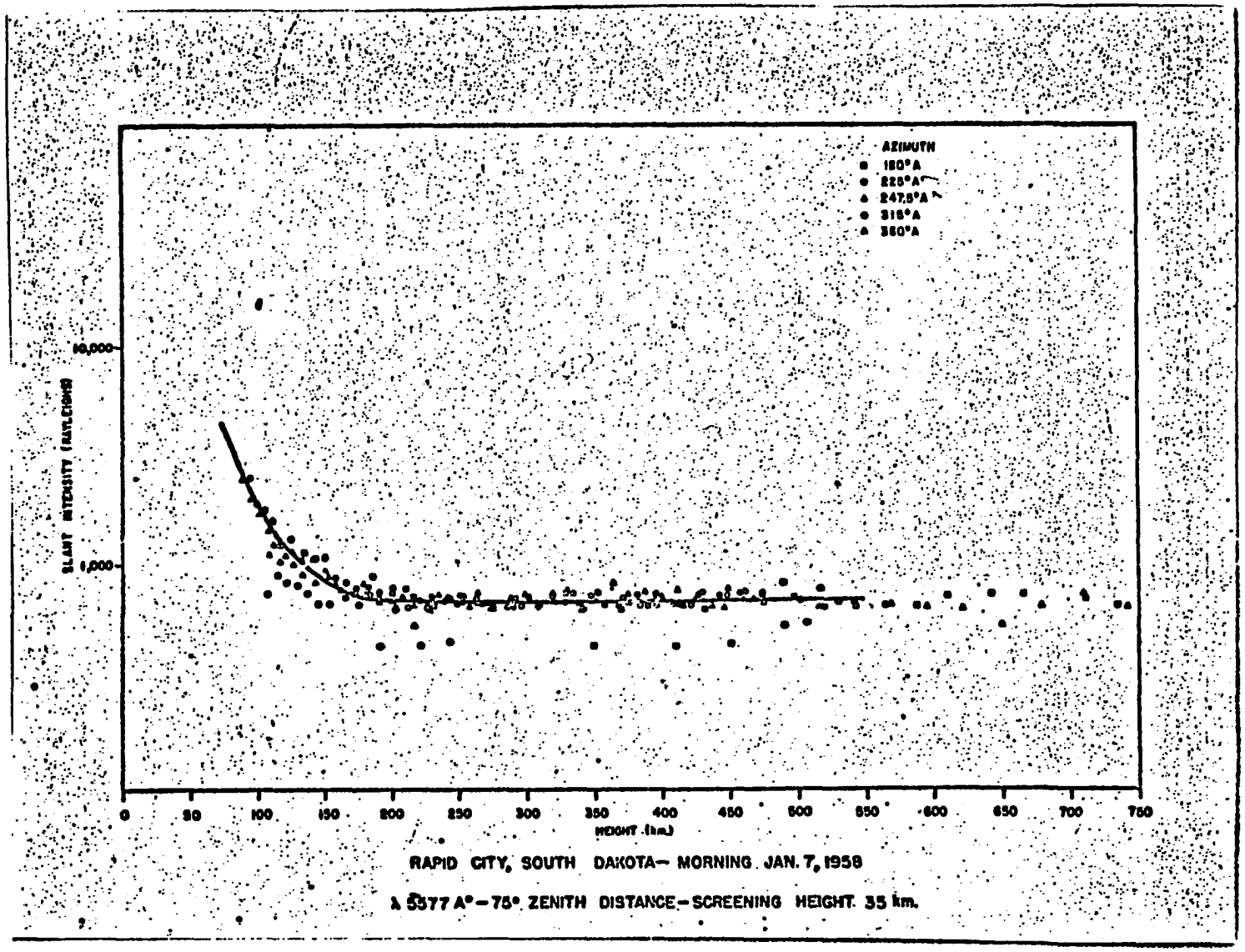

Fig. 5.15 A plot of the 5577 A slant intensity versus earth's shadow height Megill (1960).

the enhancement to occur with some frequency). The enhancements detected during the course of observations reported here could not have been detected without the rejection of the scattered solar continuum afforded by the birefringent filter and the spatial resolution possible with almucantar surveys. Two examples of the intensity versus geometric shadow-heights are given in Figs. 5.16 and 5.17.

The first example in Fig. 5.16, shows a relatively weak enhancement which is clearly indicated by the smooth change with shadow height of the intensity in the direction of the sun. Although the enhancement is not as obvious as the corresponding 6300 A emission (Fig. 5.18), the character of the traces is unmistakably the same: the intensity away from the direction of the sun is lower than one would expect, and each azimuth sweep indicates a different emission altitude.

The second example in Fig. 5.17, shows a stronger enhancement of the green line, but it appears against a fairly large auroral signal in the north. The smooth change of the intensity toward the sun is obvious, but the points away from the sun are lost in the aurora. Thus, the enhancement seems to retain its character under large changes in auroral activity (see Table 5.2). The evidence seems to justify an attempt to calculate the contribution to $O(^1S)$ which would be made in twilight by photodissociation of O_2.

The analytical expressions for the calculation of the 5577 A intensity to be expected from photodissociation of O_2 are the same as those developed above for the red line calculation. The obvious difference is in the choice of solar flux, absorption cross section, and quenching rate. The computer program for the 6300 A enhancement was modified

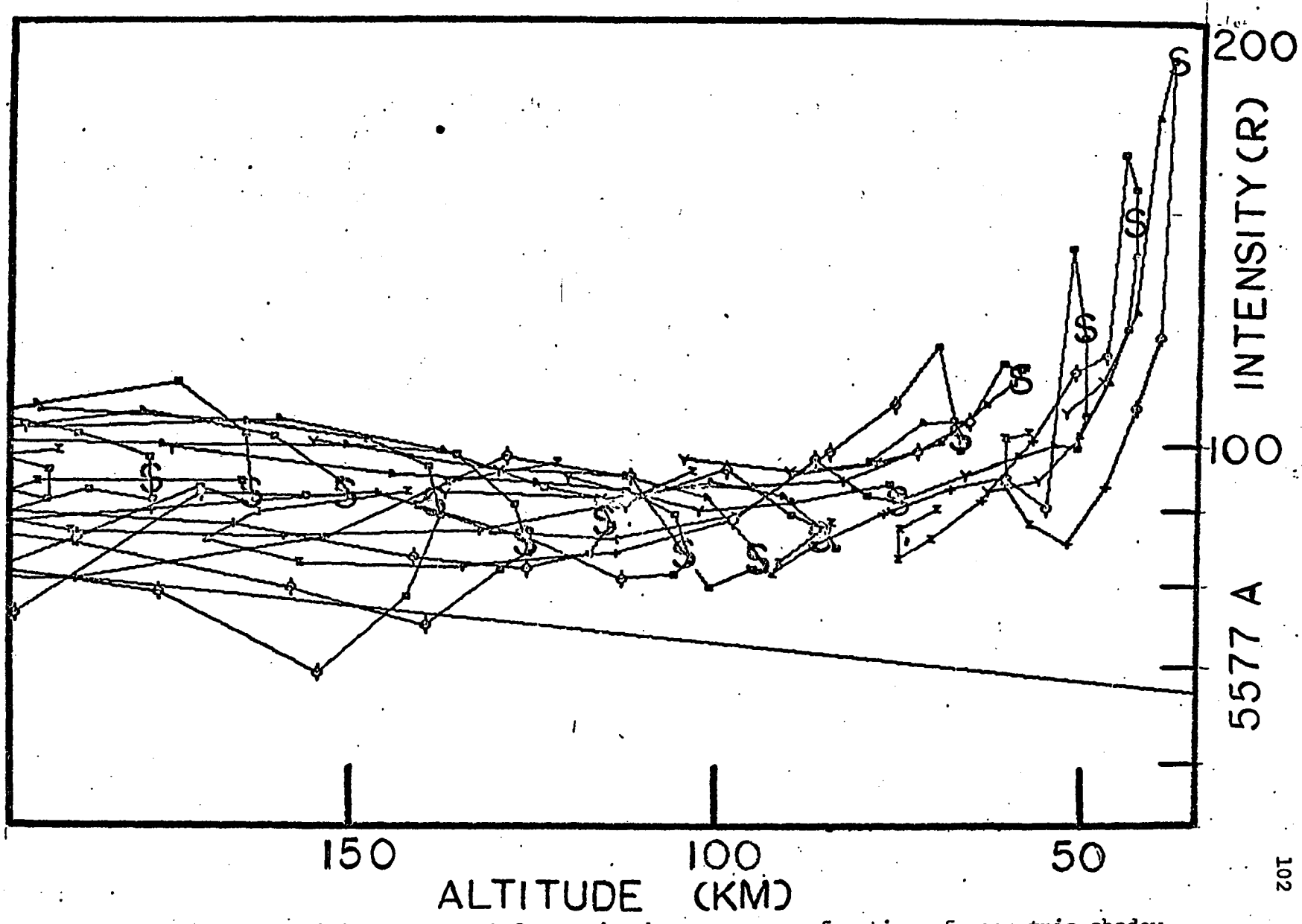

Fig. 5.16 Local zenith intensities of 5577 A from azimuth sweeps as a function of geometric shadow height. The symbols denote the azimuth angle of each observation, every 22½° measured from the sun (S is the sun; ◘ , toward the sun; ϕ, +, toward the south; Δ, Y, toward the north; Z, away from the sun). The symbols comprising a single azimuth sweep are joined by a line. The zenith angle for all the sweeps on this graph was 65°. The data are from the morning twilight of 21 January 1964 at College, Alaska.

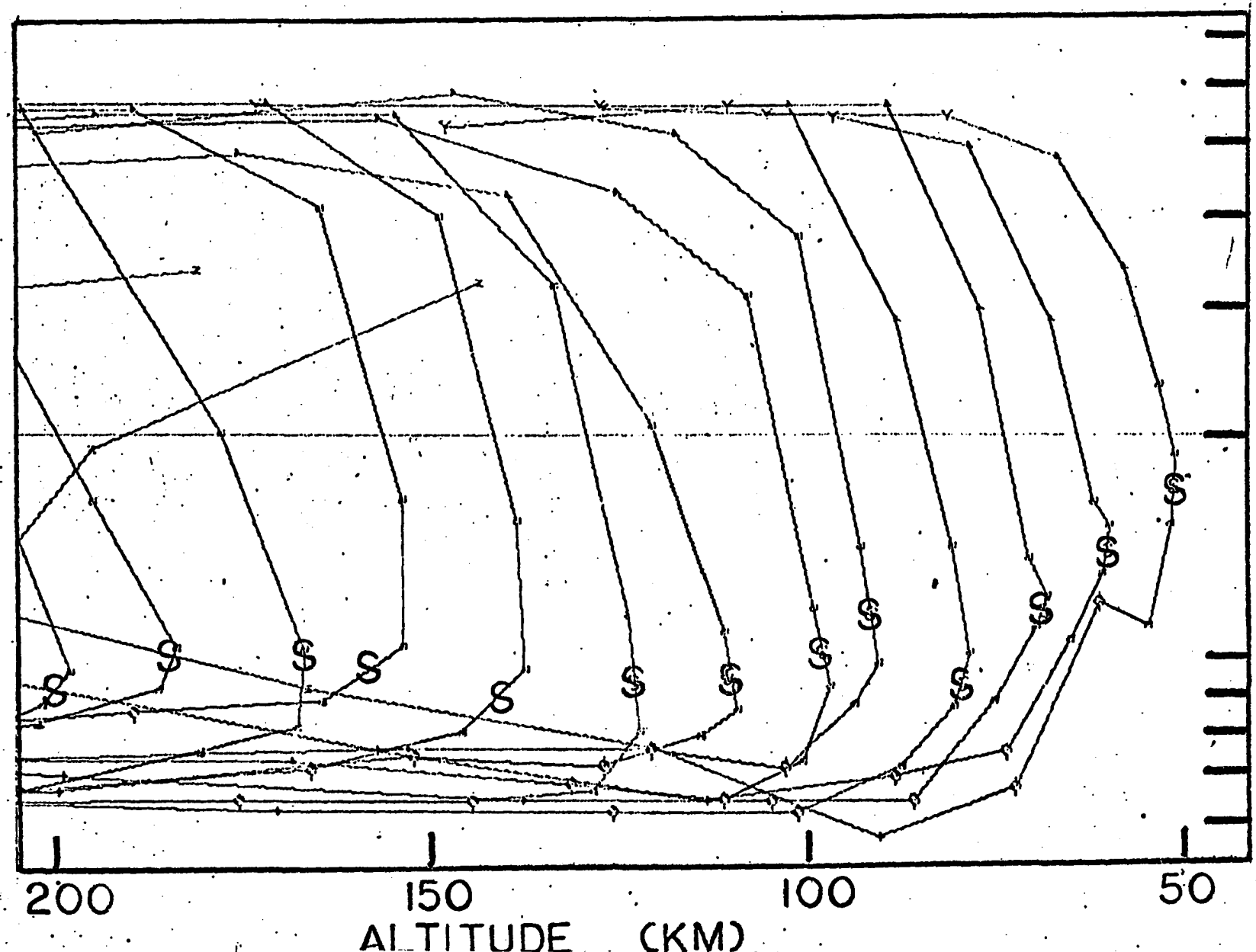

Fig. 5.17 Local zenith intensities of 5577 A from azimuth sweeps as a function of geometric shadow height. The symbols denote the azimuth angle of each observation, every 22½° measured from the sun (S is the sun; ¤ , toward the sun; ϕ, +, toward the south; Δ, Y, toward the north; Z, away from the sun). The symbols comprising a single azimuth sweep are joined by a line. The zenith angle for all the sweeps on this graph was 75°. The data are from the morning twilight of 21 January 1965 at College, Alaska.

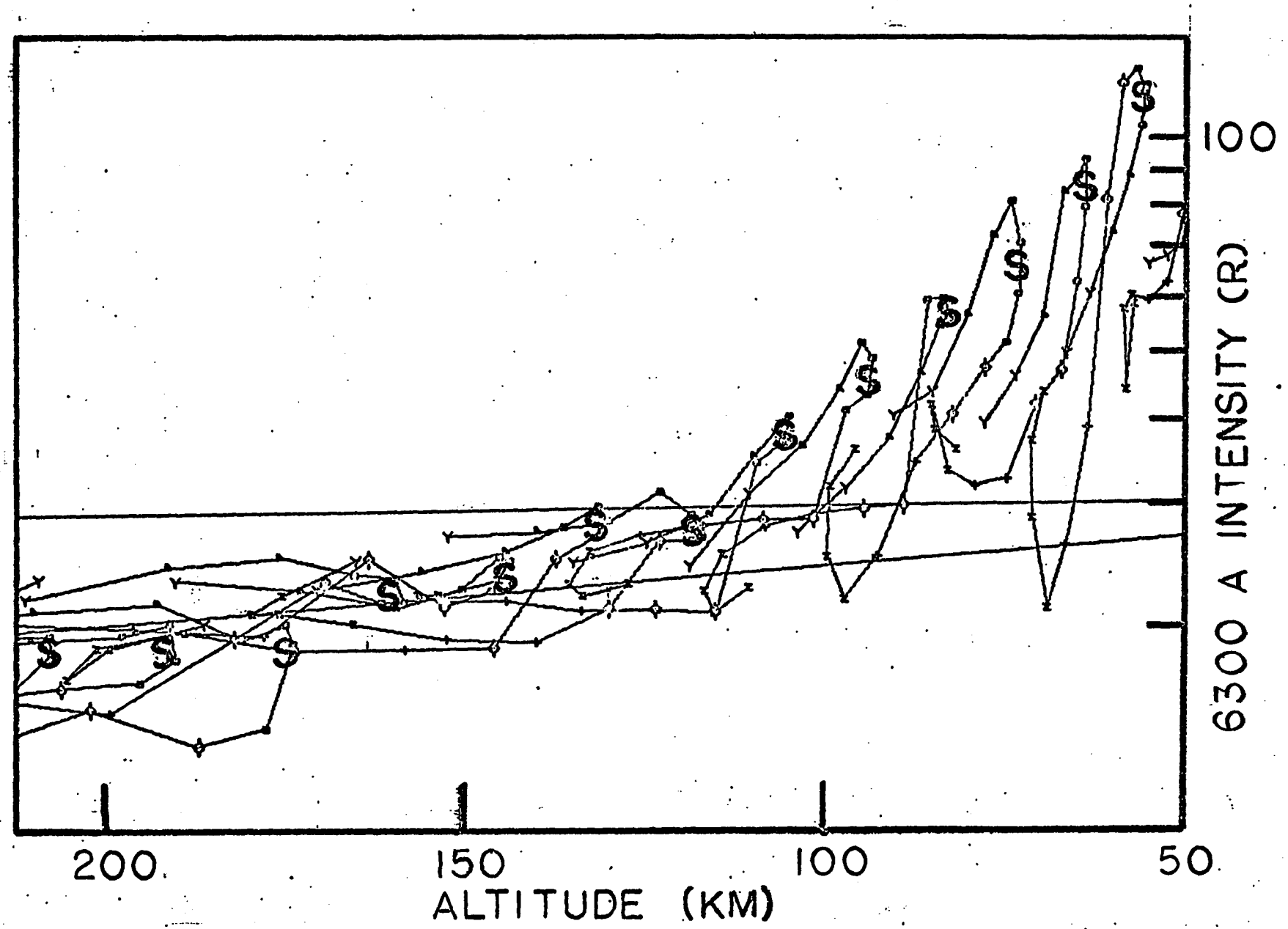

Fig. 5.18 Local zenith intensities of 6300 A from azimuth sweeps as a function of geometric shadow height. The symbols denote the azimuth angle of each observation, every 22½° measured from the sun (S is the sun; ◻, toward the sun; ϕ, +, toward the south; Δ, Y, toward the north; Z, away from the sun). The symbols comprising a single azimuth sweep are joined by a line. The zenith angle for all the sweeps on this graph was 45°. The data are from the morning twilight of 21 January 1964 at College, Alaska.

to remove the correction for quenching and substitute new values for solar flux and absorption cross section. Quenching is not important for the green line above altitudes of 120 km. The adopted values of solar flux and absorption cross section are given in Table 5.3 below.

Table 5.3

SOLAR FLUX AND ABSORPTION COEFFICIENTS USED FOR CALCULATION OF $O(^1S)$ FROM PHOTODISSOCIATION

Index	Wavelength Region	Solar Flux $\left(\frac{\text{Photons}}{\text{cm}^2 \text{ sec A interval}}\right)$	Absorption Cross Section	d factor
	1153 A	2E8	7.44E-18 cm^2	
	1205	4E9	1.60E-17	
2A	1244	1E9	4.46E-17	11.3E-8
	1292	3E9	7.75E-19	$\left(\text{sec}^{-1} \text{ molecule}^{-1}\right)$
	1210-1325	12E9	7.75E-19	
2B	2A flux doubled; 2A cross section doubled			45.2E-8
2C	2A flux, 2B cross section			22.6E-8

12E9=12x10^9

Photodissociation of O_2 leading to $O(^1S)$ was first discussed by Bates and Dalgarno (1954), who estimated that the dayglow value could be as high as 10 KR. Wallace and McElroy (1966) found the process to be of significant importance in the production of $O(^1S)$ observed by them from rockets during daytime. Walker (1965) thought the process would be of negligible importance in twilight, but he apparently did not use an adequate analytical treatment for the twilight situation. The greatest uncertainty in predicting the excitation rate is lack of knowledge of the absorption by O_2 in the spectral region between 1100 A and 1350 A.

Metzger and Cook (1964) record five "bands" in the absorption curve. There may be some continuum which is not identified, so one can only estimate the effective cross section. Table 5.3 lists the values scaled from the data of Metzger and Cook. The appropriate solar flux was read from the rocket data of Detwiler, et. al., (1961). The latter observers incidentally mention strong O_2 abosrption at 1243 A, 1163 A, and 1172 A in the altitude region 100 to 200 km. Three sets of solar flux-cross section combinations were used in the calculations in an attempt to determine an effective d-factor. Unfortunately, this was not meaningful because the variability of green line enhancement is such that it cannot be accounted for by changes in these two parameters alone (see section 5.5 below). Figure 5.19 shows the $O(^1S)$ excitation rate as a function of latitude for one observation towards the sun at SAZ=97.88°. The three curves show the effect of alternately doubling the solar flux and then the cross section. Decreasing the cross section reduces the altitude without much change in excitation rate. Increasing the solar flux increases the excitation rate without appreciably changing the altitude. There is no obvious explanation for the double maximum. It is probably an oscillation due to the greatly different values of the cross section used in the transmission function: the latter is a negative exponential and is very sensitive to large changes in cross section with wavelengths.

Integrating the volume emission rates in each direction in the same manner as with the red line calculation yields an approximation to the observed data as shown in Fig. 5.20. The observed log intensity versus geometric shadow height shown in this figure agrees quite well with the

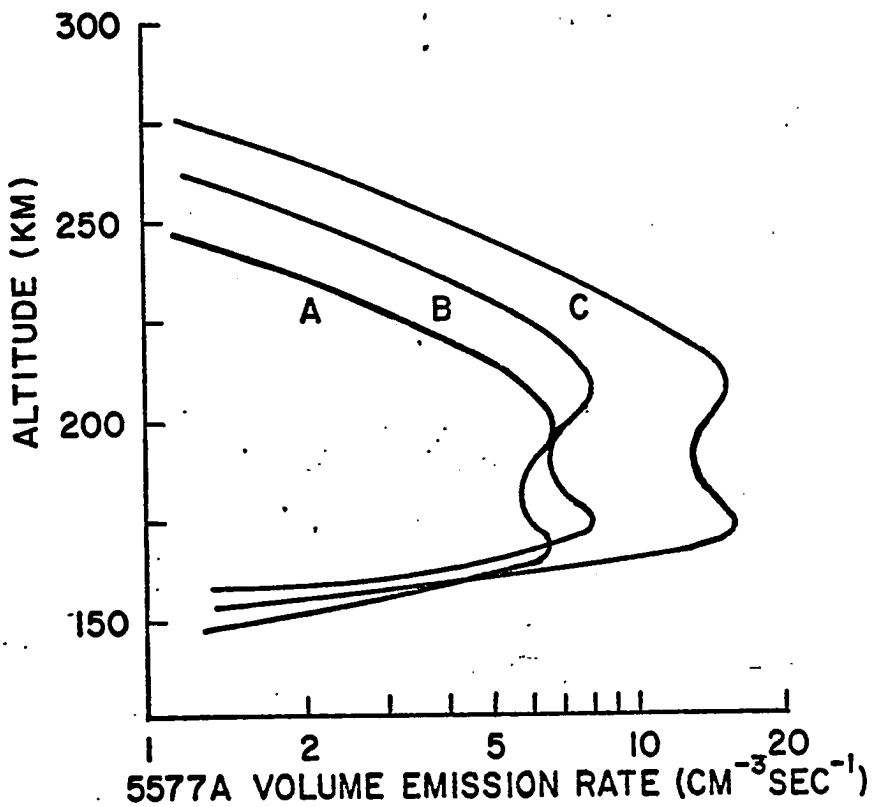

Fig. 5.20 The calculated and observed zenith intensity of 5577 A emission due to photodissociation of O_2 by sunlight in the 1100 to 1300 A region (values listed under "ZA" in Table 5.3) versus the earth's geometric shadow. The curve is calculated, with no allowance for quenching, using the CIRA 1965 Model 1, hour 04, for observations at 100.5° SZA. The numbers on the observed curve refer to the direction of observation in azimuth every 22½° clockwise from north. The azimuth sweep was at 65° ZA on 21 January 1964.

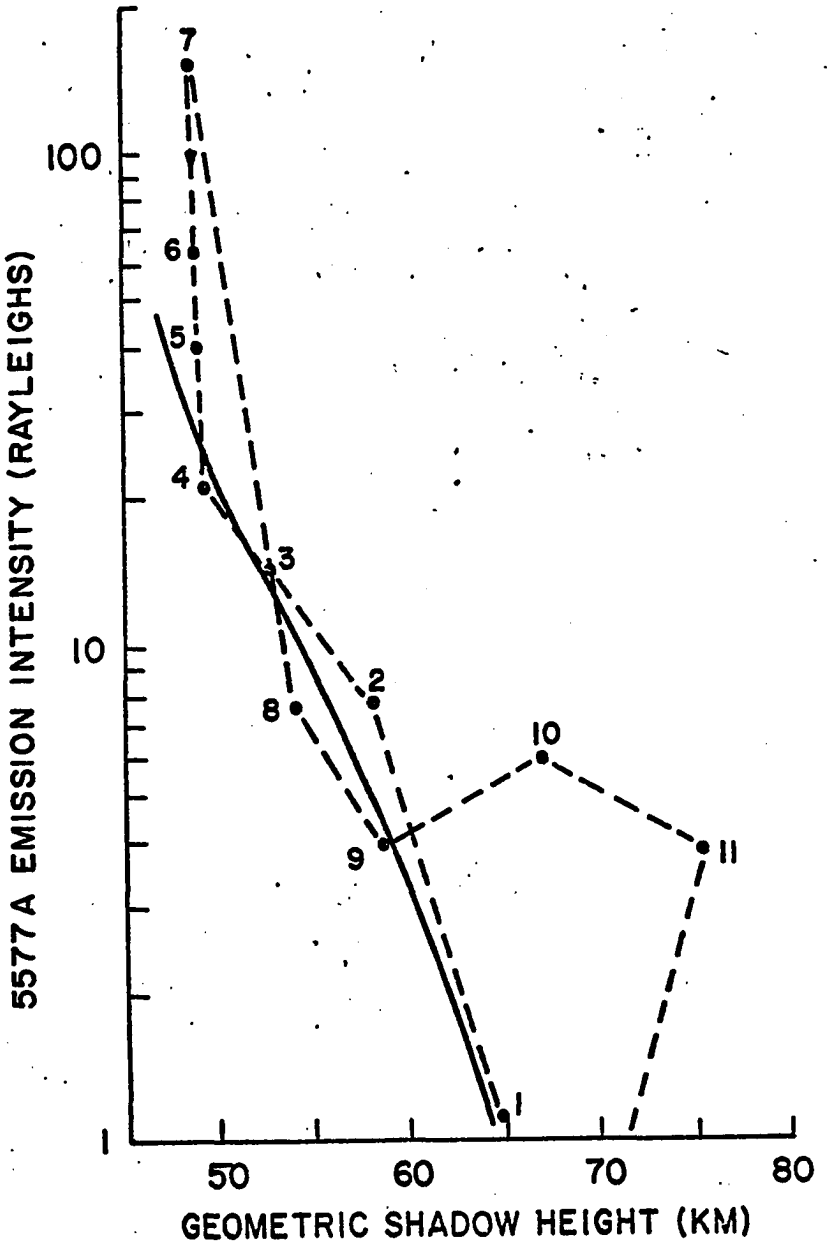

Fig. 5.19 The calculated 5577 A volume emission rate versus altitude, Z_o. The curves are calculated, with no allowance for quenching, using the CIRA 1965 Model 1, hour 04, for observations toward the sun at 65° ZA for 97.88° SZA. Curves A, B and C refer to different values of the solar flux and absorption cross section listed in Table 5.3.

calculated curve. The solar flux and absorption cross section labeled 2A seemed to fit this particular twilight, although the d-factor is probably not universally applicable, because the O_2 population may have been quite different from that of the model used for the calculation. This was, however, a "normal" 6300 A enhancement, and so perhaps the same may be said for the green line.

What can be said is that the twilight enhancement of the oxygen green line is due to photodissociation of O_2. The maximum emission for this particular observation took place between 150 km and 200 km altitude.

5.5 The Relationship Between the Red and Green Lines

The abnormally large enhancements of the red line observed both at College and Haute Provence have been described in 5.3 above. The intensity-height profile curves (Fig. 5.11) indicate that the maximum 6300 A emission rate occurs at lower altitudes during these enhancements. Another piece of evidence supporting this contention is found in the relationship between the red and the green enhancements. Figure 5.21 indicates that when the 6300 A enhancement becomes slightly larger than normal, the 5577 A emission becomes detectable. As the 6300 A enhancement becomes larger, the 5577 A enhancement grows at an even greater rate. Thus a strongly abnormal 6300 A twilight enhancement should be accompanied by very strong 5577 A emission, relatively speaking. It is reasonable to asssume that the decrease of 6300 A relative to 5577 A is due to the increased quenching of the red line as the altitude of the maximum OI emission rate becomes lower.

Table 5.4 lists the amount of enhancement for several twilights. The dependence on magnetic activity can not be shown with any certainty, nor

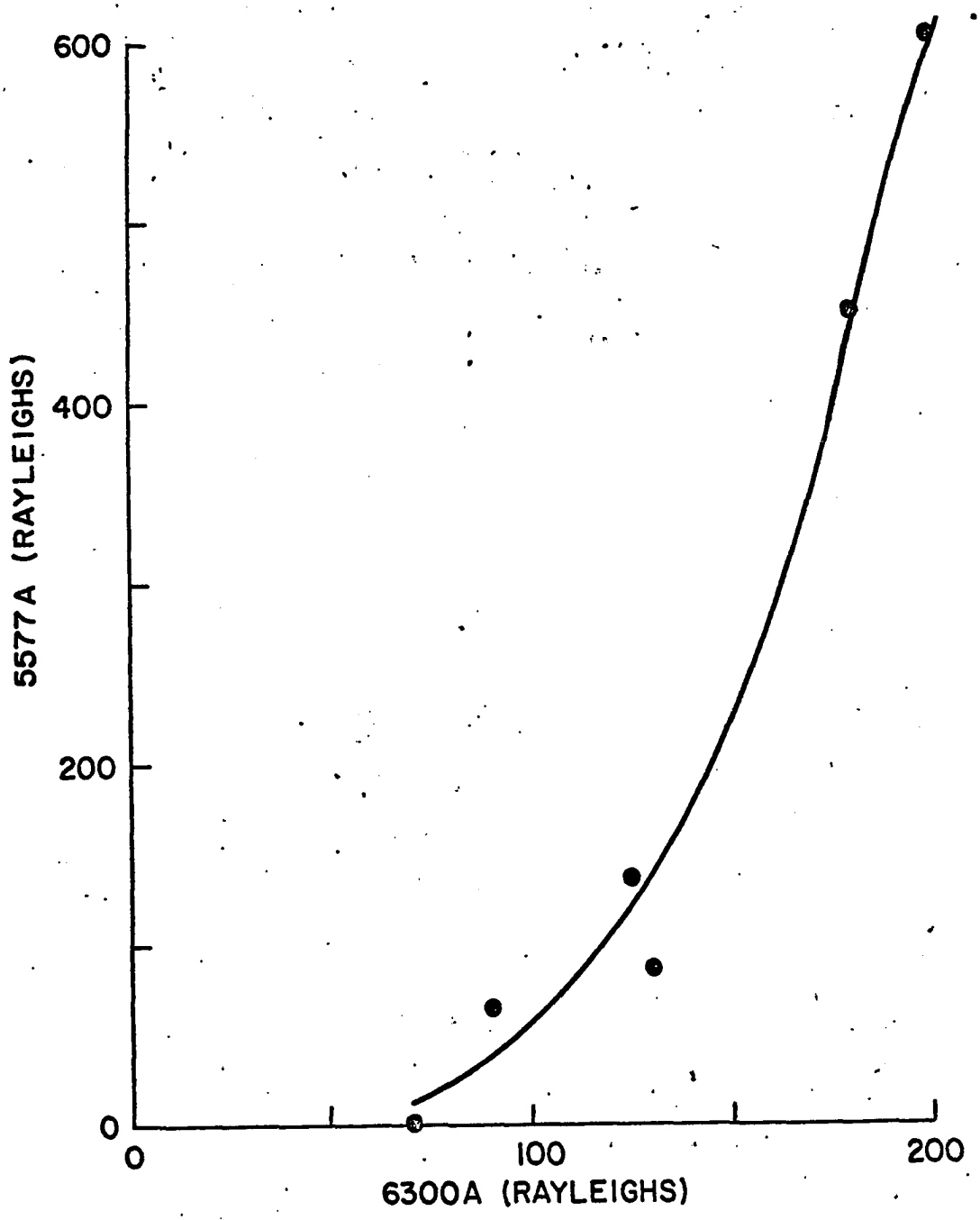

Fig. 5.21 The zenith intensity of the moving twilight enhancement of [OI] 5577 A versus the corresponding value for [OI] 6300 A. The twilight enhancement is the observed intensity at 97° SZA minus the nightglow value.

can any relationship to the solar flux at 10.7 cm be established. The number of samples is simply to small to provide any significant relation. Thus, the abnormal twilights are probably due to an increased O_2 population in the 200 km altitude region. Twilight enhancement observed in the aurora (Fig. 5.17), or with an auroral glow to the north (Fig. 5.8), shows that the auroral emission is not enhanced, but the twilight glow seems to rise independently out of the distribution of aurora luminosity. It may be concluded that the sporadic strong enhancements are not related to particle precipitation. Because an order of magnitude increase in the total O_2 population changes the observed intensity by only a factor of four (Fig. 6.4) it is probable that the O_2 is not created by a chemical process. It could be a manifestation of physical or meteorological processes above 120 km altitude; 1) There is some evidence for the accumulation of O_2 over the winter pole (Lagos and Mahoney, 1967) both as a result of less dissociation by sunlight and general poleward circulation. 2) This effect would be emphasized near 200 km altitude by the normal diurnal increase of $n(O_2)/n(N_2)$ in that region, as found by Kallmann-Bijl and Sibley (1963). 3) Another process causing an increase in density at these altitudes is the dependence of upper air density on magnetic activity, as found by Jacchia, Slowey and Veriani (1967).

Unfortunately the abnormal twilight may result from an unknown combination of all three of these effects. The latitude dependence favors 1) and 3) and the dependence on magnetic activity favors 3). However, the sensitivity of the 6300 A emission rate to $n(O_2)/n(N_2)$ may make 2) a contributor to the enhancement.

TABLE 5.4

LISTING OF MORNING TWILIGHTS, THE RELATIVE ENHANCEMENT OF THE OXYGEN LINES, AND SOME CONCURRENT GEOPHYSICAL INDICES

Date	Ap 18h ave.	Ap 12h ave.	10.7 cm Solar Flux ($\frac{\text{Watts } 10^{-22}}{\text{cm}^2 \text{ sec}}$)	k sum	6300 A Enhancement* (Rayleighs)	5577 A Enhancement* (Rayleighs)
12 March 64	18	20.1	77.0	23	200	600
21 Jan 65	11.5	4	76.6	09	180	450
15 March 65	12	10.2	71.9	19	125	120
31 Oct. 64	1.3	2	75.1	03	135	80
20 Jan. 64	7	5.1	76.0	11	80	too much aurora
21 Jan. 64	2	2	75.0	02	90	65
3 Nov. 64	5.5	3.2	73.9	05	70	0

* Zenith intensity at 87°SZA minus the nightglow value.

Whatever the cause of the sporadic enhancement, its relation to magnetic activity provides another interesting consideration. Jacchia, et. al., (1967) found an increase in atmospheric density above altitudes of 200 km as magnetic activity (Ap) increases. They assumed this density increase to manifest itself by an increase in kinetic temperature. This same assumption was made, in deducing a diurnal temperature maximum, coinciding with the density maximum, at 14 hours local time. Carru, Petit and Waldteufel (1968) find that the temperature maximum may be significantly different from this time in the 200 km altitude region. Because the

abnormal twilights can not be accounted for by an increase in the exospheric temperatures, it is possible that the relation of atmospheric density to the temperature is not reflected in this latitude region. This is reasonable because the effectiveness of the conversion from density to temperature decreases drastically as $\Delta T/\Delta h$ increases. Thus, although the diurnal density change (King-Hele and Hingston, 1967) and the density change with Ap (Jacchia, et. al., 1967) is well documented, a corresponding temperature change in the 200 km altitude region is not well defined.

CHAPTER VI

DISCUSSION

6.1 Summary

Twilight airglow observations offer unique opportunities for documenting the processes taking place in the upper atmosphere. The limiting factor in the use of ground-based observations was scattered sunlight prior to the development of the birefringent filter photometer which led to a vast improvement in the process of removing continuum emissions and scattered sunlight from airglow line emissions. Reliable line emission intensities can be observed when the signal is as much as 100 times smaller than the continuum background, and the length of the observing time afforded by this continuum rejection capability has been increased by the employment of almucantar sky surveys. This method of observation enables one to separate the several processes which normally lead to the production of the airglow emissions. The spatial and temporal characteristics of each process can then be compared to the values expected to result from the respective processes. The result is a fairly accurate description of the atmospheric condition during the twilight period; this is dependent, of course, on the relative sensitivity of the observations to the various parameters involved.

A birefringent photometer at College, Alaska (65°N, 147°W) has been used to record the red and green lines of atomic oxygen with almucantar sky surveys in the twilight. The data were corrected for atmospheric extinction and scattering and reduced to local zenith intensity. The first method of data display was to plot the logarithm of the corrected

intensity versus the geometric height of the earth's shadow at the point where it intersects the instrumental field of view. The directions of observation and the collection of points making up a single sweep were identified. In this way, the phenomena connected with the solar illumination were identified. The second method of display involved the construction of isophot plots from the almucantar survey. Thus, the time variation of certain phenomena could be associated with processes known to occur in various directions, such as aurora, etc. This type of data display permitted separation of the effects due to the different processes involved in the production of the airglow emission. When the contribution of a single process to the production of an emission is known, conclusions can be reached about the environment in which the emission took place.

The first step in the isolation of processes leading to [OI] (^{1}D) production was to determine the amount of conjugate photoelectron excitation which could have contributed to the observed intensity. The advance of the observed red line airglow associated with conjugate photoelectron impact at Observatoire de Haute Provence, France, was found to match very well with the morphology calculated to occur as a result of the conjugate sunrise. The conjugate solar zenith angle was then related to the time of arrival of red line increase at Haute Provence. Because the onset was uniquely related to the conjugate solar zenith angle, the electron production rate corresponding to various levels of solar activity was related to the appropriate Haute Provence red line intensity. From these data and the assumed electron production rate the effective absorption of the escaping photoelectrons was calculated in 100 km altitude

intervals. This absorption was then used along with the calculated photoelectron flux arriving at Haute Provence, to determine the 6300 A volume emission rate-height profile. The electron flux at Haute Provence was found to be about 10^8 electrons cm^{-2} sec^{-1}, varying with solar activity. The altitude of the maximum 6300 A emission rate was found to vary, also with solar activity, between 300 and 350 km. The physical relation of these parameters to the solar activity, in terms of the 10.7 cm solar flux, is connected to the solar EUV radiation. The latter quantity determines the average exospheric temperature of the atmosphere and hence its density gradient. It is the change of the density gradient with solar activity which affects the production and attenuation of the photoelectrons and hence the onset time, plateau intensity, and the height profile of the conjugate 6300 A emission.

Using the information accumulated from the above analysis, a map of world-wide conjugate photoelectron precipitation was made. The lines of onset and recession, corresponding to sunrise and sunset, respectively, were plotted every two hours for one twenty-four hour period at both solstices and an equinox. The effect of the changing solar declination is to change the angle at which the lines of onset and recession cross an observing station. As an example, the onset approaches College, Alaska from the east in the winter, southeast at equinox and south in summer. Another unexpected effect is due to the displacement of the magnetic poles from the geographic poles; the resulting geometry is such that the areas of the globe receiving observable (non-sunlit) continuous photoelectron precipitation sometimes include L-shells as small as 2. These areas effectively change in size with solar activity because the

solar zenith angle required for photoelectron production changes in relation to the available solar EUV. The model predicts that there should be continuous photoelectron precipitation over most of the United States, northwestern Europe and Southern Australia, to an extent which should be predictably dependent on solar activity.

The calculations made for the world-wide maps were used to predict the photoelectron induced 6300 A onset time and direction at College, Alaska for the morning twilights of interest. The enhancement of 6300 A emissions could not have been more than 5 Rayleighs. This observation placed an upper limit of 5 on the L-shell number which is capable of supporting the photoelectron travel from the conjugate region.

The photoelectron precipitation maps are useful for determining the effects of this process on other emissions. The N_2^+ resonance scattered sunlight observed at Kitt Peak has an evening winter enhancement which has been attributed previously to photoelectron precipitation. The results of this study confirm the evening enhancement and predict that it should be sensitive to the level of solar activity. The result of this dependence on solar activity is that the enhancement should appear more prominent in the morning twilight as average solar activity increases. Observations of metastable 2^3S He emission have also suggested an enhancement due to photoelectron precipitation. The calculations made here suggest that the observed northern enhancement of twilight He emission was a result of the continuous precipitation predicted above. Other asymmetries and seasonal variations can be shown to be a result of the changing onset and recession times and directions.

The true twilight enhancement of 6300 A emission was easily documented at College because of the small contributions due to aurora, dissociative recombination of O_2^+ and excitation by photoelectron impact. Unfortunately, the contribution from the aurora could not be entirely removed, but the observed intensity versus shadow height curves still could be fit to curves calculated to result from photodissociation of O_2. The latter curves were the solution of analytical expressions of the excitation rate of 6300 A emission in the field of view for various screening heights. This calculation was made at 22½° intervals from the direction of the sun to directly away from the sun. The resulting azimuth sweep showed different characteristics according to the different atmospheric parameters used. Among these parameters were the constitution of the atmosphere, the exospheric temperature, the quenching rate coefficient, the quenching species, and the absorption cross section. The comparison of the observed curves to the calculated ones resulted in the following conclusions. The calculated values of the "normal" twilight enhancement of 6300 A emission best fit the observations when the CIRA 1965 Models 1 through 4, at 04 hours were used. This implies that the exospheric temperature was between 700 and 800°K during the observations. The quenching species was probably N_2 and the rate coefficient for quenching was between 1 and 3×10^{-11} cm^3 sec^{-1}. The N_2/O_2 ratio at 120 km was 5.3. Quenching by O_2 could have had a rate coefficient as high as the gas kinetic value of 3×10^{-10} and it would still have been relatively unimportant. The values of solar flux and absorption coefficients had comparatively little effect on the twilight curves, and the normally accepted values were used.

The same analysis, without the quenching calculation, was carried out for the 5577 A emission. The calculated curves matched the observations closely enough to show that the mechanism for the twilight enhancement is almost certainly photodissociation of O_2. The efficiency of the production should be about 11 x 10^{-8} photons cm^{-3} $molecule^{-1}$. The enhancement of the green line was not always observed and it varied in magnitude by more than a factor of ten between twilights during the course of the observations. The red line also exhibits a sporadic "abnormal" increase in brightness. The magnitude of this enhancement seems to be related to magnetic activity, although the number of samples reported here was not large enough to establish a clear relationship. The enhancement of both the red and the green line is not connected with the aurora; i.e. auroral luminosity shows no obvious increase with solar illumination. Thus, the sporadic enhancement should not be connected with particle precipitation.

The enhancement of the green line is related to the "abnormal" enhancements of the red line in a fairly systematic manner. When the red line is only slightly enhanced the green line becomes observable. If the red line becomes strong the green line is exceptionally so. It is reasonable to assume that the red line would follow the green line except that it is more strongly quenched. The shape of the twilight curve corraborates the conclusion that the abnormal twilights take place at a lower altitude than do the normal ones. Attempts to change the calculated curves to match the observed ones indicate that simply increasing the exospheric temperature is not sufficient to explain the observations. The effect is more probably due to an increased O_2 population in the

200 km altitude range. This region having been too low for satellites and too high for most rockets is not well known. It is safe to say that it probably departs significantly from present atmospheric models. The observations reported here may be a sensitive indicator of conditions in this region.

6.2 Applications to Studies of Atmospheric Composition

The findings of this study indicate that routine twilight observations of the red and green lines of oxygen can provide a sensitive measure of the condition of the atmosphere above 150 km. The exospheric temperature, N_2 population and O_2 distribution could be deduced from only one azimuth sweep at 65 or 75° ZA for SZA = 97°, although a number of photometric observations could be combined to increase the signal-to-noise ratio.

The analytical expression for the expected intensity seems to need some modification. Changes in the method of calculation should include:

1) elimination of the approximation used in eq. (5.14) by numerically integrating the expression for β' from 0 to β_o.
2) elimination of the correction to local zenith intensity of observed slant intensities. The slant intensities can be easily calculated by developing an expression in terms of β_o for the slant distances between points at successive values of Z_o and integrating the volume emission rate between these points.

These changes would improve the match of the calculations to the observations at $\beta_o > 0.15$.

The ground-based observations reported here have shown that the twilight enhancement can be accounted for quantitatively. Some laboratory measurements would significantly reduce the errors in the desired results; the rate coefficient for quenching, the quenching species and the production rate are the major parameters in doubt. Unfortunately, these quantities are difficult to observe in the laboratory and such results will probably not be available for some time, with the possible exception of the efficiency of O (^{1}D) production by photodissociation.

The purpose here is to draw attention to the possibility of determining these quantities from observations in twilight. The time and place can be chosen so that only one major process contributes to the production of the O(^{1}S) and O(^{1}D) emissions. The O^1S and O^1D height-luminosity profiles from a rocket flight in this twilight situation could yield the efficiency of O(^{1}D) production and the rate of quenching of that state. That is, if the O(^{1}S) production efficiency can be observed in the laboratory and the difference between the ^{1}D and ^{1}S quenching rate is large at the altitudes of interest. The O_2 distribution resulting from the ^{1}S observed from the rocket could then be used to analyze the ^{1}D profile. Ideally, one rocket flight would improve the accuracy of the ground observations to the point that the O_2 distribution and other parameters could be measured routinely in the twilight.

6.3 Suggestions Regarding Conjugate Photoelectron Precipitation

The most efficient method of documenting the existence, and mapping the extent of the areas of continuous photoelectron precipitation

(or the onset-recession lines) is to employ an airborne observatory. A single, instrumented airplane flying north from Arecibo, and timed to encounter the equatorward boundary of continuous precipitation at about 06^h U.T., could record the position where the 6300 A intensity dropped off owing to the inability of the field lines to support the transport of 5 to 50 ev particles from the conjugate region. Unfortunately, the flight would probably have to be made in the early morning, local time, in order to avoid a large 6300 A emission background due to dissociative recombination of O_2^+ from the evening twilight. If several flights could be made at other local times and the data combined to subtract the background radiation, one could probably determine the change in latitude of the cut-off point with local time, thereby expanding the "map" of the magnetosphere with a minimum of flights. A "meridian chain" of stations in Eastern Canada might also be helpful in determining long term variations. It is not so surprising that this prediction of a region of continuous photoelectron precipitation has yet to be verified, when one considers that all of the established airglow observatories are to the south and west of the "anomaly", except during years of peak solar activity when the effect may be ill-defined owing to distortions of the field.

Suggestions can also be made for future experiments on the effects of photoelectron precipitation. A rocket fired into the F-region during a time when photoelectrons are the major contributor to the production of the red line would clarify the contribution of this process to the 6300 A emission. Previous rocket flights observing daytime airglow

(Wallace & McElroy, 1966), have illustrated the doubt which can arise from too many processes simultaneously contributing to the production of the observed emission. Correctly placed and timed, twilight observations on the other hand, offer an opportunity to evaluate some of the processes independently.

On a far more speculative basis than the above discussion, it is interesting to consider the possible relationship of the zone of continuous photoelectron precipitation to the mid-latitude red arc. As it was described in section 4.3 above, the boundaries of this precipitation zone are determined by the geometry of the magnetic field and the sunrise-sunset lines. The equatorward boundary is controlled by the line of continuous sunlight in the conjugate region and by the attenuation of photoelectron flow due to the immersion of a greater proportion of a field line in the atmosphere as L becomes smaller. The poleward boundary is determined by the ability of the field lines to support the flow of low energy electrons along its entire length. The effect of distortions in the magnetic field and in the atmosphere itself during periods of high magnetic activity is not known. However, these factors have little effect on the following argument.

Solar flare activity can increase the average solar EUV flux by three orders of magnitude. As is evident from section 4.3 above, this would tend to produce a large change in the onset time and the intensity of the 6300 A airglow produced by the precipitating photelectrons. The ionosphere under continuous solar radiation would carry a great deal of heat to the conjugate electron population where the red line would

be produced by both photoelectron and thermal electron collisions with oxygen atoms. This mechanism would produce a "monochromatic" intensity which would vary according to flare activity on the sun and the electron temperature of the ionosphere.

The boundaries of the emitting region, defined above, would be aligned along lines of constant L. The motion of the region would be related more to D_{st} than to K_p and other indices which are sensitive to polar magnetic activity. The boundaries would be quite diffuse because they would be dependent on the energy distribution of the incoming particles. The actual position of the emitting region is not obvious from the maps in Figs. 4.10, 4.11 and 4.12, and the equinox maps show what looks like an entirely different geometry. However, the onset and recession lines mapped here represent a solar minimum situation; the solar flux at maximum activity would certainly extend the zone of continuous precipitation considerably equatorward. However, because of the displacement of the geomagnetic pole from the geographic pole, the continuous precipitation would not be observed in Russia or Africa. It would be observed in North America, Northern Europe and South Australia at an altitude between 350 and 450 km. The following list (Roach and Roach, 1963) of observed properties of the mid-latitude red arc can be compared to the description in the preceding paragraphs. The mid-latitude red arcs:

1) have no other visible emissions than that of 6300 A,

2) are aligned along L-shells,

3) have been observed in North America, Northern Europe and Australia,

4) have not been observed in Russia, ironically enough,

5) are associated with radio star scintillation and F-region activity indicating enhanced electron temperatures,

6) do not seem to be related to auroral activity or K_p,

7) appear only during maximum solar activity (invariable appearance following a 3+ flare),

8) are related to Dst,

9) occur at an altitude of 350 km and are 500 to 1000 km in north-south extent,

10) arise from the evening twilight enhancement and are lost in the morning twilight enhancement.

The suggestion that photoelectrons are responsible for the production of the mid-latitude red arc is obviously only a hypothesis at this point. The continuous precipitation zones for solar maximum will be calculated in the near future; studies of the expected distribution of red line emission for documented observations of the red arcs will be made. It is encouraging to note, however, that the observed properties of the red arc can be accounted for, at least to a first approximation, by the photoelectron precipitation model.

6.4 Conclusions

The following is a condensed list of contributions from this work:

1) The true twilight enhancement of the 6300 A and 5577 A emissions of oxygen is due to photodissociation of O_2 by sunlight in the 1000 to 1700 A wavelength region.

2) The subpolar atmosphere during low solar and magnetic activity in the morning twilight can be well represented by the 1965 COSPAR Reference atmospheres with an exospheric temperature of 750°K.

3) The d-factor for the OI(^{1}S) production is about 1/200 of that for the ^{1}D state which was taken as 4.4×10^{-6} photons sec^{-1} $molecule^{-1}$.

4) The quenching of the OI(^{1}D) state was probably by N_2 with a rate of 10^{-11} cm^3 sec^{-1}.

5) The altitude of the emitting layer varies from approximately 250 km to 150 km during the course of the morning twilight observations.

6) As geomagnetic activity increases, the enhancement of both oxygen emissions increases; the 5577 A emission increases for more than that of the 6300 A line, probably because of selective quenching due to the observed effective lowering of the main emitting layer under these conditions.

7) In the advent of magnetic activity, indicated by abnomal enhancements of OI emission, the actual atmosphere cannot be represented by the model atmosphere used successfully during quiet periods, even with the substitution of larger exospheric temperatures. This indicates that density changes connected with geomagnetic perturbations are a result of mass motions by diffusion and winds rather than a change in temperature.

8) The altitude and intensity of the 6300 A emission associated with conjugate photoelectrons is proportional to the solar cycle variation in atmospheric density above 300 km.

9) The approach and departure of the emitting region with conjugate sunrise and sunset over any single station changes as much as 90° in azimuth with the yearly change in solar declination.

10) The displacement of the geomagnetic pole from the geographic pole results in the existence of a region of continuous precipitation of photoelectrons in certain areas of the earth.

11) The extent and occurrence of the photoelectron precipitation are predictably dependent on the solar activity.

12) The precipitation of conjugate photoelectrons poleward of L=5 was negligible during the period of low magnetic and solar activity.

BIBLIOGRAPHY

Barbier, D., Les Variations d'Intensite de la Raie 6300A de la Luminescence Nocturne, Ann. Geophys., 17, 3, 1961.

Barbier, D., Recherches sur la raie 6300 de la Luminescence atmospherique nocturne, 1950.

Bates, D. R. and A. Dalgarno, Theoretical considerations regarding the dayglow, J. Atmos. Terr. Phys., 5, 329-344, 1954.

Berthier, P., Etude spectrophotometrique de la luminescence nocturne des bandes des molecules OH et O_2 atmospherique, Ann. Geophys., 12, 113-143, 1956.

Broadfoot, A. L., and Hunten, D. M., N_2^+ emission in the twilight, Planet. Space Sci., 14, 1303, 1966.

Carlson, H. C., Aurora and Airglow - Proceedings of the NATO Advanced Study Institute (University of Keele), McCormac, ed. Reinhold, 1967.

Carlson, H. C., and Weill, G. M., Solar cycle variation of conjugate photoelectron flux onset timing deduced from 6300A and T_e observations, Ann. Geophys., 23, 569, 1967.

DeMore, W. B. and O. F. Raper, Deactivation of $O(^1D)$ in the Atmosphere, Astrophys. J., 139, 1381, 1964.

Detwiler, C. R., D. L. Garrett, J. D. Purcell, and R. Tousey, The intensity distribution in the ultraviolet solar spectrum, Ann. Geophys., 17, 263, 1961.

Dufay, J. and Dufay, M., Excitation de la raie verte de l'oxygene au crepuscule, C. R. Acad. Sci. Paris, 226, 1208, 1948.

Dufay, J. and Tcheng Mao-Lin, Recherches spectrophotometriques sur la lumiere du ciel nocturne dans la ciel nocturne dans la region visible, I, Ann. Geophys., 2, 189, 1946.

Dunn, R. B., and Manring, E. R., A recording night sky photometer, J. Opt. Soc. Am., 46, 572, 1955.

Elvey, C. T., Emission spectrum of the upper atmosphere at twilight, In "Emission Spectra of the Night Sky and Aurorae," (Reports of the Gassiot Committee), pp. 16-21, The Physical Society, London, 1948.

Elvey, C. T., and Farnsworth, A. H., Spectrophotometric observations of the light of the night sky, Astrophys. J., 96, 451, 1942.

Carman, E. H., and B. C. Gibson-Wilde, Seasonal Variations of the [OI] 6300A Airglow at Townsville from Isophote Sky Maps, J. Geophys. Res., 69, 487, 1964.

Carroll, P. K., Predissociation in the Schumann-Runge Bands of Oxygen, Astrophys. J., 129, 794, 1959.

Carru, H., M. Pettit, and P. Waldteufel, On the diurnal variation of the thermopause temperature, Planet. Space Sci., 15, 944-945, 1967.

Chamberlain, J. W., Physics of the Aurora and the Airglow, Academic Press, New York, 1961.

Chamberlain, J. W. and Sagan, C., The origin of nitrogen ionization in the upper atmosphere, Planet. Space Sci., 2, 157-164, 1960.

CIRA, COSPAR International Reference Atmospheres, COSPAR Working Group IV, North-Holland Publishing Co., Amsterdam, 1965.

Cole, K. D., The predawn enhancement of 6300A airglow, Ann. Geophys., 21, 156, 1965.

Fedorova, N. I., On Emission 10830A in Aurorae, Planet. Space Sci., 5, 75, 1961.

Ferguson, E. E., and Schluter, H., Metastable Helium Atom Concentrations in the Earth's Atmosphere, Planet. Space Sci., 9, 701-710, 1962.

Gilmore, F. R., Potential energy curves for N_2, N_0, 0_2, and corresponding ions, J. Quant. Spectrosc. Radiat. Transfer, 5, 369-390, 1965.

Handbook of Geophysics, United States Air Force, The MacMillan Co., New York, 1960.

Hanson, W. B., Electron Temperatures in the Upper Atmosphere, Space Res., 3, 282-302, 1963.

Hinteregger, H. E., L. A. Hall, and G. Schmidtkeg, Space Research V (ed. by D. G. King-Hele, P. Muller, and G. Righini), North-Holland Pub. Co., Amsterdam, p. 1175, 1965.

Hunten, D. M., Spectroscopic Studies of the Twilight Airglow, Space Sci. Rev., 6, 493, 1967.

Hunten, D. M., A study of sodium in twilight, I, Theory, J. Atmos. Terr. Phys., 5, 44, 1954.

Hunten, D. M., and McElroy, M. B., Quenching of Metastable States of Atomic and Molecular Oxygen and Nitrogen, Revs. Geophys., 4, 303, 1966.

Jacchia, L. G., J. Slowey, and F. Veriani, Geomagnetic perturbations and upper atmosphere heating, J. Geophys. Res., 72, 1423-1434, 1967.

Kallmann-Bijl, H. K., and W. L. Sibley, Diurnal Variation of Temperature and Particle Density Between ∿ 100 km and ∿500 km, Planet. Space Sci., 11, 1379-1394, 1963.

King-Hele, D. G., and J. Hingston, Variations in air density at heights near 150 km, from the orbit of the satellite 1966-101G, Planet. Space Sci., 15, 1883-1893, 1967.

Koomen, M. J., Packer, E. M., and Tousey, R., The use of birefringent filters in the measurements of the airglow, The Airglow and the Aurorae, (ed. by E. G. Armstrong and A. Dalgarno), Pergamon Press, London, p. 355, 1956.

Lagos, C. P., and J. R. Mahoney, Numerical studies of seasonal and latitudinal variability in a model thermosphere, J. Atmos. Sci., 24, 88-94, 1967.

Maartense, I., and D. M. Hunten, A note on N_2^+ twilight and sunlit aurora, Can. J. Phys., 41, 1729, 1963.

Manring, E. R., and H. B. Pettit, Observations of the [OI] 5577 nightglow at Sacremento Peak, New Mexico, February through June, 1955, "The Airglow and the Aurorae," (E. B. Armstrong and A. Dalgarno, eds.), pp. 29-37, Pergamon Press, 1956.

McElroy, M. B., Models for the terrestrial atmosphere above the 120 km level, Contributions from the Kitt Peak National Observatory No. 55, 1964.

Megill, L. R., The Twilight Enhancement of [OI] 5577, J. Atmos. Terr. Phys., 17, 276, 1960.

Megill, L. R., Jamnick, P. M., and Cruz, J. E., Seasonal variations in the twilight enhancement of [OI] 5577, J. Atmos. Terr. Phys., 18, 309, 1960.

Metzger, P. H., and G. R. Cook, A reinvestigation of the absorption cross sections of molecular oxygen in the 1050-1800A region, J. Quant. Spectrosc. Radiat. Transfer, 4, 107-116, 1964.

Roach, F. E., and J. R. Roach, Stable 6300A auroral arcs in mid-latitudes, Planet. Space Sci., 11, 523-545, 1963.

Tinsley, B., Measurements of twilight helium 10,830A emission, Planet. Space Sci., 16, 91, 1968.

Tohmatsu, T., Ogawa, T., and Tsuruta, H., Photoelectronic processes in the upper atmosphere, I. Energy spectrum of the primary photoelectrons, Rep. Ionosph. Space. Res. Japan, 19, 482, 1965.

Wallace, L., and McElroy, M. B., The visual dayglow, Planet. Space Sci., 14, 677-708, 1966.

Walker, J. C. G., The green line of atomic oxygen in the day airglow, J. Atmo. Sci., 22, 361-369, 1965.

Yao, I. G., Observations of the night airglow, Annals of the IGY, Pergamon Press, 1962.